

University of Windsor

## Scholarship at UWindor

---

Electronic Theses and Dissertations

Theses, Dissertations, and Major Papers

---

2011

### The Optical Response of Hydrogenated Amorphous Silicon

Jasmin Thevaril  
*University of Windsor*

Follow this and additional works at: <https://scholar.uwindsor.ca/etd>

---

#### Recommended Citation

Thevaril, Jasmin, "The Optical Response of Hydrogenated Amorphous Silicon" (2011). *Electronic Theses and Dissertations*. 440.

<https://scholar.uwindsor.ca/etd/440>

This online database contains the full-text of PhD dissertations and Masters' theses of University of Windsor students from 1954 forward. These documents are made available for personal study and research purposes only, in accordance with the Canadian Copyright Act and the Creative Commons license—CC BY-NC-ND (Attribution, Non-Commercial, No Derivative Works). Under this license, works must always be attributed to the copyright holder (original author), cannot be used for any commercial purposes, and may not be altered. Any other use would require the permission of the copyright holder. Students may inquire about withdrawing their dissertation and/or thesis from this database. For additional inquiries, please contact the repository administrator via email ([scholarship@uwindsor.ca](mailto:scholarship@uwindsor.ca)) or by telephone at 519-253-3000ext. 3208.

# The Optical Response of Hydrogenated Amorphous Silicon

by

Jasmin Joseph Thevaril

*A Dissertation*

*Submitted to the Faculty of Graduate Studies*

*Through the Department of Electrical and Computer Engineering*

*In Partial Fulfillment of the Requirements for*

*The Degree of Doctor of Philosophy at the*

*University of Windsor*

Windsor, Ontario, Canada

2011

©2011 Jasmin Joseph Thevaril

# The Optical Response of Hydrogenated Amorphous Silicon

by  
Jasmin J. Thevaril

APPROVED BY:

---

Dr. J. Sabarinathan  
University of Western Ontario

---

Dr. C. Rangan  
Department of Physics

---

Dr. J. Wu  
Department of Electrical with Computer Engineering

---

Dr. C. Chen  
Department of Electrical with Computer Engineering

---

Dr. N. Kar  
Department of Electrical with Computer Engineering

---

Dr. S. K. O'Leary  
Department of Electrical with Computer Engineering

---

Dr. S. Das, Chair of Defense  
Faculty of Graduate Studies

April 3, 2011

# Declaration of Co-Authorship / Previous Publication

## I. Co-Authorship Declaration

I hereby declare that this thesis incorporates material that is the result of research undertaken under the supervision of my supervisor, Dr. S. K. O’Leary. Results related to this research are reported in Chapters 2 through 6, inclusive.

I am aware of the University of Windsor’s Senate Policy on Authorship and I certify that I have properly acknowledged the contributions of the other researchers to my thesis, and I have obtained written permission from my co-author to include the aforementioned materials in my thesis.

I certify that, with the above qualification, this thesis, and the research to which it refers to, is the product of my own work.

## II. Declaration of Previous Publication

This thesis includes 4 original papers that have been previously published/submitted for publication to peer reviewed journals, as follows:

Thesis Chapter	Publication title/full citation	Publication status
Chapter 2	The role that conduction band tail states play in determining the optical response of hydrogenated amorphous silicon, J. J. Thevaril and S. K. O'Leary, <i>Solid State Communications</i> , v 151, no. 7, pp. 730-733, 2011.	Published
Chapter 3	A dimensionless joint density of states formalism for the quantitative characterization of the optical response of hydrogenated amorphous silicon, J. J. Thevaril and S. K. O'Leary, <i>Journal of Applied Physics</i> , v 107, no. 8, pp. 083105-1-6, 2010	Published
Chapter 4	A universal feature in the optical absorption spectrum associated with hydrogenated amorphous silicon: A dimensionless joint density of states analysis, J. J. Thevaril and S. K. O'Leary, submitted to <i>Journal of Applied Physics</i> , on June 17, 2010.	Major revisions required
Chapter 5	Defect absorption and optical transitions in hydrogenated amorphous silicon, J. J. Thevaril and S. K. O'Leary, <i>Solid State Communications</i> , v 150, no. 37-38, pp. 1851-1855, 2010	Published

I certify that I have obtained a written permission from the copyright owner(s) to include the above published materials in my thesis. I certify that the above material describes work completed during my registration as a graduate student at the University of Windsor.

I declare that, to the best of my knowledge, my thesis does not infringe upon anyone's copyright nor violate any proprietary rights and that any ideas, techniques, quotations, or any other material from the work of other people included in my thesis, published or otherwise, are fully acknowledged in accordance with standard referencing practices. Furthermore, to the extent that I have included copyrighted material that surpasses the bounds of fair dealing within the meaning of the Canada Copyright Act, I certify that I have obtained a written permission from the copyright owners to include such materials in my thesis.

I declare that this is a true copy of my thesis, including any final revisions, as approved by my thesis committee and the Graduate Studies office, and that this thesis has not been submitted for a higher degree to any other university or institution.

# ABSTRACT

Through the use of a general empirical model for the density of states functions, one that considers valence band band, valence band tail, conduction band band, and conduction band tail electronic states, the sensitivity of the joint density of states function to variations in the conduction band tail breadth, all other parameters being held fixed at nominal hydrogenated amorphous silicon values, is examined. It is found that when the conduction band tail is narrower than the valence band tail, its role in shaping the corresponding spectral dependence of the joint density of states function is relatively minor. This justifies the use of a simplified empirical model for the density of states functions that neglects the presence of the conduction band tail states in the characterization of the optical response.

A simplification of such an empirical model for the density of state functions associated with hydrogenated amorphous silicon is then suggested, reducing the number of independent modeling parameters from six to five as a result. As a consequence of this simplification, it is found that one is able to cast joint density of states evaluations into a dimensionless formalism, this formalism providing an elementary and effective platform for the determination of the underlying modeling parameters from experiment. This simplification is justified by showing, for reasonable hydrogenated amorphous silicon modeling parameter selections, that the joint density of states results are very similar to those determined using a more general approach.

Using our dimensionless joint density of states formalism for the quantitative characterization of the optical response associated with hydrogenated amorphous silicon, a critical comparative analysis of a large number of different optical absorption data sets is then considered. When these data sets are cast into this dimensionless framework, a trend is observed that is almost completely coincident for all of the data sets considered. This suggests that there is a universal character associated with the optical absorption spectrum of hydrogenated amorphous silicon.

Finally, the role that defect states play in shaping the optical response of this material are probed.

# DEDICATION

To all my well wishers. Nothing would be possible without you.

# ACKNOWLEDGEMENTS

My supervisor, Dr. S. K. O’Leary, has enabled me to pursue my studies to the best of my ability. His guidance and support have been unparalleled and I feel lucky to have found such a great mentor. I would like to thank my supervisor. The scientific approach and positive thinking that he has provided was a great base from which to conduct my research. I am indebted to my supervisor for his support, patience, guidance, and tons of hours of analysis and discussion of my research. I am sure that everything I learned from him will be valuable throughout my scientific career. I also extend my sincerest gratitude towards my committee members, Drs. C. Chen, N. Kar, C. Rangan, and J. Wu, for their valuable guidance, encouragement, and leadership throughout the course of this thesis. I am grateful to them for generously advising me and for driving me on the right path towards the successful completion of this thesis.

A special thank you to Dr. M. Ahmadi, the former Graduate Co-ordinator, Dr. X. Chen, the Graduate Co-ordinator, Dr. M. A. Sid-Ahmed, the Department Head of Electrical and Computer Engineering and Dr. J. Frank, the Dean of Graduate Studies, for mentoring me during the challenging times of my Ph.D studies.

I would like to acknowledge and express my gratitude and thanks to Ms. Andria

Ballo, the graduate secretary, for her extreme assistance, care, and kindness.

Last, but most importantly, I want to thank my family for their support, encouragement, and patience. Mom, your unending love and encouragement kept me going throughout my degree. My dad got me hooked into science and technology and provided me with invaluable advice, and allowed me to realize what I can achieve. My husband, my son, and my brother, always encouraged me and taught me never to take myself too seriously.

# Table of Contents

Declaration of Co-Authorship / Previous Publication . . . . .	iii
Abstract . . . . .	v
Dedication . . . . .	vii
Acknowledgements . . . . .	viii
List of Tables . . . . .	xii
List of Figures . . . . .	xiii
List of Abbreviations and Symbols . . . . .	xxiii
<b>1 Introduction</b>	<b>1</b>
1.1 Introduction to disordered semiconductors . . . . .	1
1.2 Distribution of atoms . . . . .	4
1.3 Device applications . . . . .	9
1.4 The optical response . . . . .	10
1.5 Distributions of electronic states . . . . .	14
1.6 Relation between the optical absorption spectrum and the DOS functions	19
1.7 Free electron density of states . . . . .	23
1.8 A review of empirical density of states models . . . . .	29
1.9 Modeling of the optical response . . . . .	40
1.10 Objective of this thesis . . . . .	53
1.11 Thesis organization . . . . .	56
References . . . . .	59
<b>2 The sensitivity of the optical response of hydrogenated amorphous silicon to variations in the conduction band tail breadth</b>	<b>62</b>
2.1 Introduction . . . . .	63
2.2 Analytical framework . . . . .	64
2.3 JDOS evaluation and analysis . . . . .	67
2.4 Conclusion . . . . .	75
References . . . . .	76
<b>3 A dimensionless joint density of states formalism for the quantitative characterization of the optical response of hydrogenated amorphous</b>	

<b>silicon</b>	<b>79</b>
3.1 Introduction . . . . .	80
3.2 Modeling the distribution of electronic states . . . . .	82
3.3 JDOS formalism . . . . .	85
3.4 The imaginary part of the dielectric function . . . . .	89
3.5 The utility of the dimensionless JDOS formalism . . . . .	91
3.6 Conclusions . . . . .	94
References . . . . .	97
<b>4 A universal feature in the optical absorption spectrum associated with hydrogenated amorphous silicon: A dimensionless joint density of states analysis</b>	<b>100</b>
4.1 Introduction . . . . .	101
4.2 Modeling the optical response of a-Si:H . . . . .	102
4.3 The experimental data of Cody <i>et al.</i> . . . . .	104
4.4 The experimental data of Viturro and Weiser and the experimental data of Remeš . . . . .	109
4.5 Critical comparative analysis . . . . .	116
4.6 Conclusions . . . . .	123
References . . . . .	124
<b>5 Defect absorption and optical transitions in hydrogenated amorphous silicon</b>	<b>128</b>
5.1 Introduction . . . . .	129
5.2 Analytical framework . . . . .	131
5.3 Results . . . . .	134
5.4 Comparison with experiment . . . . .	140
5.5 Conclusions . . . . .	141
References . . . . .	144
<b>6 Conclusions</b>	<b>148</b>
References . . . . .	151
<b>Appendix A Copyright Release - Journal of Applied Physics</b>	<b>152</b>
<b>Appendix B Copyright Release - Solid State Communications</b>	<b>154</b>
<b>Vita Auctoris</b>	<b>155</b>

# List of Tables

1.1	The nominal DOS modeling parameter selections employed for the empirical DOS models described in this section. These modeling parameters are representative of a-Si:H. . . . .	32
2.1	The nominal a-Si:H modeling parameter selections employed for the purposes of this analysis. These modeling parameters relate to Eqs. (2.5) and (2.6). . . . .	67
4.1	The model parameter selections corresponding to the fits to the experimental a-Si:H optical absorption data sets of Cody <i>et al.</i> [17] depicted in Figure 4.1. The number of excluded data points and the presence of a difference between the experimental results and the corresponding fits, for each data set considered, are also indicated. . . . .	106
4.2	The model parameter selections corresponding to the fits to the experimental a-Si:H optical absorption data sets of Viturro and Weiser [27] depicted in Figure 4.3. The number of excluded data points and the presence of a difference between the experimental results and the corresponding fits, for each data set considered, are also indicated. . . . .	111
4.3	The model parameter selections corresponding to the fits to the experimental a-Si:H optical absorption data sets of Remeš [28] depicted in Figure 4.5. The number of excluded data points and the presence of a difference between the experimental results and the corresponding fits, for each data set considered, are also indicated. . . . .	116
5.1	The nominal a-Si:H modeling parameter selections employed for the purposes of this analysis. . . . .	137
5.2	The a-Si:H modeling parameter selections employed for the purposes of the fit to the experimental data of Reměs [33] shown in Figure 5.4. . . . .	141

# List of Figures

1.1	A schematic depiction of the distribution of silicon atoms within c-Si and a-Si. The atoms are represented by the solid circles. The bonds are represented by the solid lines. The scale of the disorder within a-Si has been exaggerated for the purposes of illustration. . . . .	5
1.2	The coordination numbers associated each silicon atom in a representative sample of a-Si. The geometry has been exaggerated for the purposes of illustration. . . . .	7
1.3	A schematic representation of dangling bonds within a-Si. The atoms are represented by the solid spheres. The dangling bonds are represented by the dotted lines. The Si-Si bonds are represented by the solid lines. The ratio of the dangling bonds to the Si-Si bonds within a-Si has been exaggerated for the purposes of illustration. . . . .	8
1.4	The intensity of light as a function of the depth, $z$ , from the surface of the material, $z = 0$ , for light normally incident on a material and propagating from the left, in the absence of reflection. . . . .	11
1.5	The spectral dependence of the optical absorption coefficient, $\alpha(\hbar\omega)$ , associated with hypothetical crystalline and amorphous semiconductors. . . . .	13
1.6	A schematic representation of the distributions of electronic states associated with a hypothetical amorphous semiconductor. . . . .	15
1.7	A schematic representation of the wavefunctions associated with localized and extended electronic states. This figure is taken after Morigaki [25]. . . . .	16
1.8	The distributions of electronic states associated with a hypothetical amorphous semiconductor. The conduction band and valence band mobility edges are depicted with the dashed lines. The defect states have been neglected. . . . .	18
1.9	The number of optical transitions allowed from a single-spin state in the valence band for the cases of c-Si and a-Si:H. For the case of a-Si:H, there are $2\rho_A V$ possible optical transitions, since there is no momentum conservation. However, for the case of c-Si, there are only four possible optical transitions. The figure is taken after Jackson <i>et al.</i> [26] . . . .	21

1.10	The spectral dependence of the refractive index associated with a-Si:H. The tenth-order polynomial fit is depicted with the solid line. The experimental data points of Klazes <i>et al.</i> [27] are represented with the solid points. . . . .	24
1.11	The representation of an electron confined within a cubic volume, of dimensions, $L \times L \times L$ , surrounded by infinite potential barriers. . . .	26
1.12	The quantum numbers, $n_x$ , $n_y$ , and $n_z$ , shown in the first octet of three-dimensional $n$ -space. The density of such points is unity. . . . .	28
1.13	The empirical DOS model of Tauc <i>et al.</i> [30]. . . . .	31
1.14	The empirical DOS model of Chen <i>et al.</i> [31]. . . . .	33
1.15	The empirical DOS model of Redfield [32]. . . . .	35
1.16	The empirical DOS model of Cody [33]. . . . .	37
1.17	The empirical DOS model of O'Leary <i>et al.</i> [34]. . . . .	39
1.18	The valence band DOS function, $N_v(E)$ , for a number of selections of $\gamma_v$ , plotted on a linear scale. This function, specified in Eq. (1.31) with $E_{vT}$ set to $E_v - \frac{1}{2}\gamma_v$ , is evaluated assuming the nominal DOS modeling parameter selections $N_{vo} = 2 \times 10^{22} \text{ cm}^{-3}\text{eV}^{-3/2}$ and $E_v = 0 \text{ eV}$ for all cases. The abscissa axis represents the energy, $E$ , while the ordinate axis depicts the corresponding valence band DOS value. . . . .	41
1.19	The valence band DOS function, $N_v(E)$ , for a number of selections of $\gamma_v$ , plotted on a logarithmic scale. This function, specified in Eq. (1.31) with $E_{vT}$ set to $E_v - \frac{1}{2}\gamma_v$ , is evaluated assuming the nominal DOS modeling parameter selections $N_{vo} = 2 \times 10^{22} \text{ cm}^{-3}\text{eV}^{-3/2}$ and $E_v = 0 \text{ eV}$ for all cases. The abscissa axis represents the energy, $E$ , while the ordinate axis depicts the corresponding valence band DOS value. . . . .	42
1.20	The conduction band DOS function, $N_c(E)$ , for a number of selections of $\gamma_c$ , plotted on a linear scale. This function, specified in Eq. (1.32) with $E_{cT}$ set to $E_c + \frac{1}{2}\gamma_c$ , is evaluated assuming the nominal DOS modeling parameter selections $N_{co} = 2 \times 10^{22} \text{ cm}^{-3}\text{eV}^{-3/2}$ and $E_c = 1.7 \text{ eV}$ for all cases. The abscissa axis represents the energy, $E$ , while the ordinate axis depicts the corresponding conduction band DOS value. . . . .	43
1.21	The conduction band DOS function, $N_c(E)$ , for a number of selections of $\gamma_c$ , plotted on a logarithmic scale. This function, specified in Eq. (1.32) with $E_{cT}$ set to $E_c + \frac{1}{2}\gamma_c$ , is evaluated assuming the nominal DOS modeling parameter selections $N_{co} = 2 \times 10^{22} \text{ cm}^{-3}\text{eV}^{-3/2}$ and $E_c = 1.7 \text{ eV}$ for all cases. The abscissa axis represents the energy, $E$ , while the ordinate axis depicts the corresponding conduction band DOS value. . . . .	44
1.22	The JDOS function, $J(\hbar\omega)$ , determined through an evaluation of Eq. (1.10), for various selections of $\gamma_c$ and $\gamma_v$ , depicted on a linear scale. For all cases, the DOS modeling parameters are set to their nominal values tabulated in Table 1.1. . . . .	46

1.23	The JDOS function, $J(\hbar\omega)$ , determined through an evaluation of Eq. (1.10), for various selections of $\gamma_c$ and $\gamma_v$ , depicted on a logarithmic scale. For all cases, the DOS modeling parameters are set to their nominal values tabulated in Table 1.1. . . . .	47
1.24	The valence band and conduction band DOS functions associated with a-Si:H. The nominal DOS modeling parameter selections tabulated in Table 1.1 are employed for the purposes of this analysis. $E_{v_T}$ is set to $E_v - \frac{\gamma_v}{2}$ and $E_{c_T}$ is set to $E_c + \frac{\gamma_c}{2}$ for the purposes of this figure. The critical energies, $E_{v_T}$ and $E_{c_T}$ , that separate the square-root distributions from the exponential distributions, are clearly depicted. Representative VBB-CBB, VBB-CBT, VBT-CBB, and VBT-CBT optical transitions, are also shown. . . . .	50
1.25	The factors in the JDOS integrand, $N_v(E)$ and $N_c(E + \hbar\omega)$ , and the resultant product, $N_v(E)N_c(E + \hbar\omega)$ , for the case of $\hbar\omega$ set to 2.1 eV. The nominal DOS modeling parameter selections, tabulated in Table 1.1, are employed for the purposes of this analysis. Ranges of energy, corresponding to VBB-CBB, VBB-CBT, and VBT-CBB optical transitions, are depicted. VBT-CBT optical transitions do not occur for this selection of $\hbar\omega$ . This figure is taken after O'Leary [36].	51
1.26	The factors in the JDOS integrand, $N_v(E)$ and $N_c(E + \hbar\omega)$ , and the resultant product, $N_v(E)N_c(E + \hbar\omega)$ , for the case of $\hbar\omega$ set to 1.4 eV. The nominal DOS modeling parameter selections, tabulated in Table 1.1, are employed for the purposes of this analysis. Ranges of energy, corresponding to VBB-CBT, VBT-CBB, and VBT-CBT optical transitions, are depicted. VBB-CBB optical transitions do not occur for this selection of $\hbar\omega$ . This figure is taken after O'Leary [36].	52
1.27	The valence band and conduction band DOS functions associated with a-Si:H for the simplified empirical DOS model of O'Leary and Malik [38]. The nominal DOS modeling parameter selections tabulated in Table 1.1 are employed for the purposes of this analysis. $E_{v_T}$ is set to $E_v - \frac{\gamma_v}{2}$ . The critical energy, $E_{v_T}$ , separating the square-root valence band band distribution from the exponential valence band tail distribution, is clearly depicted. Representative VBB-CBB and VBT-CBB optical transitions are also shown. . . . .	54

2.1	The valence band and conduction band DOS functions associated with a-Si:H. The valence band DOS function, $N_v(E)$ , specified in Eq. (2.5), is determined assuming the nominal a-Si:H parameter selections $N_{vo} = 2 \times 10^{22} \text{ cm}^{-3} \text{ eV}^{-3/2}$ , $E_v = 0.0 \text{ eV}$ , and $\gamma_v = 50 \text{ meV}$ . The conduction band DOS function, $N_c(E)$ , specified in Eq. (2.6), is determined assuming the nominal a-Si:H parameter selections $N_{co} = 2 \times 10^{22} \text{ cm}^{-3} \text{ eV}^{-3/2}$ , $E_c = 1.7 \text{ eV}$ , and $\gamma_c = 27 \text{ meV}$ . Only differences between the energies $E_v$ and $E_c$ will impact upon the obtained JDOS results. The critical points at which the band states and tail states interface, $E_{vT}$ and $E_{cT}$ , are clearly marked with the dotted lines and the arrows. . . . .	68
2.2	The JDOS function, $J(\hbar\omega)$ , associated with a-Si:H, determined through an evaluation of Eq. (2.2), for various selections of $\gamma_c$ . For all cases, $N_{vo}$ , $N_{co}$ , $E_v$ , $E_c$ , and $\gamma_v$ are held at their nominal a-Si:H values, i.e., $N_{vo} = N_{co} = 2 \times 10^{22} \text{ cm}^{-3} \text{ eV}^{-3/2}$ , $E_g \equiv E_c - E_v = 1.7 \text{ eV}$ , and $\gamma_v = 50 \text{ meV}$ . . . . .	69
2.3	The dependence of $E_o$ , as defined in Eq. (2.8), on the photon energy, $\hbar\omega$ , for a number of selections of $\gamma_c$ . For all cases, $N_{vo}$ , $N_{co}$ , $E_v$ , $E_c$ , and $\gamma_v$ are held at their nominal a-Si:H values, i.e., $N_{vo} = N_{co} = 2 \times 10^{22} \text{ cm}^{-3} \text{ eV}^{-3/2}$ , $E_g \equiv E_c - E_v = 1.7 \text{ eV}$ , and $\gamma_v = 50 \text{ meV}$ . . . .	71
2.4	The dependence of $E_o$ , as defined in Eq. (2.8), on the conduction band tail breadth, $\gamma_c$ , for the photon energy, $\hbar\omega$ , set to 1 eV. For all cases, $N_{vo}$ , $N_{co}$ , $E_v$ , $E_c$ , and $\gamma_v$ are held at their nominal a-Si:H values, i.e., $N_{vo} = N_{co} = 2 \times 10^{22} \text{ cm}^{-3} \text{ eV}^{-3/2}$ , $E_g \equiv E_c - E_v = 1.7 \text{ eV}$ , and $\gamma_v = 50 \text{ meV}$ . The approximate analytical expression for $E_o$ , i.e., Eq. (2.9), is also depicted with the dotted line. . . . .	73
2.5	The dependence of $\gamma_v$ on $\gamma_c$ . Results from the experiments of Sherman <i>et al.</i> [29], Tiedje <i>et al.</i> [30], and Winer and Ley [31], are depicted. Results obtained from the modeling analysis of O'Leary [13] are also shown. . . . .	74
3.1	The valence band DOS function, $N_v(E)$ , for a number of selections of $\gamma_v$ . This function, specified in Eq. (3.3) with $E_{vT}$ set to $E_v - \frac{1}{2}\gamma_v$ , is evaluated assuming the nominal modeling parameter selections $N_{vo} = 2 \times 10^{22} \text{ cm}^{-3} \text{ eV}^{-3/2}$ and $E_v = 0 \text{ eV}$ for all cases. The abscissa axis represents the energy, $E$ , while the ordinate axis depicts the corresponding valence band DOS value. . . . .	84
3.2	The dimensionless JDOS function, $\mathcal{J}(z)$ , plotted as a function of $z$ . . . . .	87
3.3	The sensitivity of the JDOS function, $J(\hbar\omega)$ , to variations in the critical energy at which the exponential and square-root valence band distributions interface, $E_{vT}$ . All other modeling parameters are set to their nominal values for all cases, i.e., $N_{vo} = N_{co} = 2 \times 10^{22} \text{ cm}^{-3} \text{ eV}^{-3/2}$ , $E_g = 1.7 \text{ eV}$ , and $\gamma_v = 50 \text{ meV}$ . . . . .	88

- 3.4 The imaginary part of the dielectric function corresponding to a-Si:H. The experimental data of Jackson *et al.* [2] is depicted with the solid points. Our calculated result is indicated with the solid line. The characteristic energy,  $E_d$ , is indicated with the arrow. We assume that  $N_{vo} = N_{co} = 2.38 \times 10^{22} \text{ cm}^{-3} \text{ eV}^{-3/2}$ ,  $E_g = 1.68 \text{ eV}$ ,  $\gamma_v = 48 \text{ meV}$ ,  $R_o^2 = 10 \text{ \AA}^2$ , and  $E_d = 3.4 \text{ eV}$  for the purposes of this analysis. We see that there is almost complete agreement between our model and the experimental results of Jackson *et al.* [2], except for  $\hbar\omega < 1.4 \text{ eV}$ . . . . . 90
- 3.5 Three a-Si:H optical absorption data sets plotted as a function of the photon energy. The data sets considered include that corresponding to Cody *et al.* [18] (the  $T_H = 293 \text{ K}$  data set depicted in Figure 1 of Cody *et al.* [18]), plotted with the solid green points, Remeš [19] (the standard GD-a data set depicted in Figure 5.2 of Remeš [19]), plotted with the solid red points, and Viturro and Weiser [20] (the  $C_H = 1 \%$  data set depicted in Figure 4 of Viturro and Weiser [20]), plotted with the blue solid points. The optical absorption spectral dependencies obtained through our theoretical analysis, for the cases of  $\gamma_v = 68.9 \text{ meV}$  and  $E_g = 1.73 \text{ eV}$ ,  $\gamma_v = 91.2 \text{ meV}$  and  $E_g = 1.57 \text{ eV}$ , and  $\gamma_v = 193 \text{ meV}$  and  $E_g = 1.53 \text{ eV}$ , are depicted using the green, red, and blue solid lines, respectively, these parameter selections being made in order to fit the theoretical results with the experimental data of Cody *et al.* [18], Remeš [19], and Viturro and Weiser [20], respectively; for all cases, we set  $N_{vo} = N_{co} = 2.38 \times 10^{22} \text{ cm}^{-3} \text{ eV}^{-3/2}$ . The online version is depicted in color. . . . . 93
- 3.6 The rescaled a-Si:H optical absorption data sets and the dimensionless JDOS function,  $\mathcal{J}(z)$ , plotted as a function of the independent variable,  $z$ . The data sets considered include that corresponding to Cody *et al.* [18] (the  $T_H = 293 \text{ K}$  data set depicted in Figure 1 of Cody *et al.* [18]), plotted with the solid green points, Remeš [19] (the standard GD-a data set depicted in Figure 5.2 of Remeš [19]), plotted with the solid red points, and Viturro and Weiser [20] (the  $C_H = 1 \%$  data set depicted in Figure 4 of Viturro and Weiser [20]), plotted with the blue solid points. The dimensionless JDOS function,  $\mathcal{J}(z)$ , plotted as a function of  $z$ , is also shown with the solid black line. The online version is depicted in color. . . . . 95

4.1	The experimental a-Si:H optical absorption data sets of Cody <i>et al.</i> [17] and the corresponding fits. The experimental data itself is represented with the solid and open colored points. The solid colored points correspond to experimental data that is not believed to be influenced by defect absorption while the open colored points correspond to experimental data that is believed to be influenced by defect absorption. The color scheme is indicated in the legend within the figure. The identification of each data set borrows directly from the classification scheme employed by Cody <i>et al.</i> [17]; see Figure 1 of Cody <i>et al.</i> [17]. The fits to these experimental data sets are depicted with the corresponding colored lines. The model parameter selections for these fits, i.e., the corresponding $\gamma_v$ and $E_g$ values, are indicated in Table 4.1. The online version of this figure is depicted in color. . . . .	105
4.2	The rescaled experimental a-Si:H optical absorption data sets of Cody <i>et al.</i> [17] and the dimensionless JDOS function, $\mathcal{J}(z)$ , plotted as a function of the independent variable, $z$ . The rescaled experimental data is represented with the solid and open colored points. The solid colored points correspond to rescaled experimental data that is not believed to be influenced by defect absorption while the open colored points correspond to rescaled experimental data that is believed to be influenced by defect absorption. The color scheme is indicated in the legend within the figure. The identification of each data set borrows directly from the classification scheme employed by Cody <i>et al.</i> [17]; see Figure 1 of Cody <i>et al.</i> [17]. The dimensionless JDOS function, $\mathcal{J}(z)$ , plotted as a function of $z$ , is also shown with the solid black line. The online version of this figure is depicted in color. . . . .	108
4.3	The experimental a-Si:H optical absorption data sets of Viturro and Weiser [27] and the corresponding fits. The experimental data itself is represented with the solid points; for the case of Viturro and Weiser [27] there are no experimental points that are believed to be influenced by defect absorption. The color scheme is indicated in the legend within the figure. The identification of each data set borrows directly from the classification scheme employed by Viturro and Weiser [27]; see Figure 4 of Viturro and Weiser [27]. The fits to these experimental data sets are depicted with the corresponding colored lines. The model parameter selections for these fits, i.e., the corresponding $\gamma_v$ and $E_g$ values, are indicated in Table 4.2. The online version of this figure is depicted in color. . . . .	110

4.4	<p>The rescaled experimental a-Si:H optical absorption data sets of Viturro and Weiser [27] and the dimensionless JDOS function, <math>\mathcal{J}(z)</math>, plotted as a function of the independent variable, <math>z</math>. The rescaled experimental data itself is represented with the solid points; for the case of Viturro and Weiser [27] there are no experimental points that are believed to be contaminated with defect absorption. The color scheme is indicated in the legend within the figure. The identification of each data set borrows directly from the classification scheme employed by Viturro and Weiser [27]; see Figure 4 of Viturro and Weiser [27]. The dimensionless JDOS function, <math>\mathcal{J}(z)</math>, plotted as a function of <math>z</math>, is also shown with the solid black line. The online version of this figure is depicted in color. . . . .</p>	112
4.5	<p>The experimental a-Si:H optical absorption data sets of Remeš [28] and the corresponding fits. The experimental data itself is represented with the solid points; for the case of Remeš [28] there are no experimental points that are believed to be contaminated with defect absorption. The HW70 a-Si:H film of Remeš [28] is not considered as it exhibits a spectral variation that is distinct from the other spectra for high values of <math>\hbar\omega</math>; it is depicted with the open points. The color scheme is indicated in the legend within the figure. The identification of each data set borrows directly from the classification scheme employed by Remeš [28]; see Figure 5.2 of Remeš [28]. The fits to these experimental data sets are depicted with the corresponding colored lines. The model parameter selections for these fits, i.e., the corresponding <math>\gamma_v</math> and <math>E_g</math> values, are indicated in Table 4.3. The online version of this figure is depicted in color. . . . .</p>	114
4.6	<p>The rescaled experimental a-Si:H optical absorption data sets of Remeš [28] and the dimensionless JDOS function, <math>\mathcal{J}(z)</math>, plotted as a function of the independent variable, <math>z</math>. The rescaled experimental data itself is represented with the solid colored points; for the case of Remeš [28] there are no experimental points that are believed to be influenced by defect absorption. The HW70 a-Si:H film of Remeš [28] is not considered as it has not been fit to our dimensionless JDOS formalism, i.e., Eqs. (4.1), (4.2), and (4.3). The color scheme is indicated in the legend within the figure. The identification of each data set borrows directly from the classification scheme employed by Remeš [28]; see Figure 5.2 of Remeš [28]. The dimensionless JDOS function, <math>\mathcal{J}(z)</math>, plotted as a function of <math>z</math>, is also shown with the solid black line. The online version of this figure is depicted in color. . . . .</p>	115

4.7	Deviations between the experimental results and the corresponding fits as determined through a ratio of the experimental and fit results for the experimental a-Si:H optical absorption data sets of Cody <i>et al.</i> [17]. The ordinate values for this plot are obtained by dividing each experimental value, $\alpha_{\text{expt}}$ , by the corresponding fit value, $\alpha_{\text{fit}}$ , the abscissa axis being the corresponding photon energy, $\hbar\omega$ . The online version of this figure is depicted in color. . . . .	117
4.8	Deviations between the experimental results and the corresponding fits as determined through a ratio of the experimental and fit results for the experimental a-Si:H optical absorption data sets of Viturro and Weiser [27]. The ordinate values for this plot are obtained by dividing each experimental value, $\alpha_{\text{expt}}$ , by the corresponding fit value, $\alpha_{\text{fit}}$ , the abscissa axis being the corresponding photon energy, $\hbar\omega$ . The online version of this figure is depicted in color. . . . .	119
4.9	Deviations between the experimental results and the corresponding fits as determined through a ratio of the experimental and fit results for the experimental a-Si:H optical absorption data sets of Remeš [28]. The ordinate values for this plot are obtained by dividing each experimental value, $\alpha_{\text{expt}}$ , by the corresponding fit value, $\alpha_{\text{fit}}$ , the abscissa axis being the corresponding photon energy, $\hbar\omega$ . The online version of this figure is depicted in color. . . . .	120
4.10	Deviations between the experimental results and the corresponding fits as determined through a ratio of the experimental and fit results for the experimental a-Si:H optical absorption data sets of Cody <i>et al.</i> [17], Viturro and Weiser [27], and Remeš [28]. The ordinate values for this plot are obtained by dividing each experimental value, $\alpha_{\text{expt}}$ , by the corresponding fit value, $\alpha_{\text{fit}}$ , the abscissa axis being the corresponding photon energy, $\hbar\omega$ . For the optical absorption values not influenced by defect absorption, 219 of the 290 experimental points of Cody <i>et al.</i> [17], 117 of the 176 experimental points of Viturro and Weiser [27], and 136 of the 181 experimental points of Remeš [28], lie between $\frac{1}{\beta}\alpha_{\text{fit}}$ and $\beta\alpha_{\text{fit}}$ , for the specific case of $\beta$ set to 1.1. . . . .	121
4.11	The fraction of the experimental points between $\frac{1}{\beta}\alpha_{\text{fit}}$ and $\beta\alpha_{\text{fit}}$ as a function of $\beta$ . The data sets of Cody <i>et al.</i> [17], Viturro and Weiser [27], and Remeš [28] are considered in this analysis. . . . .	122

- 5.1 The valence band and conduction band DOS functions associated with a-Si:H. The valence band DOS function,  $N_v(E)$ , specified in Eq. (5.5), is determined assuming the nominal a-Si:H parameter selections  $N_{vo} = 2 \times 10^{22} \text{ cm}^{-3} \text{ eV}^{-3/2}$ ,  $E_v = 0.0 \text{ eV}$ ,  $\gamma_v = 50 \text{ meV}$ ,  $E_v - E_{v_T} = 35 \text{ meV}$ ,  $\gamma_{v_D} = 130 \text{ meV}$ , and  $E_{v_D} - E_v = 400 \text{ meV}$ . The conduction band DOS function,  $N_c(E)$ , specified in Eq. (5.6), is determined assuming the nominal parameter selections  $N_{co} = 2 \times 10^{22} \text{ cm}^{-3} \text{ eV}^{-3/2}$ ,  $E_c = 1.7 \text{ eV}$ ,  $\gamma_c = 27 \text{ meV}$ ,  $E_{c_T} - E_c = 35 \text{ meV}$ ,  $\gamma_{c_D} = 80 \text{ meV}$ , and  $E_c - E_{c_D} = 200 \text{ meV}$ . The critical points at which the band states and tail states interface,  $E_{v_T}$  and  $E_{c_T}$ , are clearly marked with the dashed lines and the arrows. The critical points at which the tail states and defect states interface,  $E_{v_D}$  and  $E_{c_D}$ , are also marked with the dashed lines and the arrows. Representative VBB-CBB, VBB-CBT, VBT-CBB, VBT-CBT, VBD-CBB, and VBD-CBT optical transitions are depicted. Representative VBB-CBD, VBT-CBD, and VBD-CBD optical transitions are not depicted as they are found to make relatively minor contributions to the JDOS function. . . . . 135
- 5.2 The JDOS function,  $J(\hbar\omega)$ , associated with a-Si:H, determined through an evaluation of Eq. (5.2). For the purposes of this analysis, we performed this evaluation with and without the defect states taken into account. In the absence of defects,  $N_v(E)$  and  $N_c(E)$  are as specified in Eqs. (5.3) and (5.4), respectively. With defects taken into account,  $N_v(E)$  and  $N_c(E)$  are as specified in Eqs. (5.5) and (5.6), respectively. The modeling parameters are set to their nominal a-Si:H values for the purposes of this analysis; recall Table 5.1.  $E_{c_T} - E_{v_T}$  and  $E_{c_T} - E_{v_D}$ , critical energies in our JDOS analysis, are clearly marked with the dashed lines and the arrows. . . . . 136

5.3	<p>The fractional contributions to the overall JDOS function associated with the various types of a-Si:H optical transitions. The contribution attributable to the VBB-CBB optical transitions is shown with the solid blue line. The contribution attributable to the VBB-CBT optical transitions is shown with the solid red line. The contribution attributable to the VBT-CBB optical transitions is shown with the solid green line. The contribution attributable to the VBT-CBT optical transitions is shown with the solid yellow line. The contribution attributable to the VBD-CBB optical transitions is shown with the solid purple line. The contribution attributable to the VBD-CBT optical transitions is shown with the solid light blue line. The contributions to the JDOS function attributable to the VBB-CBD, VBT-CBD, and VBD-CBD optical transitions are not depicted as they are found to make relatively minor contributions to the JDOS function. The modeling parameters are set to their nominal a-Si:H values for the purposes of this analysis; recall Table 5.1. <math>E_{c_T} - E_{v_T}</math> and <math>E_{c_T} - E_{v_D}</math>, critical energies in our JDOS analysis, are clearly marked with the dashed lines and the arrows. The online version is in color. . . . .</p>	138
5.4	<p>The optical absorption spectrum, <math>\alpha(\hbar\omega)</math>, associated with a-Si:H. The experimental data of Remeš [33] is depicted with the solid points; this experimental data set corresponds to the “standard GD-a” data set depicted in Figure 5.2 of Remeš [33]. The fit to this data set, determined using the modeling parameter selections specified in Table 5.2, is shown with the solid line. The fit of the lower portion of this spectrum to an exponential function, <math>\alpha_{o_D} \exp\left(\frac{\hbar\omega}{E_{o_D}}\right)</math>, is shown with the dashed line; the fit was obtained for experimental data with <math>\hbar\omega &lt; 1.4</math> eV. The dashed line corresponding to this fit has been extrapolated out to 1.45 eV so that it is observable. The determined value of <math>E_{o_D}</math> corresponding to this fit is <math>700 \pm 40</math> meV. . . . .</p>	142

# List of Abbreviations and Symbols

a-C	amorphous carbon
a-Ge	amorphous germanium
$\gamma_c$	breadth of the conduction band tail
$\gamma_v$	breadth of the valence band tail
c-Si	crystalline silicon
CBB	conduction band band
CBT	conduction band tail
$E_c$	conduction band band edge
$E_{cT}$	conduction band critical energy
$N_c(E)$	conduction band density of states function
$N_{co}$	conduction band DOS prefactor
DOS	density of states
HW	hot-wire
a-Si:H	hydrogenated amorphous silicon
$\epsilon_2(\hbar\omega)$	imaginary part of the dielectric function
$J(\hbar\omega)$	joint density of states function
JDOS	joint density of states
$\alpha, \alpha(\hbar\omega)$	optical absorption coefficient

Se	selenium
Si	silicon
$n, n(\hbar\omega)$	the refractive index
$E_v$	valence band band edge
$E_{vT}$	valence band critical energy
$N_v(E)$	valence band density of states function
$N_{vo}$	valence band DOS prefactor
VBB	valence band band
VBT	valence band tail

---

---

# CHAPTER 1

---

## Introduction

### 1.1 Introduction to disordered semiconductors

Much of the progress that has occurred in electronics over the years has arisen as a result of making the constituent electron devices within electronic systems faster, smaller, cheaper, and more reliable. These developments have occurred as a consequence of a detailed and quantitative understanding of the material properties of the materials used in the fabrication of these devices. Electron devices are fabricated from conductors, insulators, and semiconductors. While conductors and insulators have been well understood for many years, interest in the material properties of semiconductors really only found its genesis with the fabrication of the first transistor in 1947 [1, 2]; prior to that time, semiconductors were considered a laboratory curiosity. Since that time, however, there has been a considerable amount of study into the material properties of these materials. As further progress in electronics will undoubtedly require an even greater understanding of the properties of these materials, it seems likely that interest in the material properties of semiconductors will remain intense for many years to come.

While shrinking device features may be the focus of conventional electronics, there

are electron devices that require larger sizes in order to be useful. Displays [3, 4], scanners [5], solar cells [6, 7], and x-ray image detectors [8], for example, are all large area electron devices. The focus in large area electronics, as this field is now referred to as, is on substrates of the order of a square-meter [9]. This contrasts with the sub-micron device feature focus of conventional electronics. As crystalline silicon (c-Si), the material which dominates conventional electronics, can not be deposited over large areas, alternate electronic materials must be employed instead for large area electron device applications [10, 11]. Typically, the electronic materials employed for large area electronics are deposited as thin films over a substrate. Examples of such materials include hydrogenated amorphous silicon (a-Si:H), polycrystalline silicon (poly-Si), amorphous selenium (a-Se), and amorphous carbon (a-C). These materials are collectively referred to as disordered semiconductors, as the distribution of their constituent atoms does not possess the long-range order characteristic of a crystalline semiconductor.

Progress in large area electronics has occurred through advances in our understanding of the material properties of disordered semiconductors. The study of such semiconductors was initiated in the 1950s. Initially, chalcogenide semiconducting glasses [12–14], such as  $\text{As}_2\text{Se}_3$  and  $\text{GeS}_2$ , were the focus of attention; chalcogenide glasses refer to those that include the elements sulfur (S), selenium (Se), and tellurium (Te), the chalcogen elements referring to those in column VI of the periodic table. Pioneering studies into the material properties of these glasses, which are fabricated by cooling from a melt [11], allowed researchers to first probe the important role that disorder plays in shaping the electronic properties of these materials [12, 13, 15, 16]. In addition, a number of interesting device applications were implemented as a result of these studies. For example, the first xerographic copying machine was fabricated using an a-Se photoconductor [11].

Interest in amorphous silicon (a-Si) began in the 1960s. Initially, a-Si was prepared through sputtering or thermal evaporation [11]. Unfortunately, the material that was produced was of extremely poor quality. Defects, arising as a consequence of dangling bonds and vacancies, led to distributions of electronic states deep within the gap region. This rendered the material extremely difficult to dope. In addition, the disorder present made the resultant electron and hole transport very poor. In particular, the mobilities found in a-Si are orders of magnitude lower than those found for c-Si. As a result, initially at least, a-Si did not attract much attention.

Hydrogenated amorphous silicon (a-Si:H) was a late arrival in the study of disordered semiconductors [11]. It was found to exhibit much improved electronic properties when contrasted with that of its unhydrogenated counterpart. As a consequence, it is considered much more appropriate for electron device applications. This material was first fabricated in the late 1960s [11] through the use of glow discharge deposition [17]. Since that time, a variety of deposition techniques, such as hot-wire (HW), chemical vapour deposition (CVD), plasma enhanced chemical vapour deposition (PECVD), and others, have been employed in order to produce this material [18]. The improved electronic properties of a-Si:H were found to arise primarily as a consequence of the passivation of the dangling bonds with hydrogen atoms. These passivated dangling bonds do not contribute to the electronic states within the gap. As a consequence, the number of electronic states within the gap is greatly reduced for a-Si:H. This makes the material much more suitable for electron device applications.

There are a number of features associated with a-Si:H that make it a useful material for electron device applications. In particular, it can be doped [19], it exhibits a reasonable photoconductive response [11], and junctions may be readily formed [20] using a-Si:H. Using modern plasma deposition techniques, a-Si:H may be inexpensively and uniformly deposited over large substrate areas [21]. As this material is

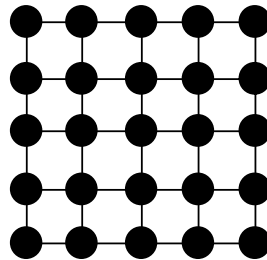
silicon based, many of the device processing techniques that have been developed for the case of c-Si can also be employed for the case of a-Si:H. Finally, the same plasma deposition technique that is used to fabricate the material itself may also be used to deposit the dielectric and passivation layers needed for the realization of actual devices [22].

## 1.2 Distribution of atoms

Crystalline silicon (c-Si) is a tetrahedrally bonded material. That is, each silicon atom within c-Si is bonded to four other nearest neighbor silicon atoms. Ideally, the bonding environment about each such atom is exactly the same as all of the other silicon atoms within the crystal. This tetrahedral structure is thus repeated periodically throughout the entire volume of the crystal. As a consequence, ideal c-Si is said to possess long-range order. A two-dimensional schematic representation of the long-range order characteristic of c-Si is shown in Figure 1.1 [23]. A defect within c-Si corresponds to any departure from this perfect order.

In amorphous silicon (a-Si), however, such long-range order is not present. While most silicon atoms within a-Si are bonded to four other silicon atoms, there are variations in the bonding environment from one silicon atom to the next. In particular, variations in the bond lengths and bond angles occur. Dangling bonds are also found, although it should be noted that dangling bonds are much rarer than their tetrahedral counterparts; within a-Si, there are typically of the order of  $10^{19}$  dangling bonds per  $\text{cm}^3$  [11] while there are of the order of  $10^{23}$  tetrahedral bonds per  $\text{cm}^3$ , i.e., there is one dangling bond for every 10,000 tetrahedral bonds in a-Si. As a result of these variations in the bond lengths and bond angles, a-Si is said to possess no long-range order. Owing to the fact that the environment around any given silicon atom is similar to that of the other silicon atoms, however, a-Si is said to possess a

crystalline  
silicon



amorphous  
silicon

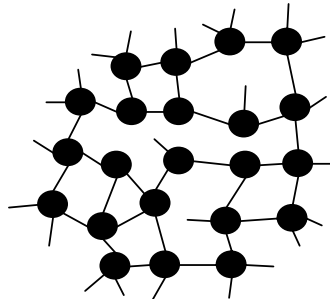


**Figure 1.1:** A schematic depiction of the distribution of silicon atoms within c-Si and a-Si. The atoms are represented by the solid circles. The bonds are represented by the solid lines. The scale of the disorder within a-Si has been exaggerated for the purposes of illustration.

form of short-range order. A two-dimensional representation of the short-range order characteristic of a-Si is also depicted in Figure 1.1 [23].

Ideal a-Si corresponds to a fully bonded tetrahedral network of silicon atoms, i.e., each silicon atom is bonded to four other silicon atoms. While such a continuous random network may be ideal for the case of a-Si, disorder is present, even within the framework of this ideal theoretical construct, i.e., variations in the bond lengths and bond angles occur, these being inherent to the amorphous state. Any departure from such an ideal network corresponds to the presence of a defect within a-Si. Vacancies and dangling bonds are examples of defects that are present within a-Si. These defects may be characterized in terms of the coordination number associated with each silicon atom, the coordination number being the number of nearest neighbor atoms associated with the atom in question. In an ideal a-Si network, all atoms are fully coordinated, i.e., the coordination number associated with each silicon atom is four. In contrast, with defects being present, variations in the coordination number of the constituent silicon atoms within a-Si are found. Such variations in the coordination number, corresponding to the specific case of a-Si, are schematically represented in Figure 1.2.

Within an a-Si network, the displacement of one silicon atom from its usual position will create dangling bonds with its four neighboring silicon atoms, each neighboring silicon atom having a dangling bond [18]. A schematic representation of silicon dangling bonds within a-Si is shown in Figure 1.3. For the case of a-Si:H, however, Si-Si bonds, Si-H bonds, and silicon dangling bonds are found. Detailed studies have found that the hydrogen atoms within a-Si:H, which are present in copious quantities during the deposition process and in the resultant a-Si:H films, bond to most of the dangling bonds that are present within a-Si; most device-quality a-Si:H films are found to have around 10 atomic % hydrogen content [11]. The density of dangling

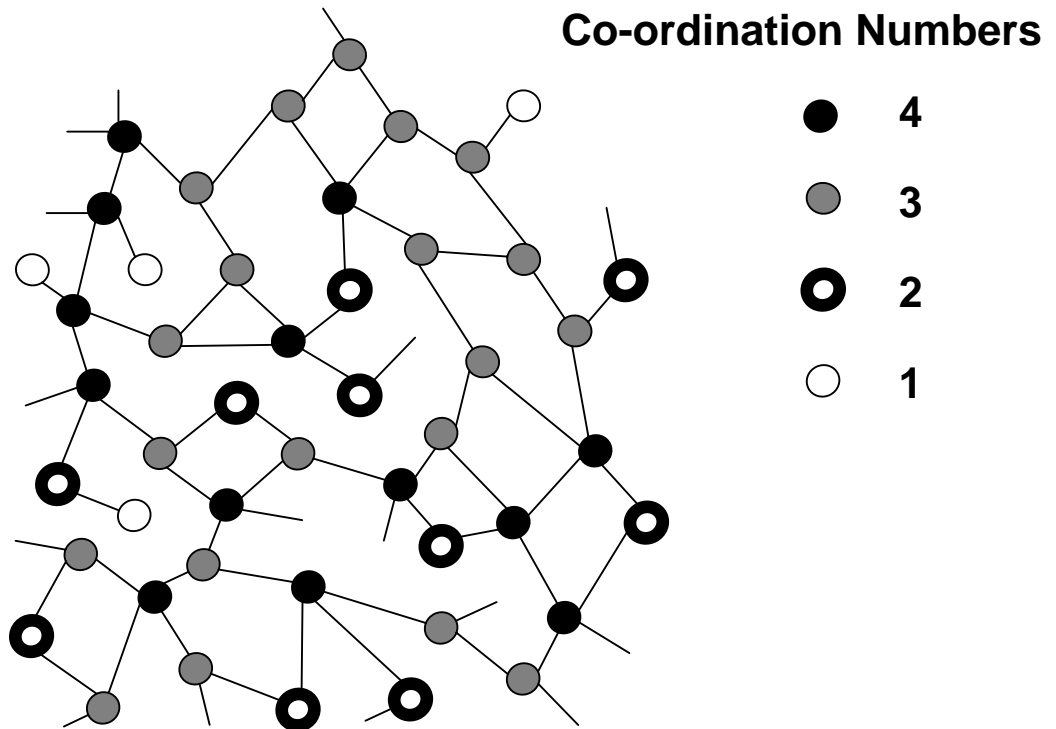


**Figure 1.2:** The coordination numbers associated each silicon atom in a representative sample of a-Si. The geometry has been exaggerated for the purposes of illustration.

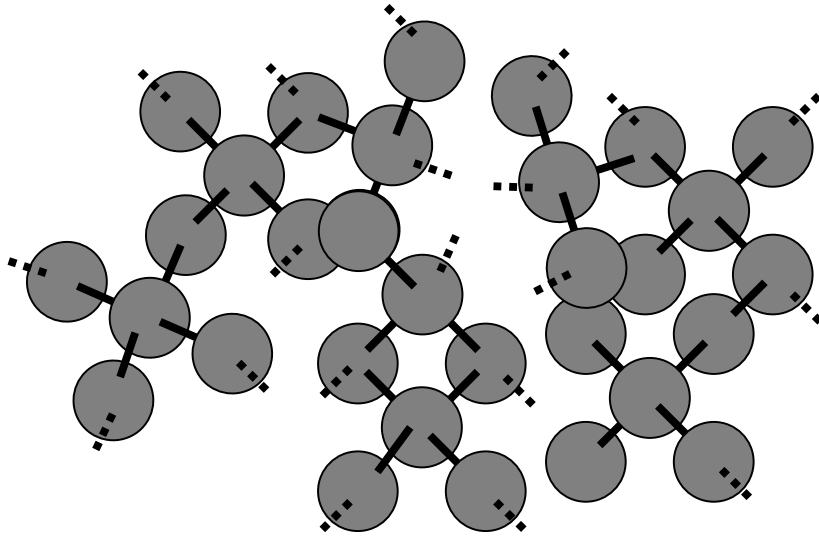


**Figure 1.3:** A schematic representation of dangling bonds within a-Si. The atoms are represented by the solid spheres. The dangling bonds are represented by the dotted lines. The Si-Si bonds are represented by the solid lines. The ratio of the dangling bonds to the Si-Si bonds within a-Si has been exaggerated for the purposes of illustration.

bonds found within a-Si:H is thus substantially reduced when contrasted with that of its unhydrogenated counterpart, a-Si; there are typically of the order of  $10^{15}$  dangling bonds per  $\text{cm}^3$  within device quality a-Si:H [11]. Many of the hydrogen atoms that are present within a-Si:H are singly coordinated with their host silicon atoms.

### 1.3 Device applications

Disordered semiconductors are employed in a variety of device applications. Early applications of disordered semiconductors include the aforementioned a-Se photoconductor based xerographic copying machine that was introduced to the market in the 1950s and the a-Si:H based photovoltaic solar cell that was introduced to the market in the 1970s. Specifically focusing on the case of a-Si:H, this being the most widely used disordered semiconductor today, current major applications for this material include displays, solar cells, thin-film opto-electronic devices, photoreceptors, sensors, light emitting diodes, x-ray imagers, and scanners [3–8]. New applications are being devised on a yearly basis.

At present, the primary use of a-Si:H is for electronic displays. These displays currently have a large market value, i.e., billions of dollars. Electronic displays are used in televisions, computers, automobiles, telecommunication systems, and biomedical systems. Each application has its own special requirements and customized optimizations must be performed with these requirements in mind. The diversity of electronic display offerings will continue to grow as new applications are developed. Variations, in terms of size, speed, power requirements, color range, brightness, contrast, and many other parameters, are being offered [24].

Solar cells is another area in which a-Si:H is finding use. Solar cells are semiconductor-based electron devices that are capable of producing electricity from solar energy through the photovoltaic effect. For large scale energy production, individual solar

cells may be connected together into an array. At present, a-Si:H based solar cells have an efficiency that ranges between 10 to 12 % [6, 7]. The solar cell panels should last for twenty or more years, with low maintenance and low environmental impact. That is, they do not produce air pollution, operate quietly, and do not interfere with the natural environment.

## 1.4 The optical response

The performance of many of the devices fabricated from disordered semiconductors depends critically on the optical properties of these materials. Light attenuates in intensity as it propagates through a material. Specifically, for monochromatic light, i.e., all photons having the same value of photon energy, the intensity of light diminishes exponentially as it passes through a material. For the case of light normally incident on a material, as shown in Figure 1.4, in the absence of any reflection, for light propagating from the left, the intensity of the light, as a function of the depth from the surface of the material,  $z$ , may be expressed as

$$I(z) = I_o \exp(-\alpha z), \quad (1.1)$$

where  $I_o$  denotes the intensity at the surface of the material,  $z = 0$ , and  $\alpha$  represents the optical absorption coefficient. This coefficient describes the rate at which this exponential attenuation occurs. A quantitative determination of this optical absorption coefficient,  $\alpha$ , for various values of photon energy, will allow for the quantitative analysis of the optical response of these materials. This in turn will allow for the quantitative prediction of the device performance of many disordered semiconductor based devices. Optimization of proposed designs may thus be considered.

The optical absorption coefficient exhibits a spectral variation. That is, the op-

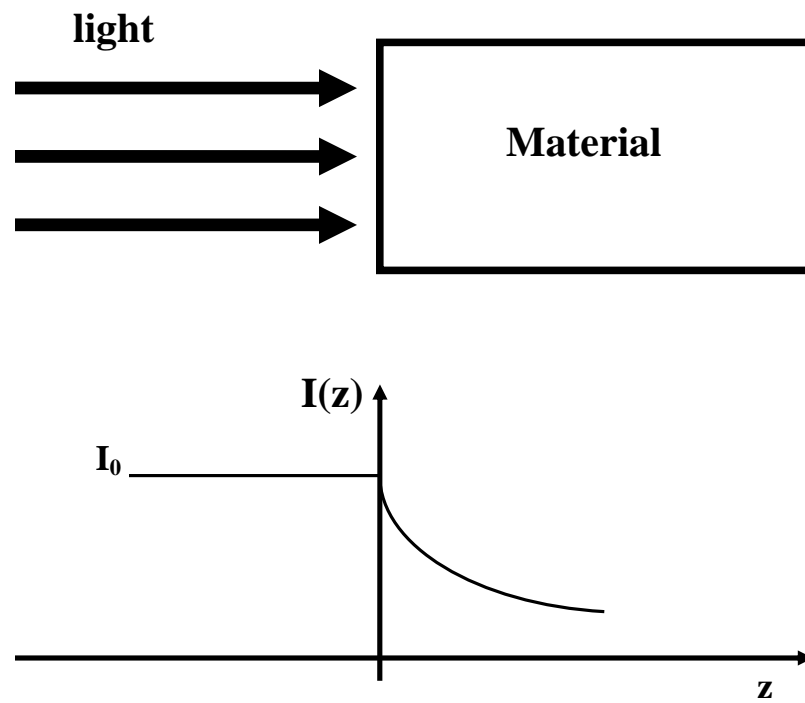


**Figure 1.4:** The intensity of light as a function of the depth,  $z$ , from the surface of the material,  $z = 0$ , for light normally incident on a material and propagating from the left, in the absence of reflection.

tical absorption coefficient,  $\alpha$ , depends on the photon energy,  $\hbar\omega$ , i.e.,  $\alpha(\hbar\omega)$ . From the spectral dependence of the optical absorption coefficient, insights into the character of these materials may be gleaned. In a disorderless crystalline semiconductor, the optical absorption spectrum terminates abruptly at the energy gap. In an amorphous semiconductor, however, the optical absorption spectrum instead encroaches into the otherwise empty gap region. In Figure 1.5, the optical absorption spectrum associated with a hypothetical crystalline semiconductor is contrasted with that of its amorphous counterpart. While the optical absorption spectrum terminates abruptly at the energy gap for the case of the hypothetical crystalline semiconductor, for the case of an amorphous semiconductor, three distinct regions are observed. The low-absorption region, i.e.,  $\alpha < 10^0 \text{ cm}^{-1}$ , denoted Region A in Figure 1.5, exhibits a broad exponential dependence that encroaches deeply into the otherwise empty gap region. The mid-absorption region, i.e.,  $10^0 \text{ cm}^{-1} < \alpha < 10^4 \text{ cm}^{-1}$ , Region B in Figure 1.5, exhibits a sharp exponential increase corresponding to increased photon energies, its breadth being much narrower than that exhibited by Region A. This region is often referred to as the Urbach tail region, its breadth being referred to as the Urbach tail breadth. It plays an important role in the physics of amorphous semiconductors, and has been the focus of a considerable amount of analysis. Finally, the high-absorption region, i.e.,  $\alpha > 10^4 \text{ cm}^{-1}$ , denoted Region C in Figure 1.5, exhibits an algebraic functional dependence.

This thesis aims to develop models that will allow for the quantitative analysis of the spectral dependence of the optical absorption coefficient,  $\alpha(\hbar\omega)$ , associated with a-Si:H. These models will stem from empirical models for the distributions of electronic states, these distribution of electronic states models being rooted in a-Si:H phenomenology. The ultimate aim of this analysis is to provide a framework for the critical comparative analysis of disparate a-Si:H optical spectra, that will allow for

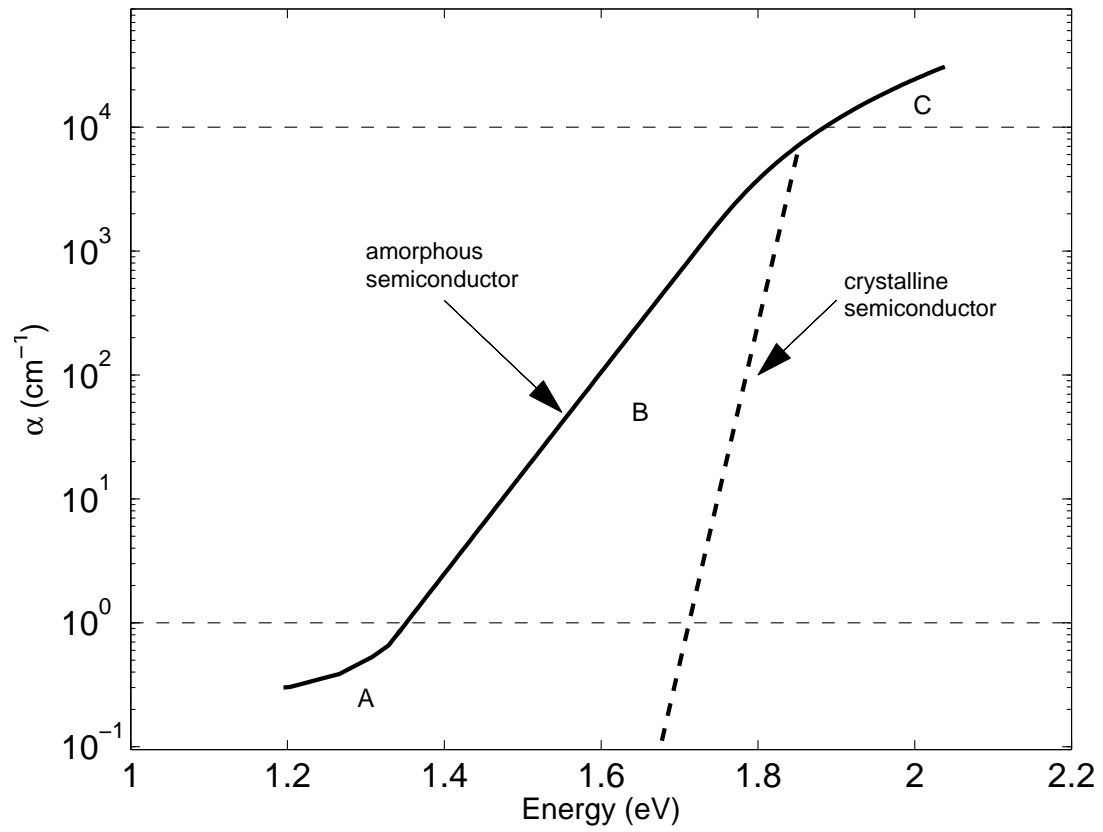


**Figure 1.5:** The spectral dependence of the optical absorption coefficient,  $\alpha(\hbar\omega)$ , associated with hypothetical crystalline and amorphous semiconductors.

the identification of general trends in these spectra. From the insights gleaned from this study, greater understanding into the material properties of this semiconductor will be obtained. These insights could be used in order to improve the performance of future generations of a-Si:H based devices.

## 1.5 Distributions of electronic states

The disorder present within a-Si and a-Si:H has a profound impact on the distributions of electronic states. Accordingly, the electronic properties associated with these materials are somewhat distinct from those exhibited by c-Si [11]. In a disorderless material, these distributions terminate abruptly at the valence band and conduction band band edges. This leads to a well defined energy gap that separates the distribution of electronic states associated with the valence band from that associated with the conduction band. In contrast, in a-Si and a-Si:H, distributions of electronic states encroach into the otherwise empty gap region. These tail states, as the encroaching distributions of electronic states are often referred to as, are associated with the intrinsic disorder associated with a-Si and a-Si:H, i.e., the unavoidable variations in the bond lengths and bond angles. Defects, i.e., dangling bonds and vacancies, are responsible for states deeper in the gap region. A schematic representation of these distributions of electronic states is depicted in Figure 1.6.

Detailed analyzes have demonstrated that some of the electronic states associated with the tail states are actually localized by the disorder. That is, the wavefunctions associated with such states are confined to a small volume rather than extending throughout the entire volume of the material; all the wavefunctions associated with ideal (disorderless) crystalline semiconductors extend throughout the entire volume of the material. A comparison of the wavefunctions associated with localized and extended electronic states is depicted in Figure 1.7 [25]. Further studies have demon-

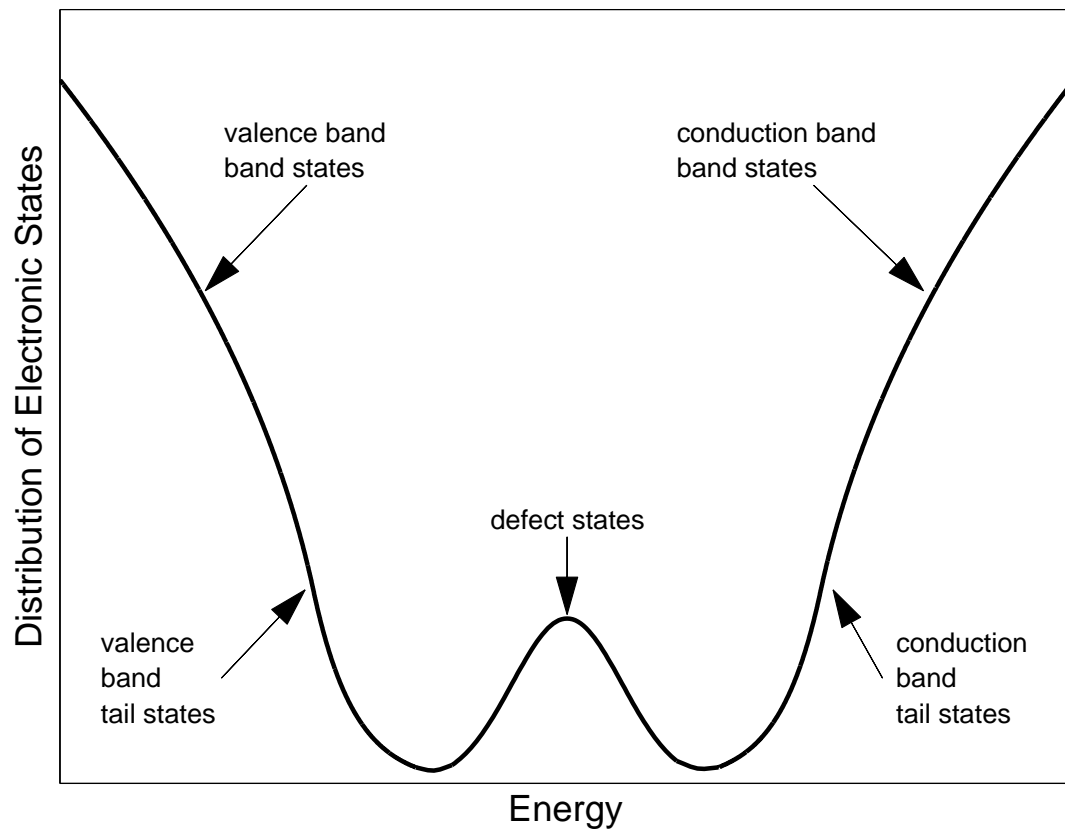


**Figure 1.6:** A schematic representation of the distributions of electronic states associated with a hypothetical amorphous semiconductor.

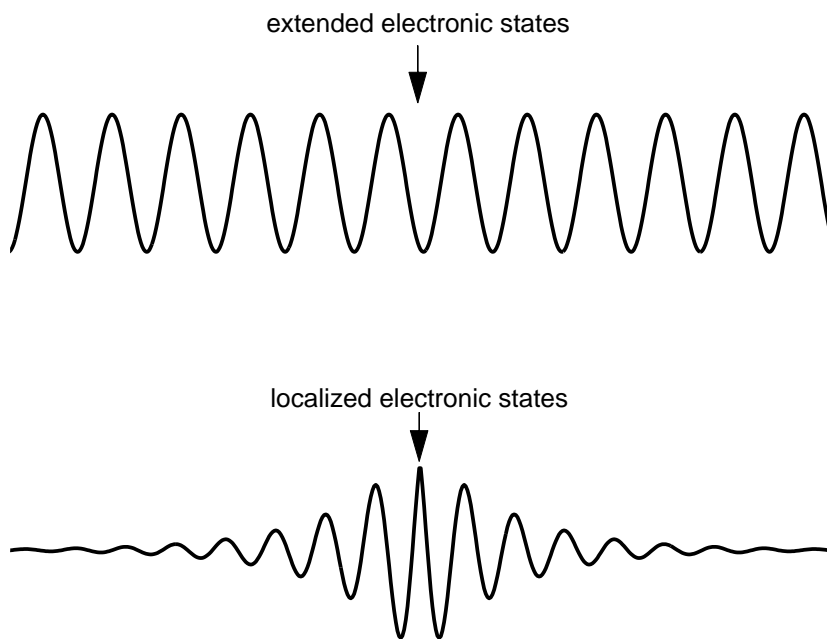


**Figure 1.7:** A schematic representation of the wavefunctions associated with localized and extended electronic states. This figure is taken after Morigaki [25].

strated that there exist critical energies, termed mobility edges, which separate the localized electronic states from their extended counterparts, one associated with the valence band, the other associated with the conduction band. That is, there is a mobility edge associated with the valence band that separates the localized valence band electronic states from their extended counterparts. Similarly, there is a mobility edge associated with the conduction band that separates the localized conduction band electronic states from their extended counterparts. These mobility edges are depicted in Figure 1.8. The difference in energy between these mobility edges is referred to as the mobility gap.

In the study of crystalline semiconductors, the periodicity inherent to the distribution of atoms allows for the quantitative determination of the energy levels of the electronic states in terms of the electron wave-vector,  $\vec{k}$ . The distributions of electronic states that result may thus be characterized in terms of a band diagram that specifies how the electronic energy levels vary with  $\vec{k}$ . In the case of a disordered semiconductor, however, such as a-Si and a-Si:H, the disorder renders  $\vec{k}$  a poor quantum number. As a result, band diagrams can not be used for the analysis of these materials. Nevertheless, as it is the nearest neighbor environment that primarily determines the electronic character of a material, it seems reasonable to expect the existence of bands within a-Si and a-Si:H, of similar shape and character to those found within c-Si. As a consequence, it is expected that many of the properties found for a-Si and a-Si:H are similar to those exhibited by c-Si.

In order to provide a quantitative framework for the determination of the properties associated with disordered semiconductors, an alternate approach to the band diagrams used for the analysis of crystalline semiconductors must be sought. It is found that the distributions of electronic states associated with these materials may be quantitatively characterized through the valence band and conduction band density of

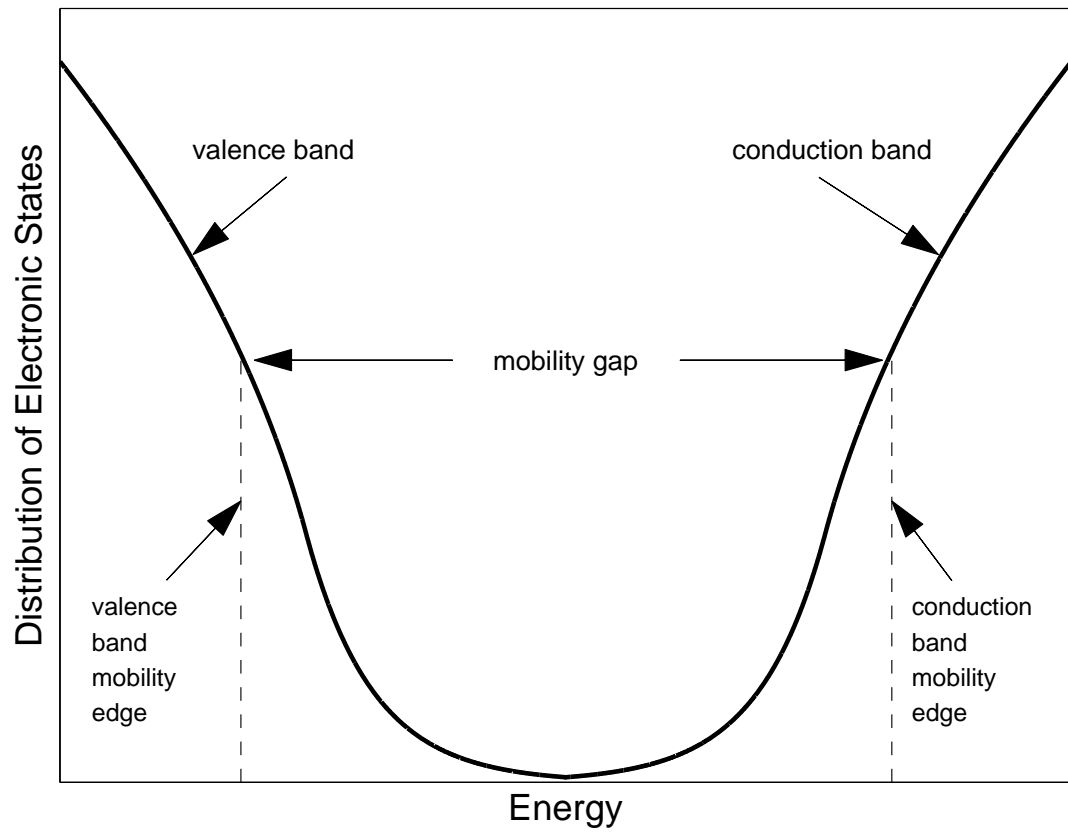


**Figure 1.8:** The distributions of electronic states associated with a hypothetical amorphous semiconductor. The conduction band and valence band mobility edges are depicted with the dashed lines. The defect states have been neglected.

states (DOS) functions,  $N_v(E)$  and  $N_c(E)$ , respectively,  $N_v(E) \Delta E$  and  $N_c(E) \Delta E$  representing the number of valence band and conduction band electronic states, per unit volume, between energies  $[E, E + \Delta E]$ . This means of characterizing the corresponding distributions of electronic states may be employed both for crystalline semiconductors and their amorphous counterparts.

## 1.6 Relation between the optical absorption spectrum and the DOS functions

For the specific case of a-Si:H, Jackson *et al.* [26] developed a relationship between the spectral dependence of the imaginary part of the dielectric function,  $\epsilon_2(\hbar\omega)$ , and the valence band and conduction band DOS functions,  $N_v(E)$  and  $N_c(E)$ , respectively. This relationship is key to the analysis presented in this thesis. Accordingly, a review of the analysis of Jackson *et al.* [26], relating  $\epsilon_2(\hbar\omega)$  with  $N_v(E)$  and  $N_c(E)$ , is presented in this section. The application of this relationship to the interpretation of the optical properties associated with a-Si:H will be presented later in the thesis.

Jackson *et al.* [26] employ a linear response approach within the framework of a one-electron formalism, i.e., many electron effects are neglected. Assuming zero-temperature statistics, i.e., that all valence band states are completely filled and that all conduction band states are completely empty, Jackson *et al.* [26] contend that

$$\epsilon_2(\hbar\omega) = (2\pi q)^2 \frac{2}{V} \sum_{v,c} |\vec{\eta} \cdot \vec{R}_{v,c}|^2 \delta(E_c - E_v - \hbar\omega), \quad (1.2)$$

where  $q$  is the electron charge,  $V$  is the illuminated volume,  $\vec{\eta}$  is the polarization vector, and  $\vec{R}_{v,c} = \langle c | \vec{r} | v \rangle$  is the dipole matrix element associated with the valence band and conduction band electronic states,  $|v\rangle$  and  $|c\rangle$ , respectively, the sum in Eq. (1.2) being taken over all the single-spin states of the valence band and conduction

band; as this expression for  $\epsilon_2(\hbar\omega)$  is expressed in terms of the dipole matrix elements, the general approach adopted by Jackson *et al.* [26] is referred to as a dipole operator based formalism. For unpolarized light, on average,  $|\vec{\eta} \cdot \vec{R}_{v,c}|^2$  reduces to  $\frac{|R_{v,c}|^2}{3}$ , where  $|R_{v,c}|$  denotes the amplitude of the dipole matrix element. Accordingly, Eq. (1.2) reduces to

$$\epsilon_2(\hbar\omega) = (2\pi q)^2 \frac{2}{3V} \sum_{v,c} |R_{v,c}|^2 \delta(E_c - E_v - \hbar\omega). \quad (1.3)$$

Defining the average squared dipole matrix element

$$[R'(\hbar\omega)]^2 \equiv \frac{\sum_{v,c} |R_{v,c}|^2 \delta(E_c - E_v - \hbar\omega)}{\sum_{v,c} \delta(E_c - E_v - \hbar\omega)}, \quad (1.4)$$

Jackson *et al.* [26] conclude that

$$\epsilon_2(\hbar\omega) = (2\pi q)^2 \frac{2}{3V} [R'(\hbar\omega)]^2 \sum_{v,c} \delta(E_c - E_v - \hbar\omega). \quad (1.5)$$

Thus far, the expression for  $\epsilon_2(\hbar\omega)$  that has been derived, i.e., Eq. (1.5), applies equally to both c-Si and a-Si:H. In order to facilitate a direct comparison between the spectral dependencies of  $[R'(\hbar\omega)]^2$  associated with these two distinct materials, it would seem reasonable that this matrix element should be normalized by the number of optical transitions corresponding to each material. The number of optical transitions from any given single-spin state in the valence band, associated with a-Si:H and c-Si, are shown in Figure 1.9. In a-Si:H, the number of optical transitions from any given single-spin state in the valence band is  $2\rho_A V$ ,  $\rho_A$  denoting the density of silicon atoms within a-Si:H. In contrast, for the case of c-Si, the number of optical transitions from any given single-spin state in the valence band is four; all of these optical transitions conserve  $\vec{k}$ . Clearly, the number of optical transitions that can

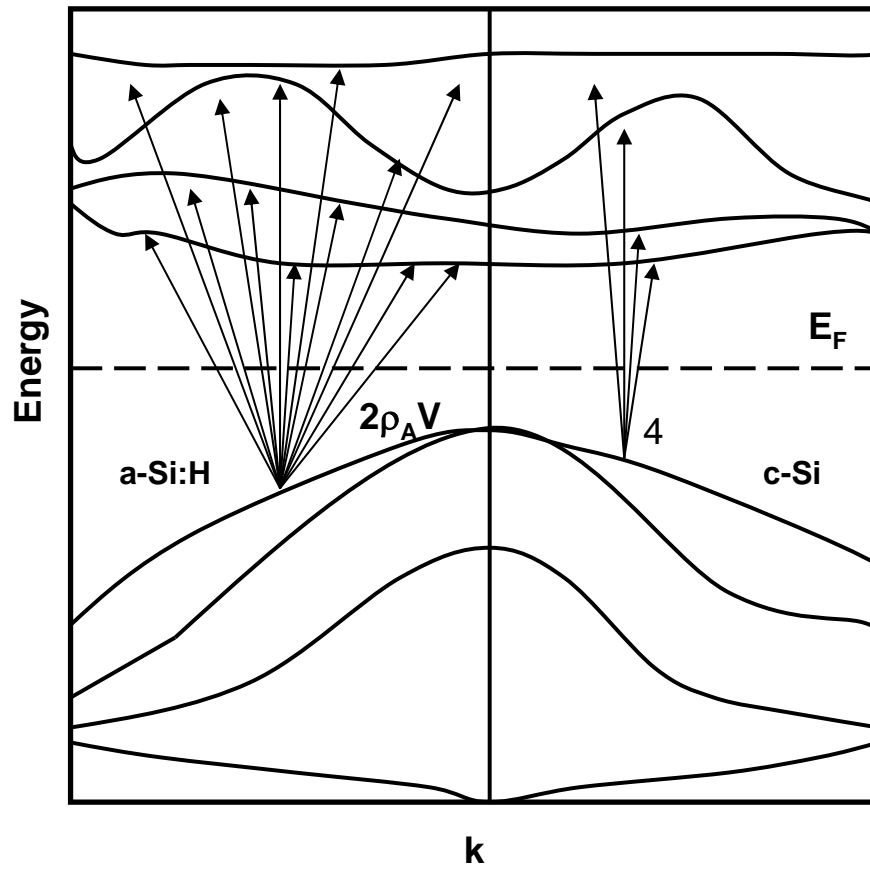


**Figure 1.9:** The number of optical transitions allowed from a single-spin state in the valence band for the cases of c-Si and a-Si:H. For the case of a-Si:H, there are  $2\rho_A V$  possible optical transitions, since there is no momentum conservation. However, for the case of c-Si, there are only four possible optical transitions. The figure is taken after Jackson *et al.* [26]

occur from any given single-spin state in the valence band associated with a-Si:H is greater than that associated with c-Si, and thus, it might be expected that the dipole matrix elements associated with these transitions are of a lesser magnitude than those associated with c-Si. Thus, a normalized average squared dipole matrix element,

$$\mathcal{R}^2(\hbar\omega) \equiv [R'(\hbar\omega)]^2 \left( \frac{2\rho_A V}{4} \right), \quad (1.6)$$

is introduced, this matrix element being normalized by the ratio of the number of optical transitions allowed for the case of a-Si:H with respect to that allowed for the case of c-Si. Accordingly, Eq. (1.5) reduces to

$$\epsilon_2(\hbar\omega) = (2\pi q)^2 \frac{1}{3\rho_A} \mathcal{R}^2(\hbar\omega) \frac{4}{V^2} \sum_{v,c} \delta(E_c - E_v - \hbar\omega). \quad (1.7)$$

From the definition of a single-spin state, it may be seen that

$$N_v(E) = \frac{2}{V} \sum_v \delta(E - E_v), \quad (1.8)$$

and

$$N_c(E) = \frac{2}{V} \sum_c \delta(E - E_c). \quad (1.9)$$

By introducing the joint density of states (JDOS) function

$$J(\hbar\omega) \equiv \int_{-\infty}^{\infty} N_v(E) N_c(E + \hbar\omega), \quad (1.10)$$

from Eqs. (1.8) and (1.9), it can be shown that

$$J(\hbar\omega) = \frac{4}{V^2} \sum_{v,c} \delta(E_c - E_v - \hbar\omega). \quad (1.11)$$

Thus, using Eq. (1.11), Eq. (1.7) may be represented as

$$\epsilon_2(\hbar\omega) = (2\pi q)^2 \frac{1}{3\rho_A} \mathcal{R}^2(\hbar\omega) J(\hbar\omega). \quad (1.12)$$

For the specific case of a-Si:H, where  $\rho_A$  is roughly  $5 \times 10^{22}$  per  $\text{cm}^{-3}$ , Eq. (1.12) may be simply expressed as

$$\epsilon_2(\hbar\omega) = 4.3 \times 10^{-45} \mathcal{R}^2(\hbar\omega) J(\hbar\omega), \quad (1.13)$$

where  $\mathcal{R}^2(\hbar\omega)$  is in units of  $\text{\AA}^2$  and  $J(\hbar\omega)$  is in units of  $\text{states}^2 \text{eV}^{-1} \text{cm}^{-6}$ . It is upon this expression that the subsequent analysis is built.

The spectral dependence of the optical absorption coefficient,  $\alpha(\hbar\omega)$ , may be determined by noting that

$$\alpha(\hbar\omega) = \frac{\omega}{n(\hbar\omega)c} \epsilon_2(\hbar\omega), \quad (1.14)$$

where  $n(\hbar\omega)$  denotes the spectral dependence of the refractive index and  $c$  represents the speed of light in a vacuum. For the purposes of this analysis, the spectral dependence of  $n(\hbar\omega)$  is determined by fitting a tenth-order polynomial to the experimental data of Klazes *et al.* [27]; the original experimental data is depicted in Figure 4 of Klazes *et al.* [27]. The resultant fit, and the original experimental data, are depicted in Figure 1.10. This fit is only valid over the range of the experimental data of Klazes *et al.* [27], i.e., for  $0.77 \text{ eV} < \hbar\omega < 3.2 \text{ eV}$ .

## 1.7 Free electron density of states

In light of the important role that the form of the valence band and conduction band DOS functions,  $N_v(E)$  and  $N_c(E)$ , respectively, play in determining the form

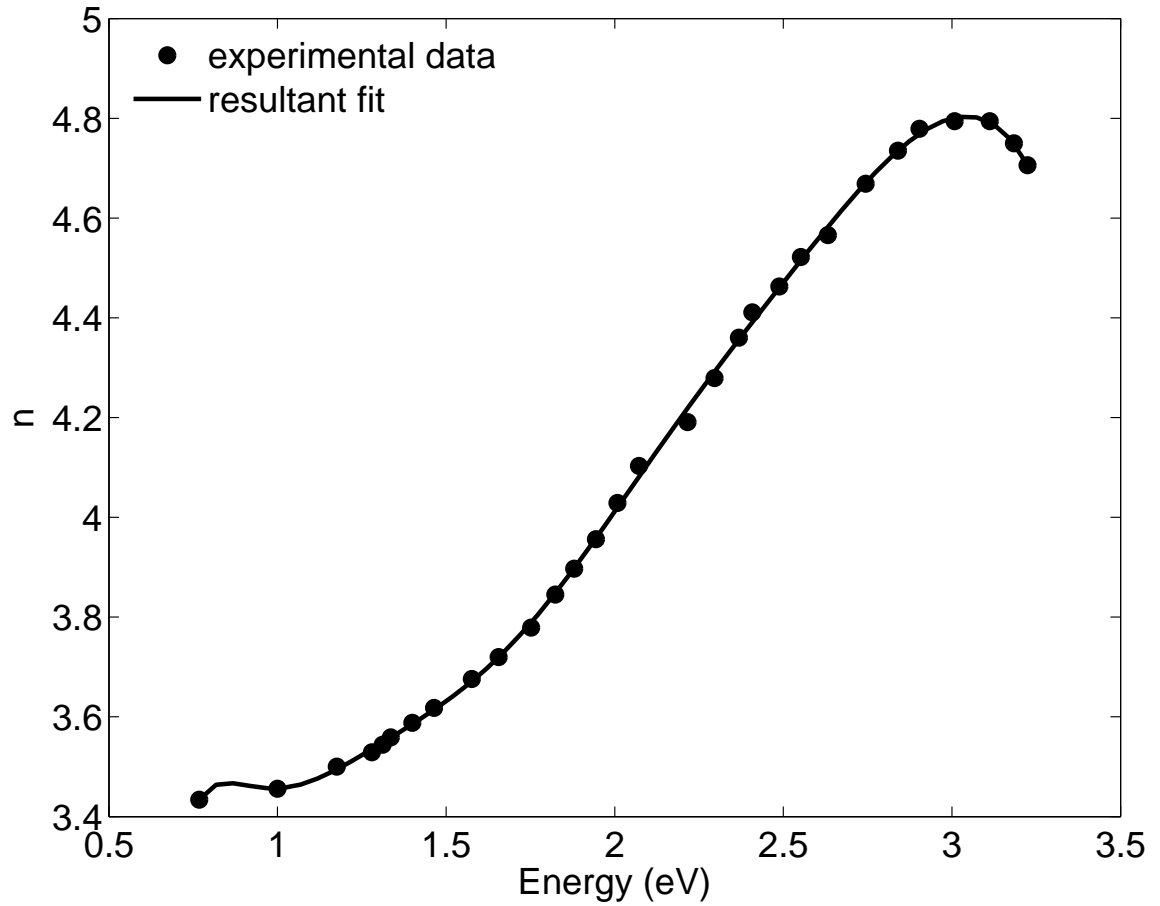


**Figure 1.10:** The spectral dependence of the refractive index associated with a-Si:H. The tenth-order polynomial fit is depicted with the solid line. The experimental data points of Klazes *et al.* [27] are represented with the solid points.

of the optical absorption spectra, it is obvious that they must be determined in order for this analysis to proceed. It is instructive to consider the form of the density of states for the free electron case. Consider an electron confined within a cubic volume, of dimensions  $L \times L \times L$ , surrounded by infinite potential barriers; see Figure 1.11. According to quantum mechanics, in steady-state, the wavefunctions associated with this electron may be described by Schrödinger's equation, i.e.,

$$-\frac{\hbar^2}{2m} \nabla^2 \Psi(\vec{r}) + V(\vec{r}) \Psi(\vec{r}) = E \Psi(\vec{r}), \quad (1.15)$$

where  $\hbar$  denotes the reduced Planck's constant,  $m$  represents the mass of the electron,  $V(\vec{r})$  is the potential energy, and  $E$  is the electron energy; in three-dimensions,  $\nabla^2$  represents the mathematical operator  $\frac{\partial^2}{\partial x^2} + \frac{\partial^2}{\partial y^2} + \frac{\partial^2}{\partial z^2}$ . If the electron is free within the cubic volume, i.e.,  $V(\vec{r}) = 0$  for  $0 \leq x \leq L$ ,  $0 \leq y \leq L$ , and  $0 \leq z \leq L$ , and if the potential is infinite elsewhere, then it may be shown that

$$\Psi(\vec{r}) = \Psi_{n_x, n_y, n_z}(x, y, z) = \left(\frac{2}{L}\right)^{3/2} \sin\left(\frac{\pi n_x}{L} x\right) \sin\left(\frac{\pi n_y}{L} y\right) \sin\left(\frac{\pi n_z}{L} z\right), \quad (1.16)$$

where  $n_x$ ,  $n_y$ , and  $n_z$  denote the quantum numbers, i.e., positive integers, associated with electron motion in the  $x$ ,  $y$ , and  $z$  directions, respectively. It should be noted that on account of the electron spin, there are actually two electronic states associated with each unique selection of  $n_x$ ,  $n_y$ , and  $n_z$ .

Substituting the solution for the wavefunction, i.e., Eq. (1.16), back into Schrödinger's equation, it is seen that

$$E_{n_x, n_y, n_z} = \frac{\hbar^2}{2m} \left[ \left(\frac{\pi n_x}{L}\right)^2 + \left(\frac{\pi n_y}{L}\right)^2 + \left(\frac{\pi n_z}{L}\right)^2 \right], \quad (1.17)$$

where  $E_{n_x, n_y, n_z}$  denotes the energy level corresponding to the wavefunction,  $\Psi_{n_x, n_y, n_z}(x, y, z)$ .

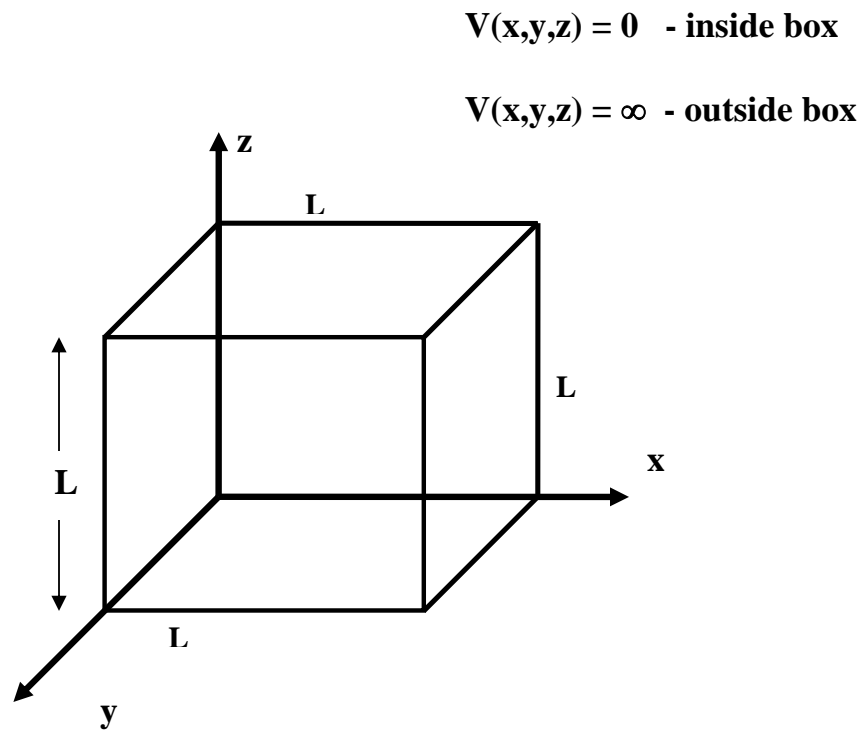


**Figure 1.11:** The representation of an electron confined within a cubic volume, of dimensions,  $L \times L \times L$ , surrounded by infinite potential barriers.

If one was to consider each unique combination of quantum numbers,  $n_x$ ,  $n_y$ , and  $n_z$ , as a unique point in a constellation of such points in the first octet of three-dimensional  $n$ -space, such as that shown in Figure 1.12, for sufficiently high energies, i.e., when the granularity of these points becomes a continuum, it is seen that the radial quantum number, i.e., the radius within which all selections of  $n_x$ ,  $n_y$ , and  $n_z$ , yield energies less than or equal to  $E$ ,

$$\tilde{n}(E) = \sqrt{\frac{2mL^2E}{\hbar^2\pi^2}}. \quad (1.18)$$

Thus, the number of electronic states, per unit volume, up to and including energy  $E$ , may be expressed as an integral over the DOS function, i.e.,

$$\int_{-\infty}^E N(u) du = 2 \left( \frac{4\pi}{3} \right) \frac{1}{8} \frac{1}{L^3} \tilde{n}(E)^3, \quad (1.19)$$

where the factor of two refers to the two spin levels per unique selection of  $n_x$ ,  $n_y$ , and  $n_z$ , the factor of  $\frac{4\pi}{3}$  denotes the prefactor for a spherical volume, the factor of eight in the denominator corresponding to the fact the  $n_x$ ,  $n_y$ , and  $n_z$  integers only occupy the first octet of three-dimensional  $n$ -space, and the factor of  $L^3$  represents the fact that this is defined on a per unit volume basis; there is a unity density of points in the first octet of three-dimensional  $n$ -space. Differentiation of Eq. (1.19) yields

$$N(E) = \frac{\sqrt{2}m^{3/2}}{\pi^2\hbar^3} \sqrt{E}. \quad (1.20)$$

It is seen that this DOS function has no dependence on  $L$ . That is, when the electron becomes completely free, i.e., when  $L \rightarrow \infty$ , the DOS function is exactly the same. This square-root DOS function, also known as the free-electron DOS, will form the cornerstone of the subsequent analysis.

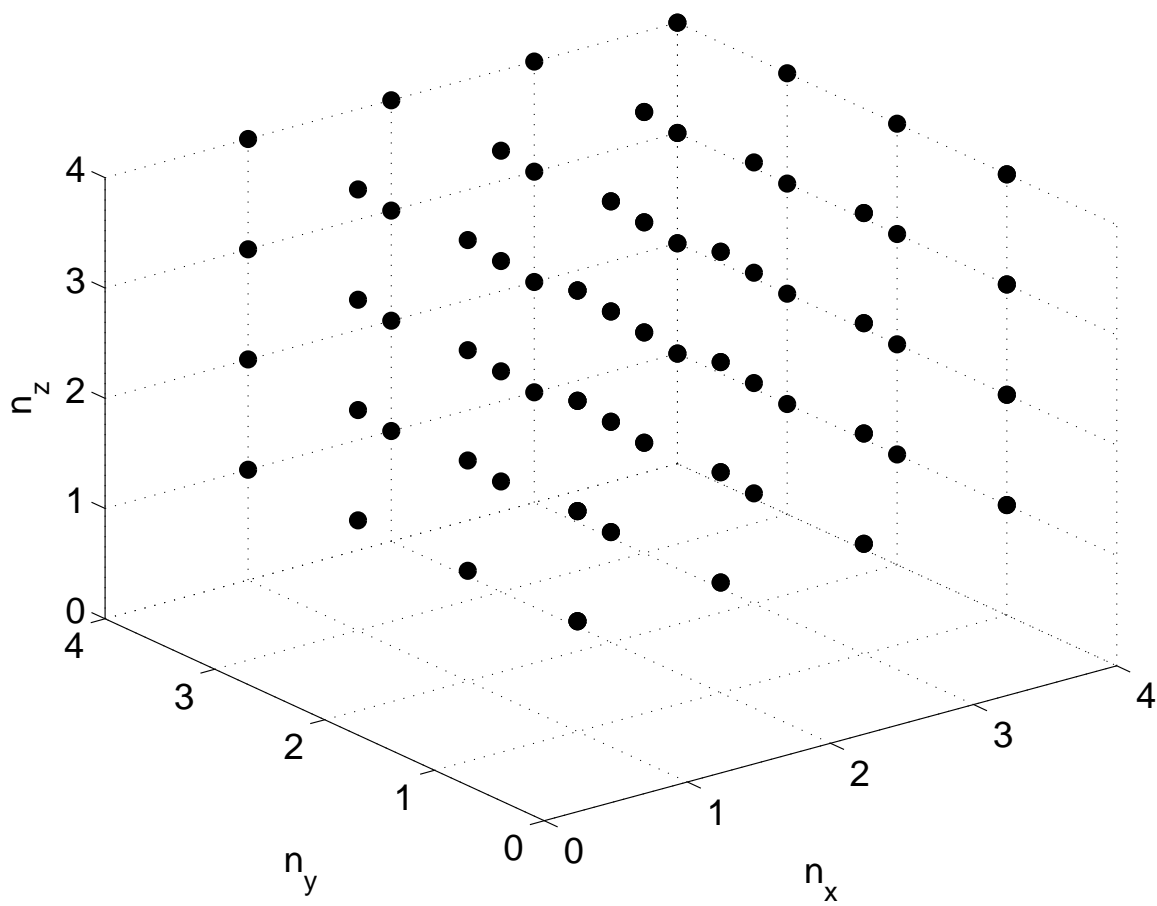


**Figure 1.12:** The quantum numbers,  $n_x$ ,  $n_y$ , and  $n_z$ , shown in the first octet of three-dimensional  $n$ -space. The density of such points is unity.

## 1.8 A review of empirical density of states models

The exact form of the DOS functions associated with disordered semiconductors remains the focus of considerable debate. There are fundamental questions related to the nature of the band states and the tail states associated with each band. In addition, the form of the defect states remains unknown. In fact, despite many years of study, the exact role that disorder plays in shaping these DOS functions remains unknown. Even for the case of a-Si:H, the most well studied disordered semiconductor, the band tailing that occurs has been attributed both to disorder [28] and to the presence of hydrogen atoms [29]. As a consequence, a specification for the DOS functions,  $N_v(E)$  and  $N_c(E)$ , that stems directly from first-principles, would likely be too complex in order to allow for insights into the material properties of these semiconductors to be gleaned.

For the purposes of materials characterization, and in order to predict device performance, a number of empirical models for the valence band and conduction band DOS functions,  $N_v(E)$  and  $N_c(E)$ , respectively, associated with disordered semiconductors, have been devised. These models provide an elementary means whereby the properties associated with disordered semiconductors may be determined. Most empirical DOS models are built upon disordered semiconductor phenomenology. A brief review of the empirical DOS models that have been developed for the analysis of the optical properties of disordered semiconductors is provided next.

In 1966, Tauc *et al.* [30] introduced an empirical model for the valence band and conduction band DOS functions. Tauc *et al.* [30] assumed the free electron DOS model, i.e., Eq. (1.20), for both the valence band and conduction band DOS functions.

That is, Tauc *et al.* [30] assumed that

$$N_v(E) = \begin{cases} 0, & E > E_v \\ N_{vo}\sqrt{E_v - E}, & E \leq E_v \end{cases}, \quad (1.21)$$

and

$$N_c(E) = \begin{cases} N_{co}\sqrt{E - E_c}, & E \geq E_c \\ 0, & E < E_c \end{cases}, \quad (1.22)$$

where  $N_{vo}$  and  $N_{co}$  denote the valence band and conduction band DOS prefactors, respectively,  $E_v$  and  $E_c$  representing the valence band and conduction band band edges. This model for the DOS functions associated with a disordered semiconductor, i.e., Eqs. (1.21) and (1.22), forms the basis for the most common interpretation for the determination of the energy gap associated with such semiconductors. The resultant DOS functions, for the nominal selection of DOS modeling parameters tabulated in Table 1.1, are depicted in Figure 1.13. The use of this model in determining the energy gap associated with a disordered semiconductor is further discussed in the literature.

In 1981, Chen *et al.* [31] improved on the empirical DOS model of Tauc *et al.* [30] by grafting an exponential distribution of valence band tail states onto the square-root distribution of valence band band states, the conduction band DOS function,  $N_c(E)$ , being exactly the same as that assumed by Tauc *et al.* [30]. In particular,

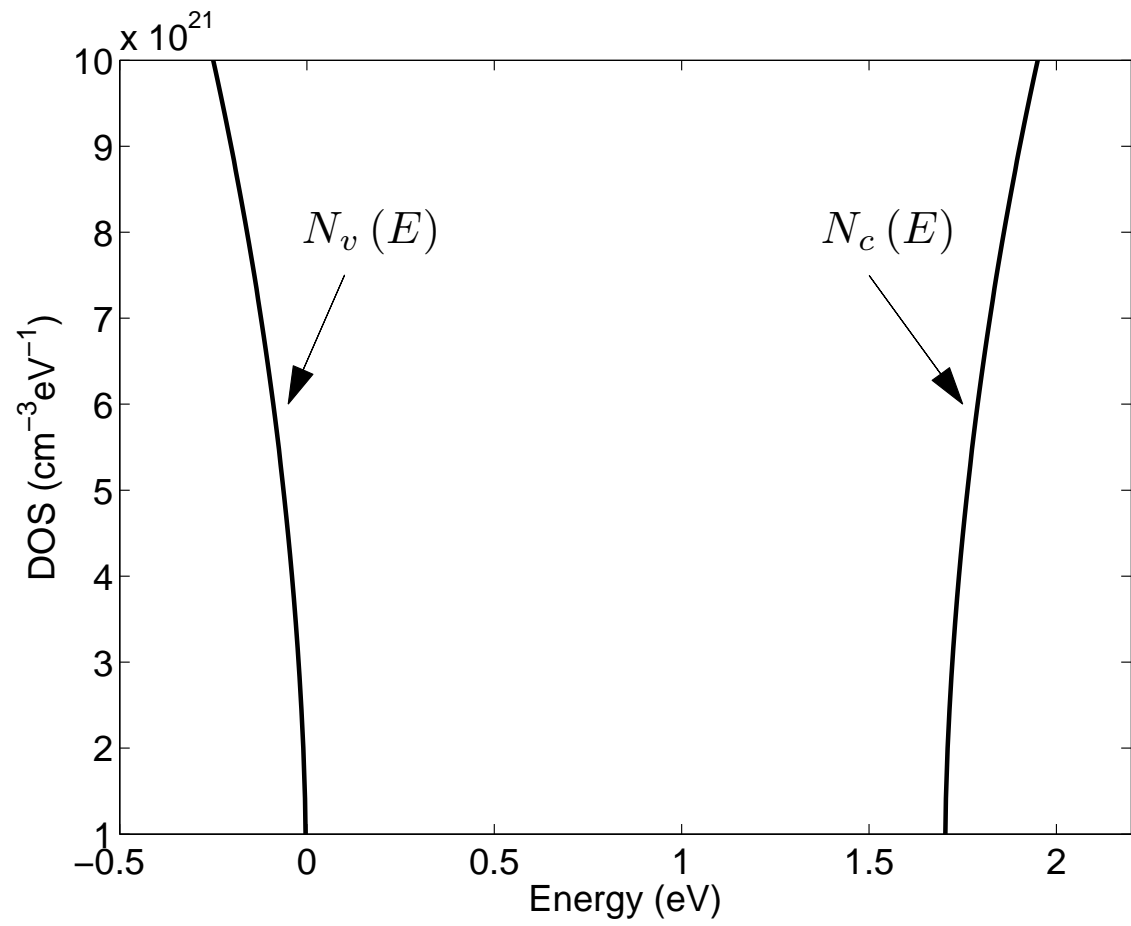


**Figure 1.13:** The empirical DOS model of Tauc *et al.* [30].

**Table 1.1:** The nominal DOS modeling parameter selections employed for the empirical DOS models described in this section. These modeling parameters are representative of a-Si:H.

Parameter (units)	Tauc <i>et al.</i> [30]	Chen <i>et al.</i> [31]	Redfield [32]	Cody [33]	O’Leary <i>et al.</i> [34]
$N_{vo}$ ( $\text{cm}^{-3}\text{eV}^{-3/2}$ )	$2 \times 10^{22}$	$2 \times 10^{22}$	-	$2 \times 10^{22}$	$2 \times 10^{22}$
$N_{co}$ ( $\text{cm}^{-3}\text{eV}^{-3/2}$ )	$2 \times 10^{22}$	$2 \times 10^{22}$	-	$2 \times 10^{22}$	$2 \times 10^{22}$
$N_{vo}^*$ ( $\text{cm}^{-3}\text{eV}^{-3/2}$ )	-	$5 \times 10^{21}$	$5 \times 10^{21}$	-	-
$N_{co}^*$ ( $\text{cm}^{-3}\text{eV}^{-3/2}$ )	-	-	$5 \times 10^{21}$	-	-
$E_v$ (eV)	0.0	0.0	0.0	0.0	0.0
$E_c$ (eV)	1.7	1.7	1.7	1.7	1.7
$E_v - E_{vT}$ (meV)	-	-	-	-	25
$E_{cT} - E_c$ (meV)	-	-	-	-	13.5
$\gamma_v$ (meV)	-	50	50	50	50
$\gamma_c$ (meV)	-	-	27	-	27

Chen *et al.* [31] assumed that

$$N_v(E) = \begin{cases} N_{vo}^* \exp\left(\frac{E_v - E}{\gamma_v}\right), & E > E_v \\ N_{vo} \sqrt{E_v - E}, & E \leq E_v \end{cases}, \quad (1.23)$$

and

$$N_c(E) = \begin{cases} N_{co} \sqrt{E - E_c}, & E \geq E_c \\ 0, & E < E_c \end{cases}, \quad (1.24)$$

where  $N_{vo}^*$  denotes the valence band tail DOS prefactor and  $\gamma_v$  represents the valence band tail breadth,  $N_{vo}$ ,  $N_{co}$ ,  $E_v$ , and  $E_c$  being as defined earlier. The resultant DOS functions, for the nominal selection of DOS modeling parameters tabulated in Table 1.1, are depicted in Figure 1.14.

In an effort to understand how the valence band tail states and the conduction band tail states influence the resultant optical properties, in 1982 Redfield [32] in-

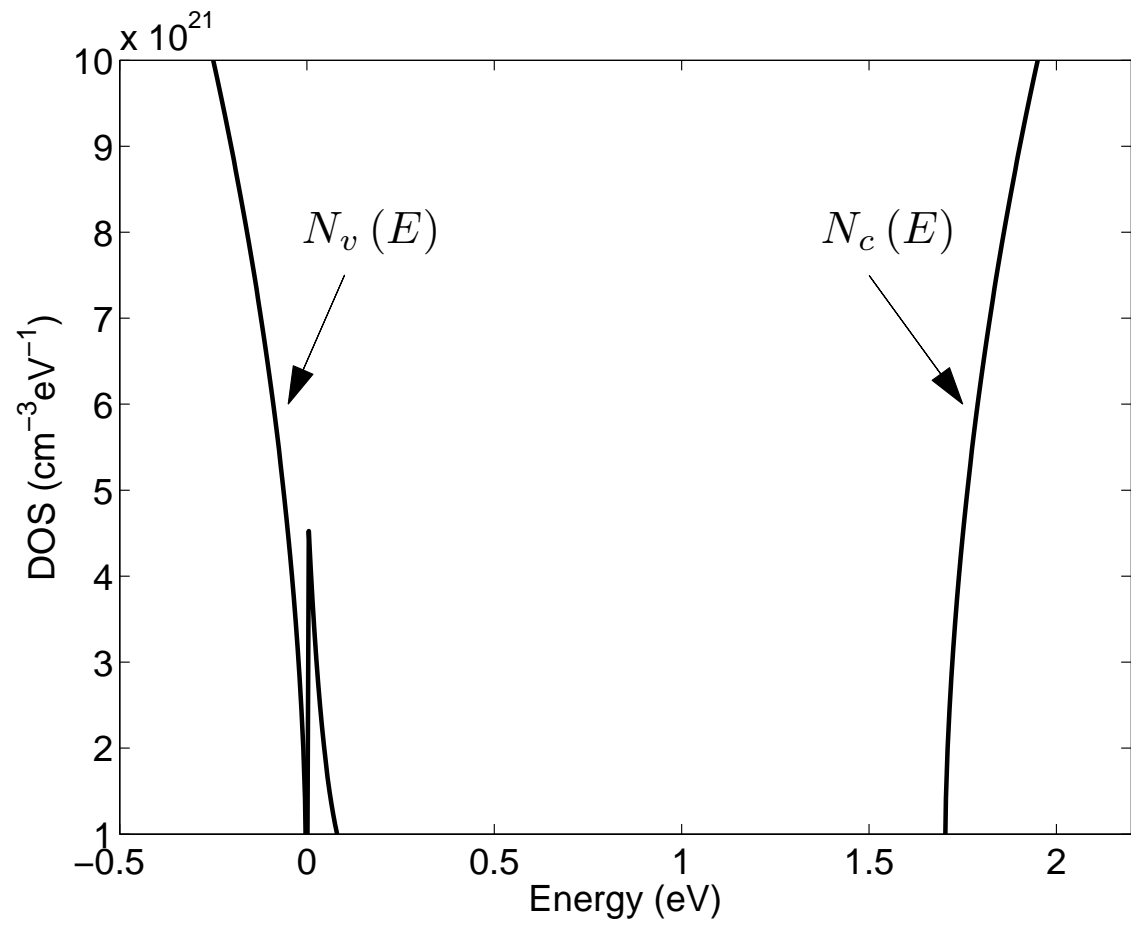


**Figure 1.14:** The empirical DOS model of Chen *et al.* [31].

roduced an alternate empirical DOS model that includes both exponential valence band tail states and exponential conduction band tail states. Redfield [32], however, assumes flat distributions of valence band band states and conduction band band states. That is, Redfield [32] assumes that

$$N_v(E) = \begin{cases} N_{vo}^* \exp\left(\frac{E_v - E}{\gamma_v}\right), & E > E_v \\ N_{vo}^*, & E \leq E_v \end{cases}, \quad (1.25)$$

and

$$N_c(E) = \begin{cases} N_{co}^*, & E \geq E_c \\ N_{co}^* \exp\left(\frac{E - E_c}{\gamma_c}\right), & E < E_c \end{cases}, \quad (1.26)$$

where  $N_{co}^*$  denotes the conduction band tail DOS prefactor and  $\gamma_c$  represents the conduction band tail breadth,  $N_{vo}^*$ ,  $E_v$ ,  $E_c$ , and  $\gamma_v$  being as defined earlier. The resultant DOS functions, for the nominal selection of DOS modeling parameters tabulated in Table 1.1, are depicted in Figure 1.15.

In 1984, Cody [33] developed an empirical model that builds upon the empirical DOS model of Chen *et al.* [31]. While Chen *et al.* [31] just added an exponential valence band tail onto a terminated square-root valence band DOS function, Cody [33] instead assumed that the interface between the square-root and exponential regions of the valence band occurs below the valence band band edge,  $E_v$ . That is, drawing

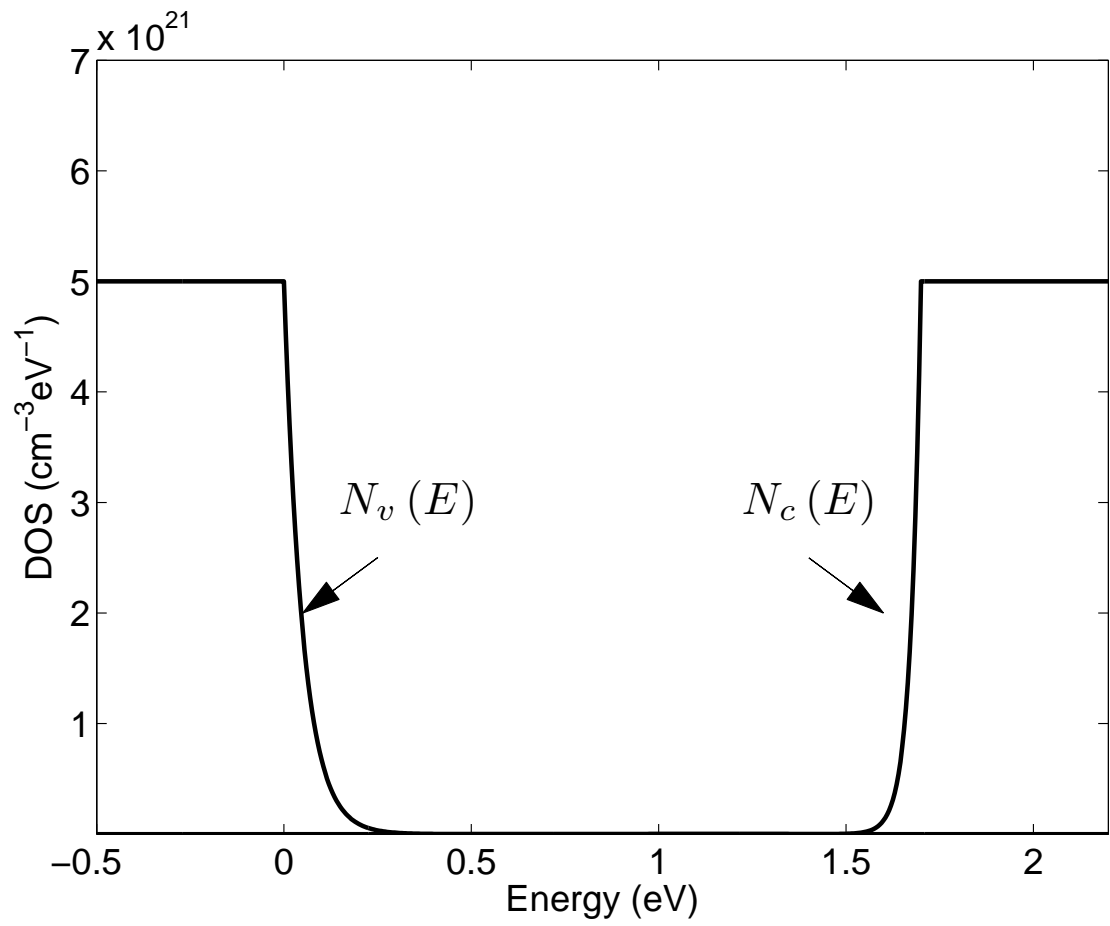


**Figure 1.15:** The empirical DOS model of Redfield [32].

upon a conservation of states argument, Cody [33] assert that

$$N_v(E) = \begin{cases} N_{vo} \sqrt{\frac{3}{2}} \gamma_v \exp\left(-\frac{3}{2}\right) \exp\left(\frac{E_v - E}{\gamma_v}\right), & E > E_v - \frac{3}{2}\gamma_v \\ N_{vo} \sqrt{E_v - E}, & E \leq E_v - \frac{3}{2}\gamma_v \end{cases}, \quad (1.27)$$

and

$$N_c(E) = \begin{cases} N_{co} \sqrt{E - E_c}, & E \geq E_c \\ 0, & E < E_c \end{cases}, \quad (1.28)$$

where  $N_{vo}$ ,  $N_{co}$ ,  $E_v$ ,  $E_c$ , and  $\gamma_v$  are as defined earlier. The resultant DOS functions, for the nominal selection of DOS modeling parameters tabulated in Table 1.1, are depicted in Figure 1.16.

In 1997, O'Leary *et al.* [34] proposed an empirical DOS model that further builds upon this rich tradition. In particular, square-root distributions of band states and exponential distributions of tail states are assumed, both for the valence band and for the conduction band. O'Leary *et al.* [34] further assume that the valence band and conduction band DOS functions,  $N_v(E)$  and  $N_c(E)$ , and their derivatives, are continuous at the critical energies at which the square-root and exponential distributions interface. That is, O'Leary *et al.* [34] assume that

$$N_v(E) = N_{vo} \begin{cases} \sqrt{\frac{\gamma_v}{2}} \exp\left(-\frac{1}{2}\right) \exp\left(\frac{E_v - E}{\gamma_v}\right), & E > E_v - \frac{\gamma_v}{2} \\ \sqrt{E_v - E}, & E \leq E_v - \frac{\gamma_v}{2} \end{cases}, \quad (1.29)$$

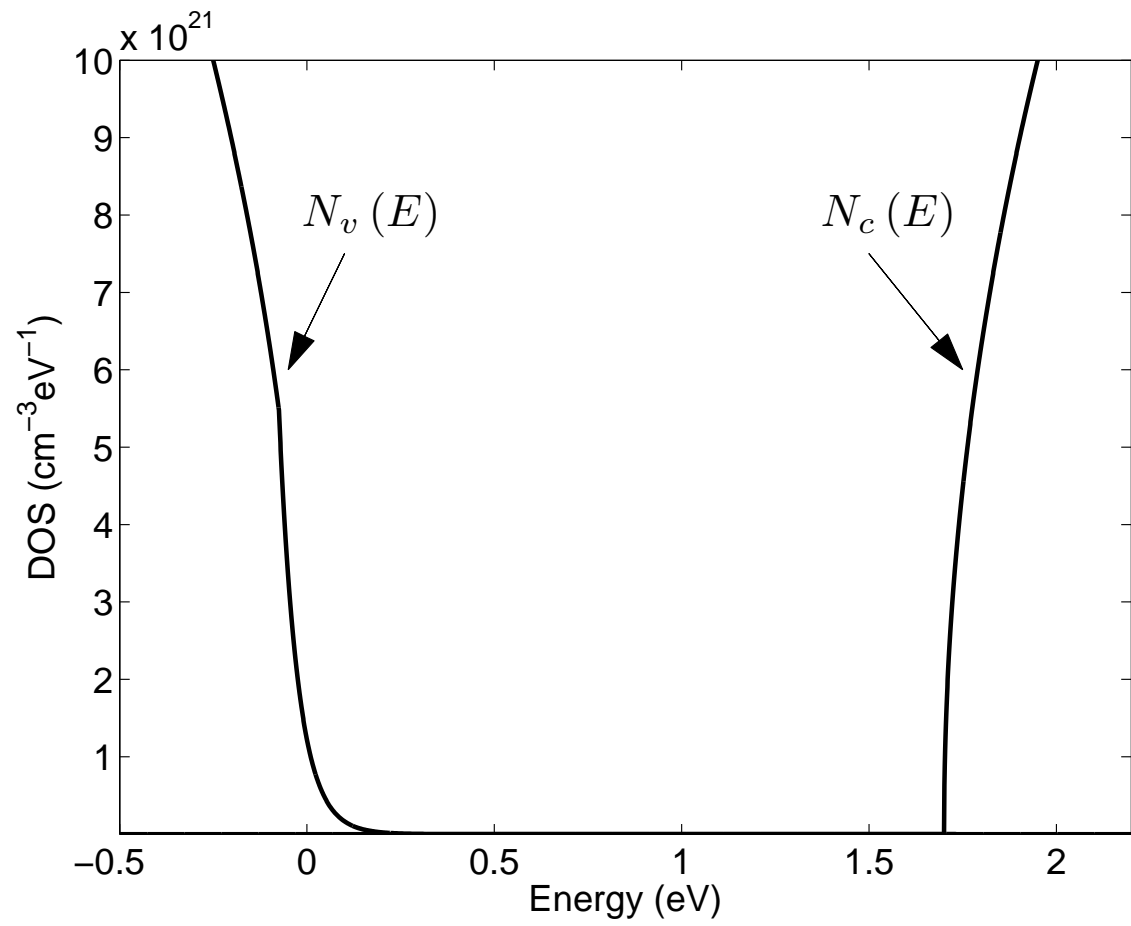


**Figure 1.16:** The empirical DOS model of Cody [33].

and

$$N_c(E) = N_{co} \begin{cases} \sqrt{E - E_c}, & E \geq E_c + \frac{\gamma_c}{2} \\ \sqrt{\frac{\gamma_c}{2}} \exp\left(-\frac{1}{2}\right) \exp\left(\frac{E - E_c}{\gamma_c}\right), & E < E_c + \frac{\gamma_c}{2} \end{cases}, \quad (1.30)$$

where  $N_{vo}$ ,  $N_{co}$ ,  $E_v$ ,  $E_c$ ,  $\gamma_v$ , and  $\gamma_c$  are as defined previously. The resultant DOS functions, for the nominal selection of DOS modeling parameters tabulated in Table 1.1, are depicted in Figure 1.17. The critical energies at which point the square-root and exponentials interface,  $E_v - \frac{\gamma_v}{2}$  for the valence band and  $E_c + \frac{\gamma_c}{2}$  for the conduction band, are clearly marked.

The empirical DOS model of O'Leary *et al.* [34] was further generalized by Jiao *et al.* [35] in 1998. As with the model of O'Leary *et al.* [34], the empirical model of Jiao *et al.* [35] assumes square-root distributions of band states and exponential distributions of tail states. While the valence band and conduction band DOS functions are continuous in the model of Jiao *et al.* [35], the further assumption of O'Leary *et al.* [34], that their derivatives must also be continuous, is relaxed. In particular, Jiao *et al.* [35] assume that

$$N_v(E) = N_{vo} \begin{cases} \sqrt{E_v - E_{vT}} \exp\left(\frac{E_{vT} - E_v}{\gamma_v}\right) \exp\left(\frac{E_v - E}{\gamma_v}\right), & E > E_{vT} \\ \sqrt{E_v - E}, & E \leq E_{vT} \end{cases}, \quad (1.31)$$

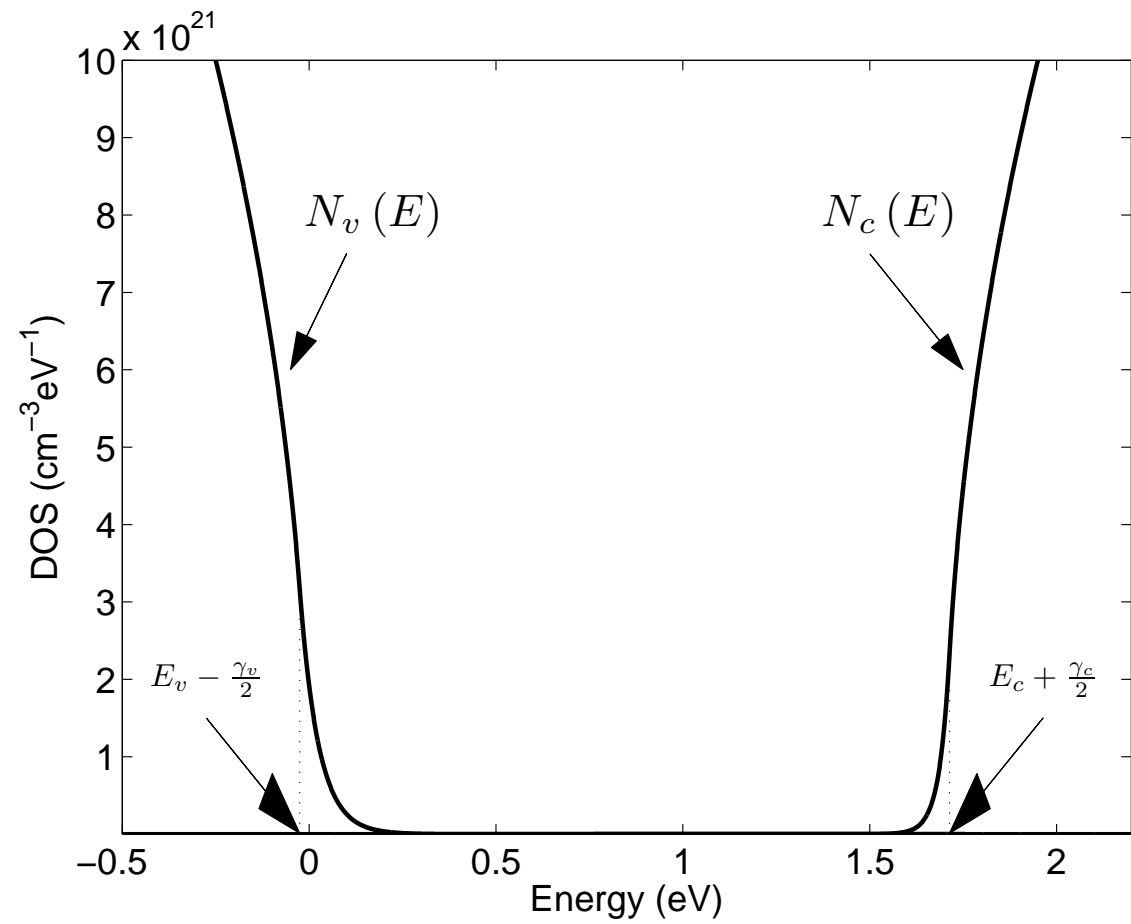


Figure 1.17: The empirical DOS model of O'Leary *et al.* [34].

and

$$N_c(E) = N_{co} \begin{cases} \sqrt{E - E_c}, & E \geq E_{cT} \\ \sqrt{E_{cT} - E_c} \exp\left(\frac{E_c - E_{cT}}{\gamma_c}\right) \exp\left(\frac{E - E_c}{\gamma_c}\right), & E < E_{cT} \end{cases}, \quad (1.32)$$

where  $E_{vT}$  and  $E_{cT}$  are the critical energies at which point the square-root and exponential distributions interface,  $N_{vo}$ ,  $N_{co}$ ,  $E_v$ ,  $E_c$ ,  $\gamma_v$ , and  $\gamma_c$  being as defined previously. It should be noted that in this case,  $E_{vT} \leq E_v$  and  $E_{cT} \geq E_c$ . It is seen that for the special case of  $E_{vT}$  set to  $E_v - \frac{\gamma_v}{2}$  and  $E_{cT}$  set to  $E_c + \frac{\gamma_c}{2}$ , the empirical DOS model of Jiao *et al.* [35] reduces to that of O’Leary *et al.* [34]. That is, Eqs. (1.31) and (1.32) reduce to Eqs. (1.29) and (1.30), respectively.

## 1.9 Modeling of the optical response

In this thesis, an empirical model for the DOS functions will be used in order to compute the optical properties associated with a-Si:H. The analysis starts with the general empirical DOS model of Jiao *et al.* [35], i.e., Eqs. (1.31) and (1.32). Focusing on the specific case of the valence band DOS function,  $N_v(E)$ , an examination of how the valence band tail breadth,  $\gamma_v$ , influences the form of this function is provided in Figures 1.18 and 1.19. For  $N_{vo}$  and  $E_v$  set to the nominal DOS modeling parameter selections provided in Table 1.1, i.e., the selections of O’Leary *et al.* [34], for the case of  $E_{vT}$  set to  $E_v - \frac{\gamma_v}{2}$ , a number of valence band DOS results, for different selections of  $\gamma_v$ , are depicted in these figures, Figure 1.18 being depicted on a linear scale and Figure 1.19 being cast on a logarithmic scale. It is seen that as  $\gamma_v$  is increased from 0 meV, that a tail of electronic states, of increasing breadth, encroaches into the otherwise empty gap region. A similar observation is observed for the conduction band, as may be seen from Figures 1.20 and 1.21. It is noted that for the case that

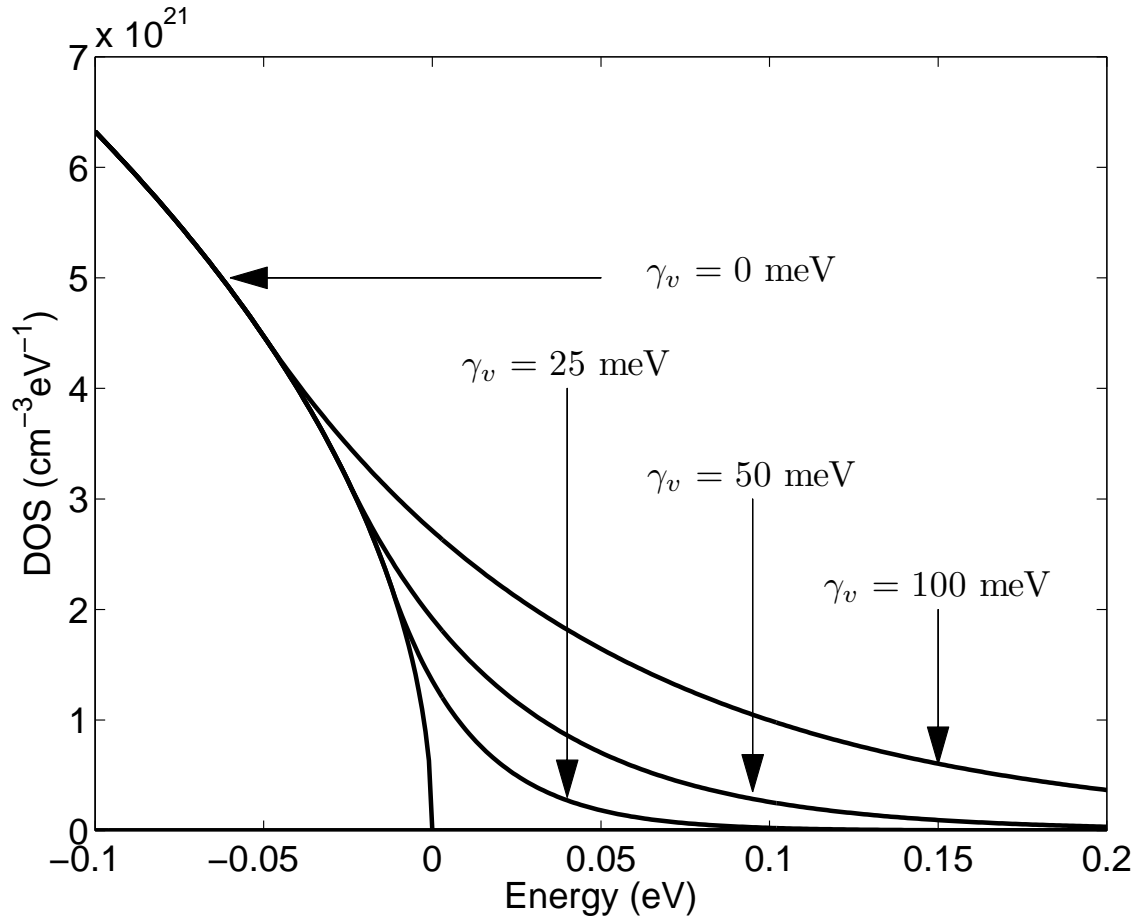


**Figure 1.18:** The valence band DOS function,  $N_v(E)$ , for a number of selections of  $\gamma_v$ , plotted on a linear scale. This function, specified in Eq. (1.31) with  $E_{vT}$  set to  $E_v - \frac{1}{2}\gamma_v$ , is evaluated assuming the nominal DOS modeling parameter selections  $N_{vo} = 2 \times 10^{22} \text{ cm}^{-3} \text{ eV}^{-3/2}$  and  $E_v = 0 \text{ eV}$  for all cases. The abscissa axis represents the energy,  $E$ , while the ordinate axis depicts the corresponding valence band DOS value.

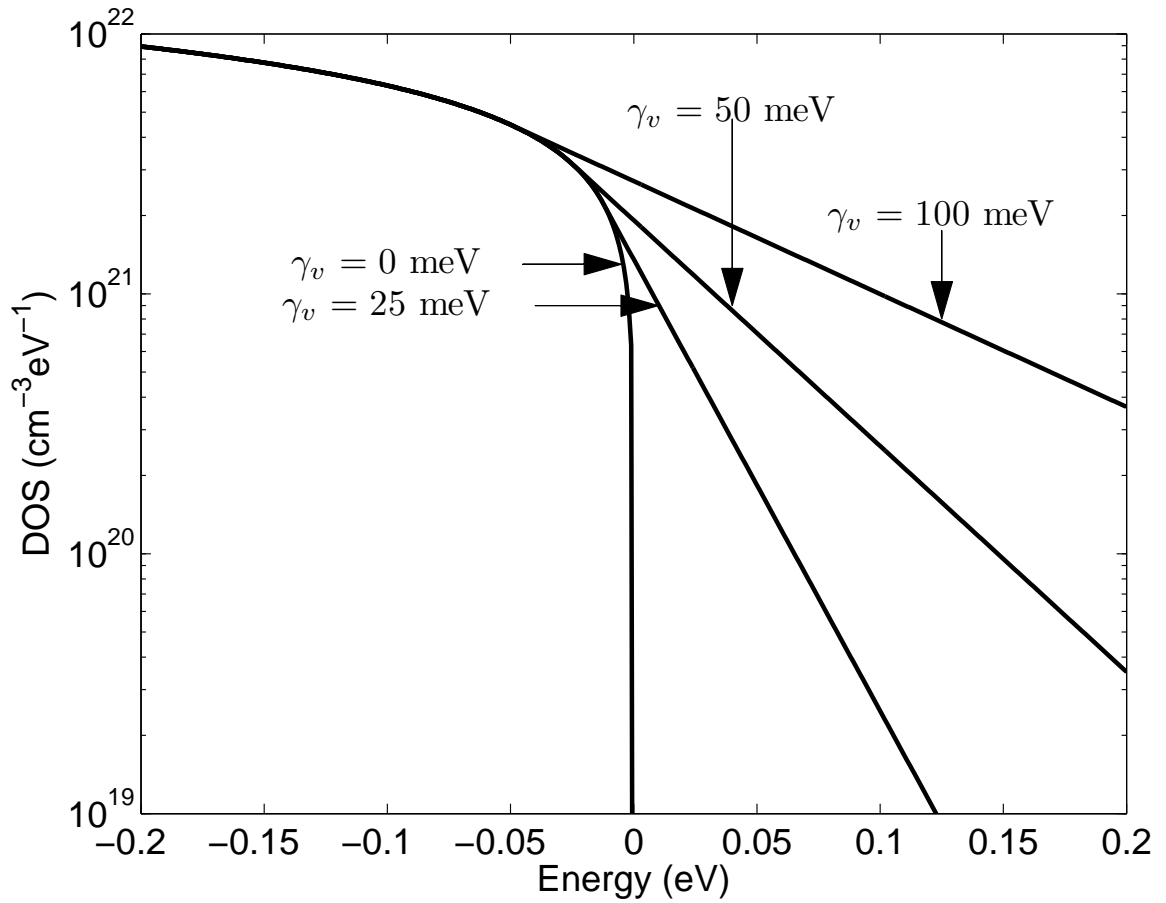


**Figure 1.19:** The valence band DOS function,  $N_v(E)$ , for a number of selections of  $\gamma_v$ , plotted on a logarithmic scale. This function, specified in Eq. (1.31) with  $E_{vT}$  set to  $E_v - \frac{1}{2}\gamma_v$ , is evaluated assuming the nominal DOS modeling parameter selections  $N_{vo} = 2 \times 10^{22} \text{ cm}^{-3} \text{ eV}^{-3/2}$  and  $E_v = 0 \text{ eV}$  for all cases. The abscissa axis represents the energy,  $E$ , while the ordinate axis depicts the corresponding valence band DOS value.

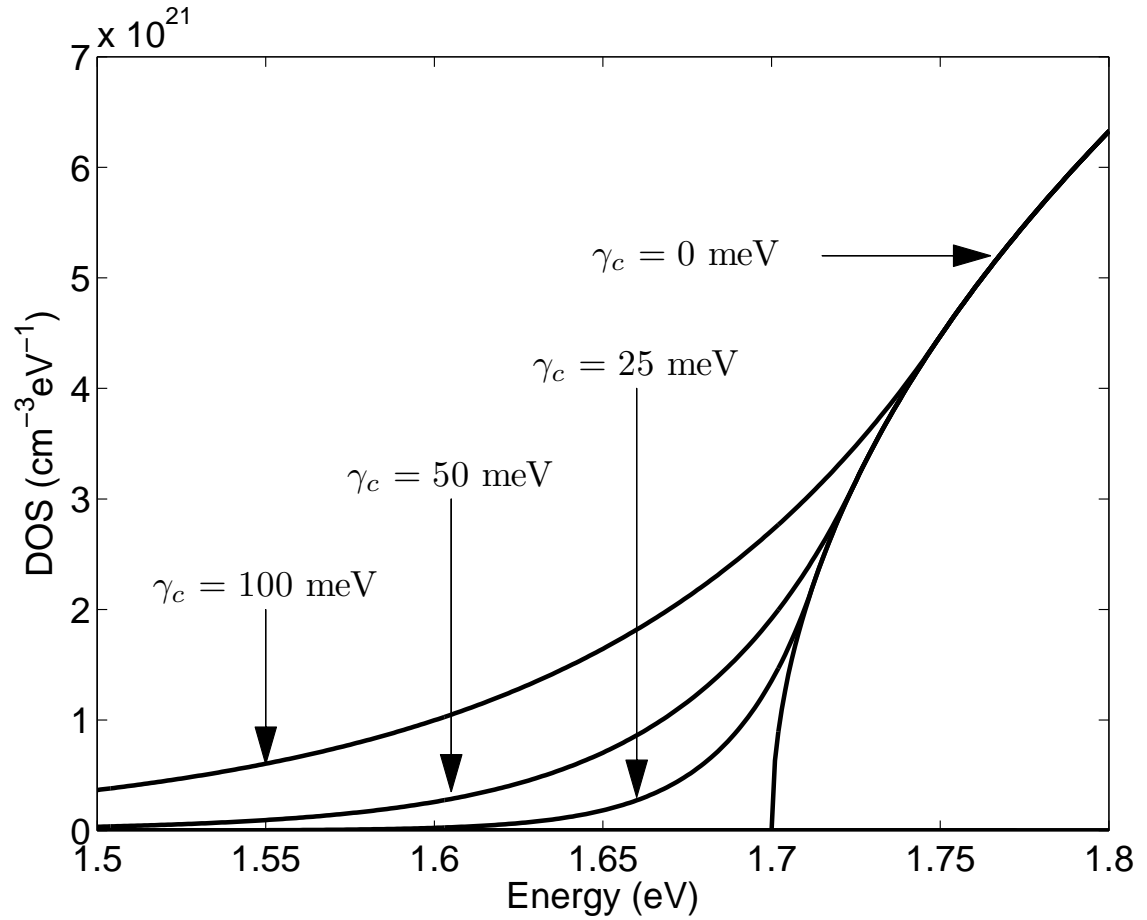


**Figure 1.20:** The conduction band DOS function,  $N_c(E)$ , for a number of selections of  $\gamma_c$ , plotted on a linear scale. This function, specified in Eq. (1.32) with  $E_{cT}$  set to  $E_c + \frac{1}{2}\gamma_c$ , is evaluated assuming the nominal DOS modeling parameter selections  $N_{co} = 2 \times 10^{22} \text{ cm}^{-3} \text{ eV}^{-3/2}$  and  $E_c = 1.7 \text{ eV}$  for all cases. The abscissa axis represents the energy,  $E$ , while the ordinate axis depicts the corresponding conduction band DOS value.

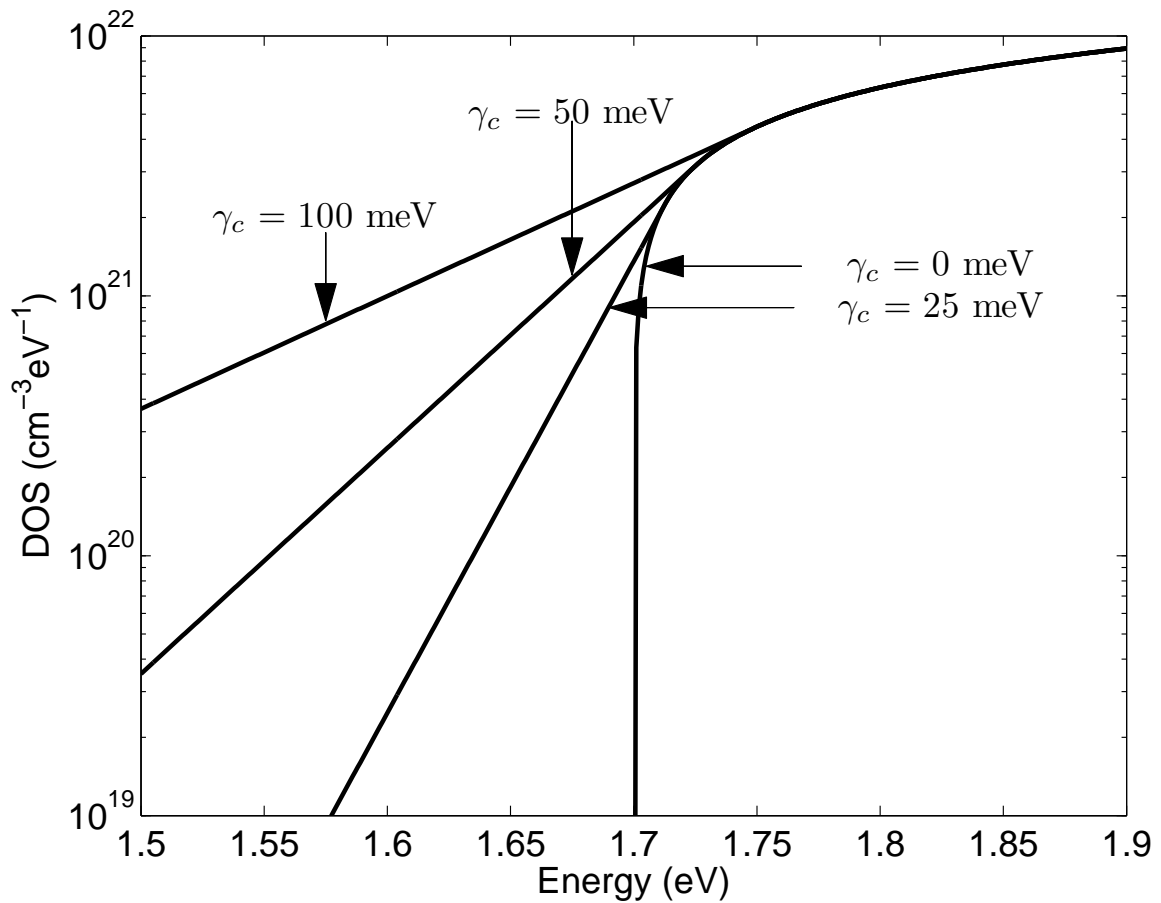


**Figure 1.21:** The conduction band DOS function,  $N_c(E)$ , for a number of selections of  $\gamma_c$ , plotted on a logarithmic scale. This function, specified in Eq. (1.32) with  $E_{cT}$  set to  $E_c + \frac{1}{2}\gamma_c$ , is evaluated assuming the nominal DOS modeling parameter selections  $N_{co} = 2 \times 10^{22} \text{ cm}^{-3} \text{ eV}^{-3/2}$  and  $E_c = 1.7 \text{ eV}$  for all cases. The abscissa axis represents the energy,  $E$ , while the ordinate axis depicts the corresponding conduction band DOS value.

$E_{vT}$  is set to  $E_v - \frac{\gamma_v}{2}$ , that as  $\gamma_v \rightarrow 0$ , that Eq.(1.31) reduces to

$$N_v(E) \rightarrow \begin{cases} 0, & E > E_v \\ N_{vo}\sqrt{E_v - E}, & E \leq E_v \end{cases}. \quad (1.33)$$

Similarly, for the case that  $E_{cT}$  is set to  $E_c + \frac{\gamma_c}{2}$ , that as  $\gamma_c \rightarrow 0$ , that Eq.(1.32) reduces to

$$N_c(E) \rightarrow \begin{cases} N_{co}\sqrt{E - E_c}, & E \geq E_c \\ 0, & E < E_c \end{cases}. \quad (1.34)$$

That is, the empirical DOS model of Jiao *et al.* [35], for the special case of  $E_{vT}$  set to  $E_v - \frac{\gamma_v}{2}$  and  $E_{cT}$  set to  $E_c + \frac{\gamma_c}{2}$ , i.e, the empirical DOS model of O'Leary *et al.* [34], reduces to that of Tauc *et al.* [30], i.e., Eqs. (1.21) and (1.22), in the limit that  $\gamma_v \rightarrow 0$  and  $\gamma_c \rightarrow 0$ . This limit is henceforth referred to as the disorderless limit,  $\gamma_v$  and  $\gamma_c$  providing a measure of the amount of disorder present.

A closed form expression for the resultant JDOS function was determined by O'Leary in 2004 [36]. For the special case of  $\gamma_v = \gamma_c = \gamma$ , for the nominal DOS modeling parameter selections tabulated in Table 1.1, for the special case of  $E_{vT}$  set to  $E_v - \frac{\gamma_v}{2}$  and  $E_{cT}$  set to  $E_c + \frac{\gamma_c}{2}$ , the resultant JDOS functions are shown in Figures 1.22 and 1.23, for a number of different  $\gamma$  selections; Figure 1.22 is depicted on a linear scale while Figure 1.23 is cast on a logarithmic scale. It is seen that as  $\gamma$  increases, the JDOS function further encroaches into the otherwise empty gap region. For each value of  $\gamma$  considered, an exponential tail, of tail breadth  $\gamma$ , is observed. In the limit of  $\gamma \rightarrow 0$ , i.e., the disorderless limit, it is seen that the JDOS function terminates abruptly at the energy difference between  $E_v$  and  $E_c$ . Analytically, for the special case of  $E_{vT}$  set to  $E_v - \frac{\gamma_v}{2}$  and  $E_{cT}$  set to  $E_c + \frac{\gamma_c}{2}$ , i.e, the empirical DOS

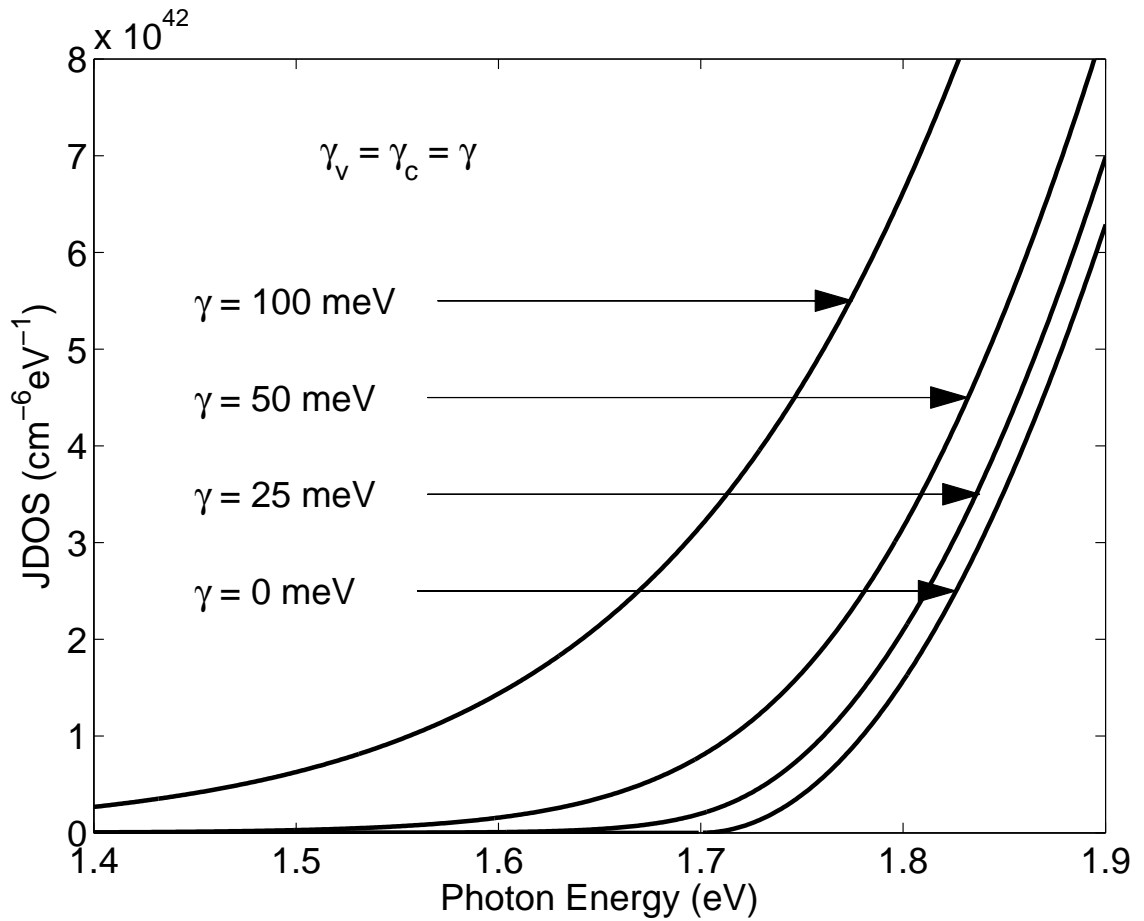


**Figure 1.22:** The JDOS function,  $J(\hbar\omega)$ , determined through an evaluation of Eq. (1.10), for various selections of  $\gamma_c$  and  $\gamma_v$ , depicted on a linear scale. For all cases, the DOS modeling parameters are set to their nominal values tabulated in Table 1.1.

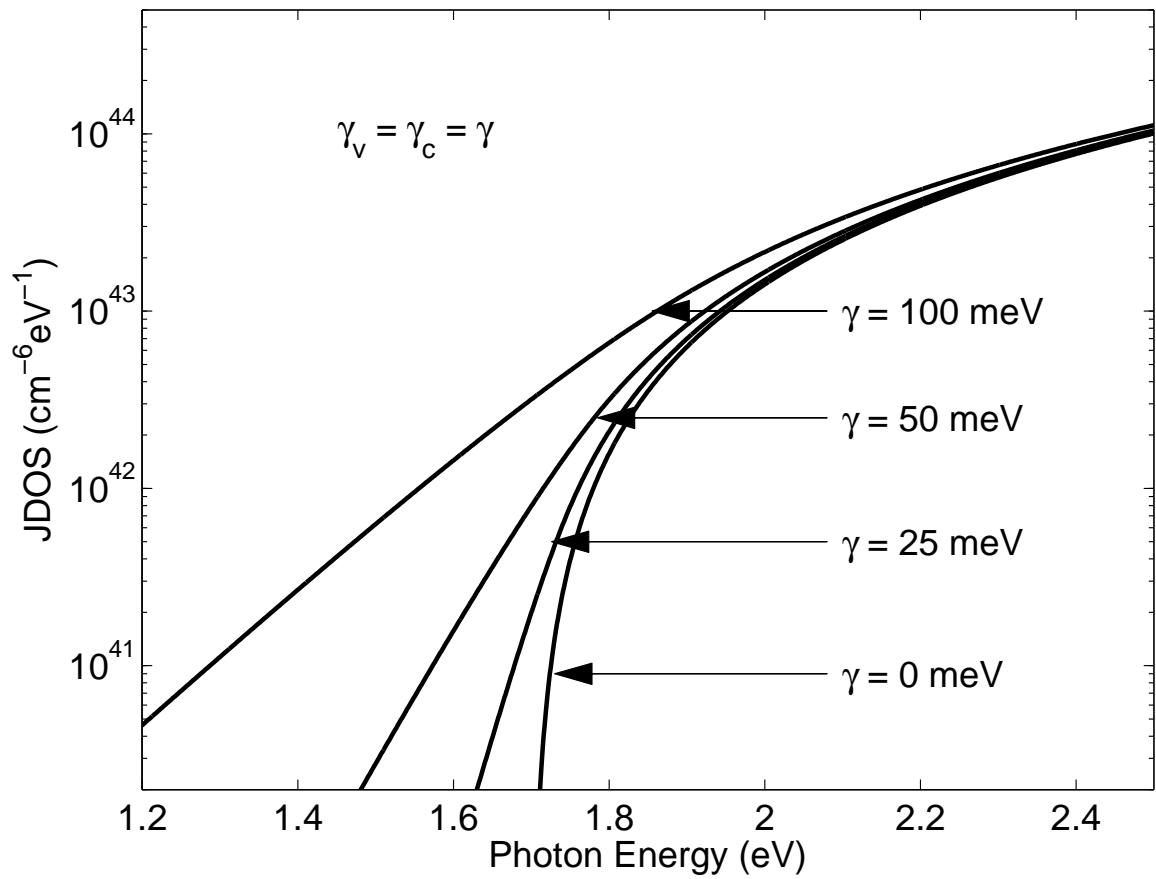


**Figure 1.23:** The JDOS function,  $J(\hbar\omega)$ , determined through an evaluation of Eq. (1.10), for various selections of  $\gamma_c$  and  $\gamma_v$ , depicted on a logarithmic scale. For all cases, the DOS modeling parameters are set to their nominal values tabulated in Table 1.1.

model of O'Leary *et al.* [34], from Eqs. (1.31) and (1.32), for  $\gamma_v = \gamma_c = \gamma = 0$  meV, it may be shown that

$$J(\hbar\omega) \rightarrow \begin{cases} N_{vo}N_{co}\frac{\pi}{8}(\hbar\omega - E_g)^2, & \hbar\omega \geq E_g \\ 0, & \hbar\omega < E_g \end{cases}, \quad (1.35)$$

where the energy gap

$$E_g \equiv E_c - E_v. \quad (1.36)$$

This result also corresponds to that determined using the empirical DOS model of Tauc *et al.* [30], i.e., Eqs. (1.21) and (1.22).

The empirical DOS model of Jiao *et al.* [35], i.e., Eqs. (1.31) and (1.32), allows for the consideration of four different types of optical transitions. In the valence band DOS function,  $N_v(E)$ , there are valence band band (VBB) and valence band tail (VBT) electronic states, these states being separated by the critical energy,  $E_{vT}$ , that separates the square-root and exponential distributions. Similarly, in the conduction band DOS function,  $N_c(E)$ , there are conduction band band (CBB) and conduction band tail (CBT) electronic states, these states being separated by the critical energy,  $E_{cT}$ , that separates the square-root and exponential distributions. Optical transitions from the VBB states to the CBB states (VBB-CBB optical transitions), from the VBB states to the CBT states (VBB-CBT optical transitions), from the VBT states to the CBB states (VBT-CBB optical transitions), and from the VBT states to the CBT states, are thus considered within the framework of the empirical DOS model of Jiao *et al.* [35]. For the special case of  $E_{vT}$  set to  $E_v - \frac{\gamma_v}{2}$  and  $E_{cT}$  set to  $E_c + \frac{\gamma_c}{2}$ , for the nominal DOS modeling parameter selections tabulated in Table 1.1, representative VBB-CBB, VBB-CBT, VBT-CBB, and VBT-CBT optical transitions are depicted

in Figure 1.24.

In 2002, Malik and O’Leary [37] determined the contributions to the JDOS function attributable to each type of optical transition. A means of evaluating the various contributions to the JDOS function attributable to these four types of optical transitions is depicted in Figures 1.25 and 1.26. In particular, the functional dependence of  $N_v(E)$  and  $N_c(E + \hbar\omega)$  independently, and their product,  $N_v(E) N_c(E + \hbar\omega)$ , are depicted, for the cases of  $\hbar\omega$  set to 2.1 eV and  $\hbar\omega$  set to 1.4 eV, i.e., above and below the separation in energy between  $E_{v_T}$  and  $E_{c_T}$ . For the case of  $\hbar\omega$  set to 2.1 eV, a considerable amount of overlap in these DOS functions is found, the resultant JDOS integrand,  $N_v(E) N_c(E + \hbar\omega)$ , being quite large in magnitude. In contrast, for the case of  $\hbar\omega$  set to 1.4 eV, the overlap is found to be considerably smaller. The contributions to the JDOS function corresponding to the four different types of optical transitions, i.e., VBB-CBB, VBB-CBT, VBT-CBB, and VBT-CBT, corresponds to the regions of overlap of the respective DOS functions. That is, the contribution to the JDOS function attributable to the VBB-CBB optical transitions corresponds to the values of  $E$  over which  $N_v(E)$  is in the VBB region and  $N_c(E + \hbar\omega)$  is in the CBB region. The overall contribution to the JDOS function attributable to VBB-CBB optical transitions may be obtained by integrating over the range of energies over which this condition is satisfied. The other contributions to the JDOS function may be obtained in a similar manner.

In an effort to simplify matters, for the specific case of a-Si:H, O’Leary and Malik [38] introduced a simplified empirical DOS model. Noting, for the specific case of a-Si:H, that the valence band tail associated with this material is much broader than the corresponding conduction band tail, O’Leary and Malik [38] suggest neglecting the CBT in their modeling of the DOS functions. That is, O’Leary and Malik [38]

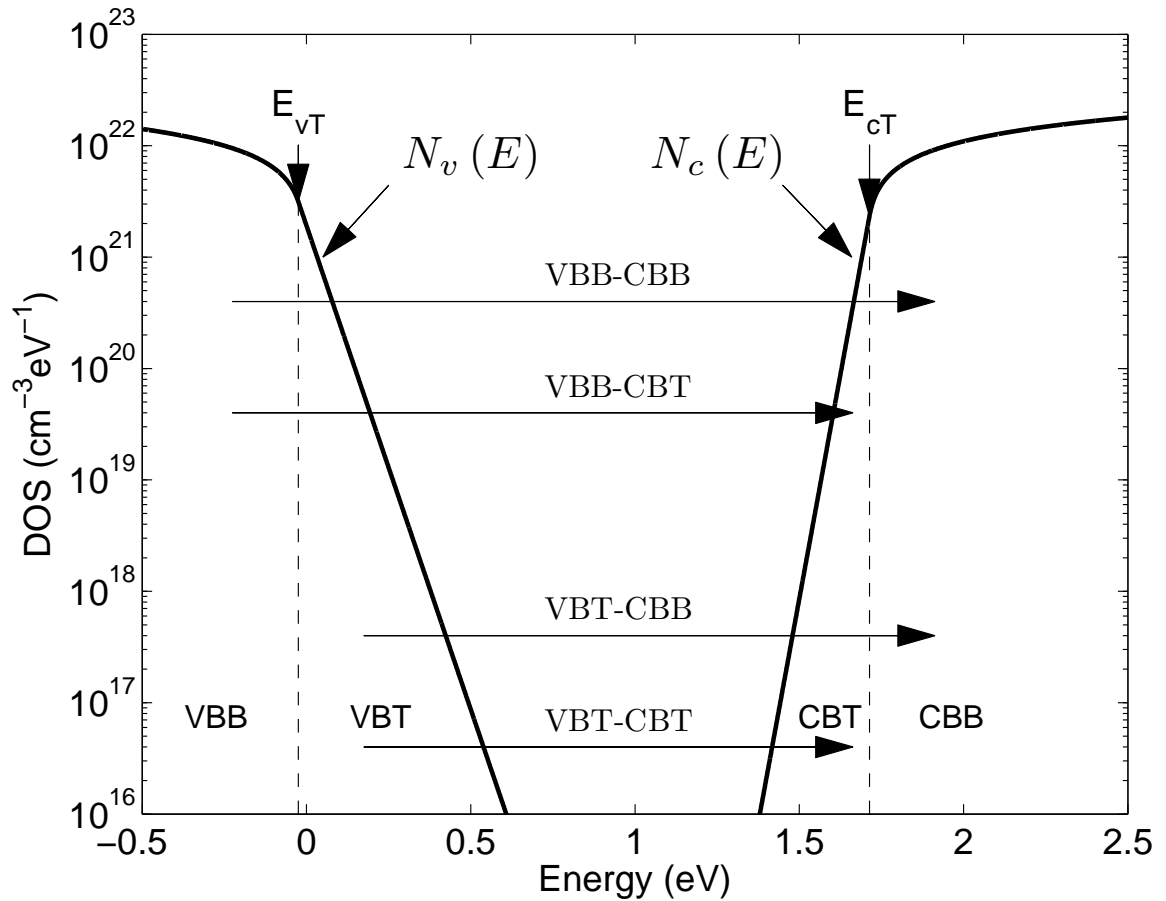
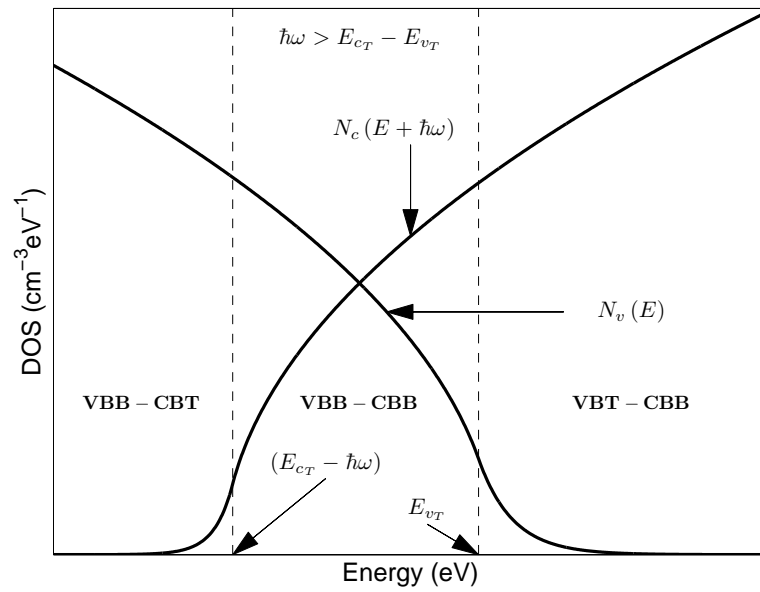
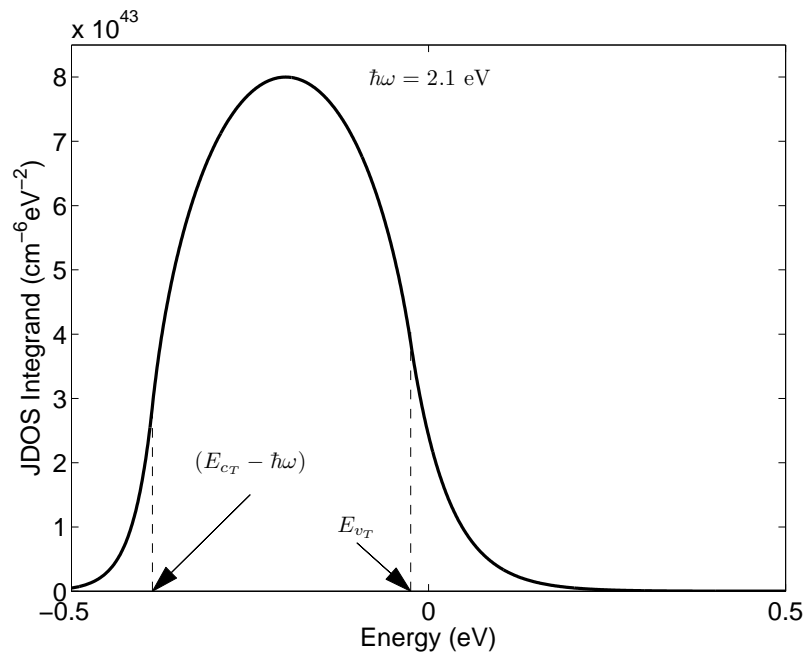


**Figure 1.24:** The valence band and conduction band DOS functions associated with a-Si:H. The nominal DOS modeling parameter selections tabulated in Table 1.1 are employed for the purposes of this analysis.  $E_{vT}$  is set to  $E_v - \frac{\gamma_v}{2}$  and  $E_{cT}$  is set to  $E_c + \frac{\gamma_c}{2}$  for the purposes of this figure. The critical energies,  $E_{vT}$  and  $E_{cT}$ , that separate the square-root distributions from the exponential distributions, are clearly depicted. Representative VBB-CBB, VBB-CBT, VBT-CBB, and VBT-CBT optical transitions, are also shown.



(a)



(b)

**Figure 1.25:** The factors in the JDOS integrand,  $N_v(E)$  and  $N_c(E + \hbar\omega)$ , and the resultant product,  $N_v(E)N_c(E + \hbar\omega)$ , for the case of  $\hbar\omega$  set to 2.1 eV. The nominal DOS modeling parameter selections, tabulated in Table 1.1, are employed for the purposes of this analysis. Ranges of energy, corresponding to VBB-CBB, VBB-CBT, and VBT-CBB optical transitions, are depicted. VBT-CBT optical transitions do not occur for this selection of  $\hbar\omega$ . This figure is taken after O’Leary [36].

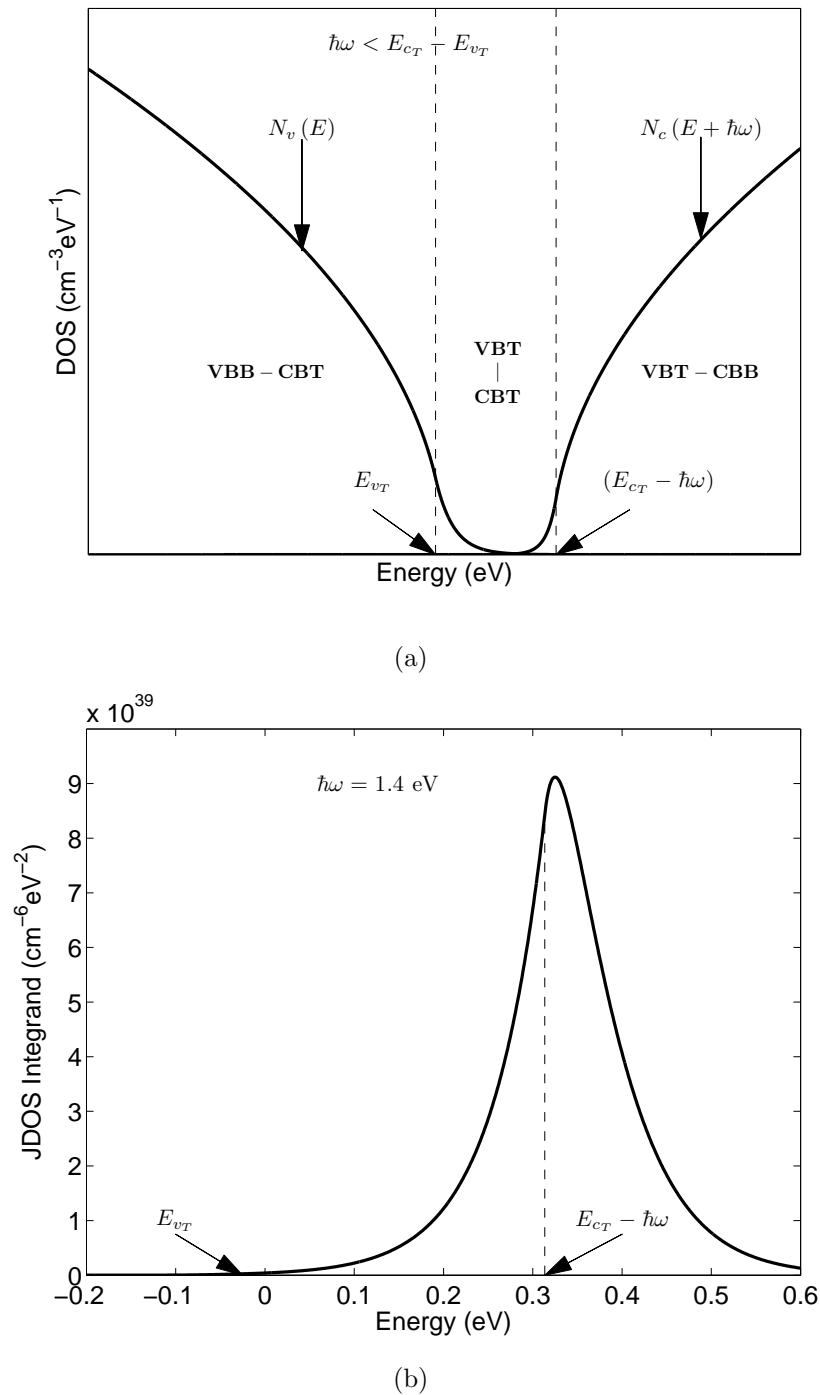


**Figure 1.26:** The factors in the JDOS integrand,  $N_v(E)$  and  $N_c(E + \hbar\omega)$ , and the resultant product,  $N_v(E) N_c(E + \hbar\omega)$ , for the case of  $\hbar\omega$  set to 1.4 eV. The nominal DOS modeling parameter selections, tabulated in Table 1.1, are employed for the purposes of this analysis. Ranges of energy, corresponding to VBB-CBT, VBT-CBB, and VBT-CBT optical transitions, are depicted. VBB-CBB optical transitions do not occur for this selection of  $\hbar\omega$ . This figure is taken after O’Leary [36].

assume that

$$N_v(E) = N_{vo} \begin{cases} \sqrt{E_v - E_{vT}} \exp\left(\frac{E_{vT} - E_v}{\gamma_v}\right) \exp\left(\frac{E_v - E}{\gamma_v}\right), & E > E_{vT} \\ \sqrt{E_v - E}, & E \leq E_{vT} \end{cases}, \quad (1.37)$$

and

$$N_c(E) = \begin{cases} N_{co} \sqrt{E - E_c}, & E \geq E_c \\ 0, & E < E_c \end{cases}, \quad (1.38)$$

where  $N_{vo}$ ,  $N_{co}$ ,  $E_v$ ,  $E_c$ ,  $\gamma_v$ , and  $E_{vT}$  are as defined previously. For the special case of  $E_{vT}$  set to  $E_v - \frac{\gamma_v}{2}$ , for the nominal DOS modeling parameter selections tabulated in Table 1.1, the resultant DOS functions are depicted in Figure 1.27. Note that now only VBB-CBB and VBT-CBB optical transitions are considered. The simplified empirical DOS model of O'Leary and Malik [38], i.e., Eqs. (1.37) and (1.38), forms the basis of the analysis presented in this thesis.

## 1.10 Objective of this thesis

This thesis aims to devise a quantitative model for the spectral dependence of the optical properties associated with a-Si:H, which allows for the ready determination of the underlying modeling parameters from the results of experiment. This analysis stems directly from a simplified empirical model for the DOS functions,  $N_v(E)$  and  $N_c(E)$ , that only considers VBB, VBT, and CBB electronic states, i.e., the CBT electronic states are neglected. This model assumes square-root distributions of VBB and CBB electronic states, and an exponential distribution of VBT states. The optical properties of a-Si:H will then be determined through the evaluation of the corresponding JDOS function,  $J(\hbar\omega)$ . A comparison with the results of experiment

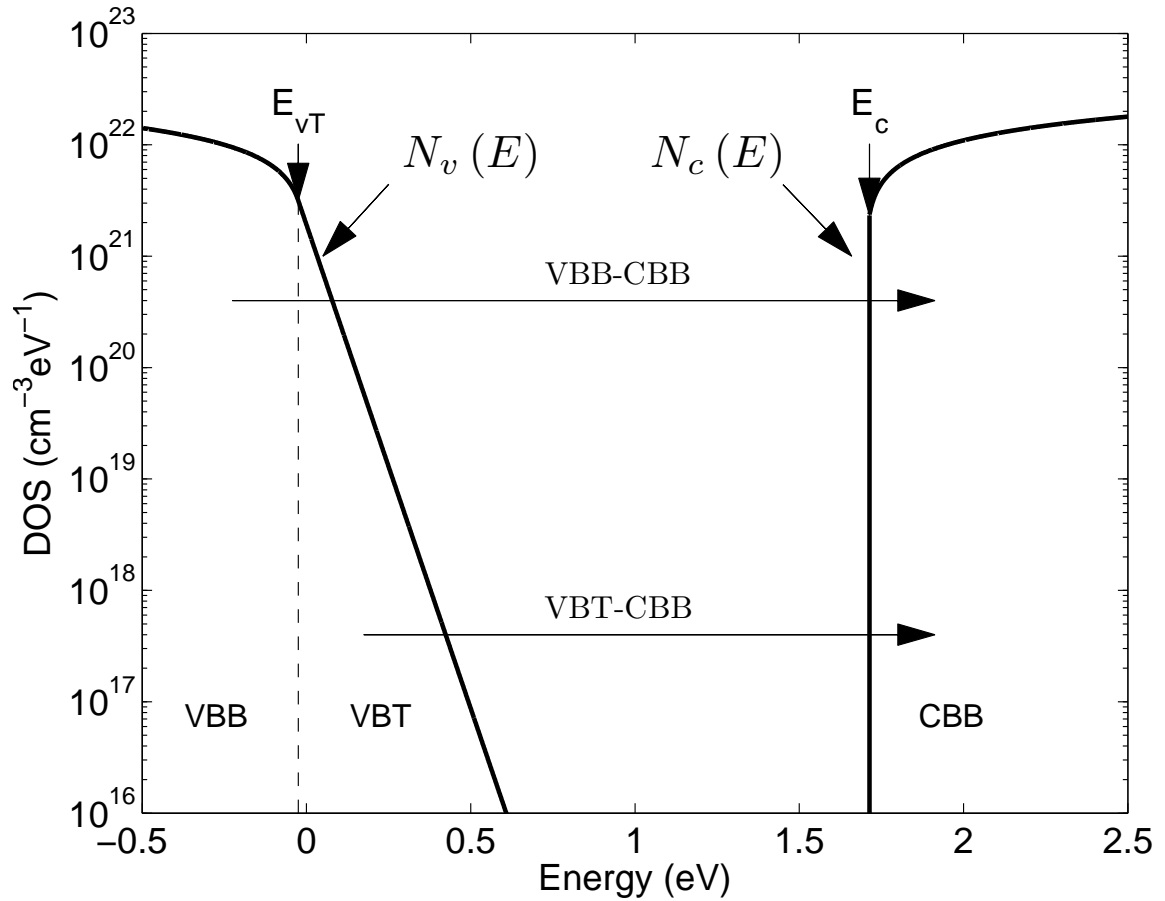


**Figure 1.27:** The valence band and conduction band DOS functions associated with a-Si:H for the simplified empirical DOS model of O’Leary and Malik [38]. The nominal DOS modeling parameter selections tabulated in Table 1.1 are employed for the purposes of this analysis.  $E_{vT}$  is set to  $E_v - \frac{\gamma_v}{2}$ . The critical energy,  $E_{vT}$ , separating the square-root valence band band distribution from the exponential valence band tail distribution, is clearly depicted. Representative VBB-CBB and VBT-CBB optical transitions are also shown.

will be used in order to validate the model and in order to gain insight into the character of the optical response of a-Si:H.

In order to justify the neglect of the CBT states, initially, for the specific case of a-Si:H, it will be shown that the neglect of the CBT states has no real impact on the obtained JDOS function, and that, therefore, the optical properties of a-Si:H may be accurately determined using this simplified empirical model for the DOS functions. This will be done through the use of the general empirical model for the DOS functions of O’Leary *et al.* [36]; this model is the same as that suggested by Jiao *et al.* [35], i.e., Eqs. (1.31) and (1.32), this model including VBB, VBT, CBB, and CBT electronic states. Square-root distributions of VBB and CBB states and exponential distributions of VBT and CBT are employed for the purposes of this analysis. By examining the role that the conduction band tail breadth,  $\gamma_c$ , plays in determining the form of the resultant JDOS function,  $J(\hbar\omega)$ , it will be shown that when the conduction band tail breadth,  $\gamma_c$ , is significantly less than the valence band tail breadth,  $\gamma_v$ , that the CBT states can be ignored in the determination of the JDOS function,  $J(\hbar\omega)$ . Experimental evidence will be presented that confirms this to be the case for the specific case of a-Si:H. Thus, the use of a simplified empirical DOS model, that neglects CBT states, is justified for the specific case of this material.

In order to further simplify this empirical model for the DOS functions, it will be further assumed that the derivative of the valence band DOS function is continuous at the energy at which the square-root and exponential functional dependencies interface; it was already assumed that the valence band DOS function is continuous at this interface. This simplification allows for the casting of the JDOS evaluation into a dimensionless format. This dimensionless formalism for the JDOS function will be shown to provide a platform for the comparison of disparate optical absorption spectra, with differing energy gaps and Urbach tail breadths. The applicability of this

formalism is then tested through an analysis of a large number of a-Si:H experimental data sets. From this analysis, insights into the optical response of this material may be gleaned.

Finally, the role that defect states play in shaping the optical response of a-Si:H will be probed. In order to perform this analysis, the empirical model for the DOS functions will be modified in order to include valence band defect (VBD) and conduction band defect (CBD) states. This is done through splining exponential tails, of greater breadth than the VBT and CBT tail breadths, onto the VBT and CBT distributions, these new exponential distributions modeling the distributions of defect states. With this model for the VBD and CBD states established, the contributions to the JDOS function, attributable to the various types of optical transitions involving these defect states, may then be assessed. A comparison with the results of experiment is used in order to validate this modeling approach.

## 1.11 Thesis organization

This thesis is organized into 6 chapters. Chapter One provides the background material relevant to this analysis. In particular, an introduction to disordered semiconductors, a brief history of research into disordered semiconductors, and an overview of their electronic and optical properties is provided. A detailed review of empirical models for the DOS functions, and their use in determining the optical response of these materials, is also provided, this analytical framework forming the background to this thesis.

In Chapter 2, the use of an empirical model for the DOS functions, that neglects the presence of CBT states, is justified. In particular, using a general empirical model for the DOS functions, that includes VBB, VBT, CBB, and CBT states, the resultant JDOS function is determined, for a number of parameter selections. Assuming square-

root distributions of VBB and CBB states and exponential distributions of VBT and CBT states, for a fixed selection of the valence band tail breadth,  $\gamma_v$ , the sensitivity of the JDOS function to variations in the conduction band tail breadth,  $\gamma_c$ , is examined. It is found that when  $\gamma_c$  is smaller than  $\gamma_v$ , the JDOS function is virtually independent of  $\gamma_c$ . Through a comparison with the results of experiment, for the specific case of a-Si:H, it is shown that  $\gamma_c$  is always less than  $\gamma_v$  for the case of this material. As a result, an empirical model for the DOS functions, that neglects the CBT states, is justified for the case of a-Si:H.

In Chapter 3, this empirical DOS model is further simplified. In particular, by assuming that the valence band DOS function,  $N_v(E)$ , and its derivative, are continuous at the interface between the exponential and square-root distributions, the number of empirical DOS modeling parameters can be reduced. As a consequence, the JDOS evaluations may be cast into a dimensionless form, one that allows for the ready extraction of parameters from the results of experiment. Moreover, it is found that this dimensionless JDOS function provides a means whereby disparate optical absorption spectra, with differing energy gaps and differing Urbach tails, may be directly compared. Through an analysis of three a-Si:H optical absorption experimental data sets, a general ‘universal’ character in the optical absorption spectrum associated with this material is hinted at.

In Chapter 4, using the dimensionless JDOS formalism devised in Chapter 3, a critical comparative analysis of a large number of different a-Si:H experimental optical absorption data sets is considered. When these data sets are cast into this dimensionless framework, a trend that is almost completely coincident for all of the data sets considered is observed. This suggests that there is a ‘universal’ character associated with the optical absorption spectrum of a-Si:H

In Chapter 5, the empirical DOS model is modified in order to account for the

presence of defect states. This is done by splining additional exponential distributions onto the VBT and CBT distributions, these exponential distributions corresponding to the electronic states related to defects. With this model established, how the distributions of such states shape the optical response of this material is examined. The contributions to this response, attributable to the various types of optical transitions, are also determined. Finally, it is demonstrated that this formalism is able to capture the spectral dependence of the optical absorption coefficient associated with a defect absorption influenced sample of a-Si:H.

Finally, the conclusions of this thesis are presented in Chapter 6. Recommendations for further study are also presented.

## References

- [1] M. Riordan and H. Lillian, "The Moses of silicon valley," *Physics Today*, vol. 50, no. 12, pp. 42-47, 1997.
- [2] I. M. Ross, "The foundation of the silicon age," *Physics Today*, vol. 50, no. 12, pp. 34-39, 1997.
- [3] A. J. Snell, K. D. Mackenzie, W. E. Spear, P. G. Le Comber, and A. J. Hughes, "Application of amorphous silicon field effect transistors in addressable liquid crystal display panels," *Applied Physics Letters*, vol. 24, no. 4, pp. 357-362, 1981.
- [4] P. G. Le Comber, W. E. Spear, and A. Ghaith, "Amorphous-silicon field-effect device and possible application," *Electronics Letters*, vol. 15, no. 6, pp. 179-181, 1979.
- [5] M. G. Clark, "Current status and future prospects of poly-Si devices," *IEEE Proceedings-Circuits, Devices and Systems*, vol. 141, no. 1, pp. 3-8, 1994.
- [6] H. Fujioka, M. Oshima, C. Hu, M. Sumiya, N. Matsuki, K. Miyazaki, and H. Koinuma, "Characteristics of field effect a-Si:H solar cell," *Journal of Non-Crystalline Solids*, vol. 227-230, pt. B, pp. 1287-1290, 1998.
- [7] H. Pawlikiewicz and S. Guha, "Performance comparison of triple and tandem multi-junction a-Si:H solar cells: A numerical study," *IEEE Transactions on Electron Devices*, vol. 37, no. 7, pp. 1758-1762, 1990.
- [8] S. O. Kasap and J. A. Rowlands, "X-ray photoconductors and stabilized a-Se for direct conversion digital flat-panel X-ray image-detectors," *Journal of Materials Science: Materials in Electronics*, vol. 11, no. 3, pp. 179-198, 2000.
- [9] R. A. Street, Editor, *Technology and Applications of Amorphous Silicon*. New York, New York: Springer-Verlag, 2000.
- [10] A. Goetzberger and C. Hebling, "Photovoltaic materials, past, present, future," *Solar Energy Materials and Solar Cells*, vol. 62, no. 1-2, pp. 1-19, 2000.
- [11] R. A. Street, *Hydrogenated Amorphous Silicon*. New York, New York: Cambridge University Press, 1991.
- [12] National Research Council, *Physics through the 1990s: Condensed-Matter Physics*. Washington D.C., National Academy Press, pp. 113-126, 1986.
- [13] D. Lezal, J. Pedlikova, and J. Zavadil, "Chalcogenide glasses for optical and photonics applications," *Chalcogenide Letters*, vol. 1, no. 1, pp. 11-15, 2004.
- [14] D. Lezal, "Chalcogenide glasses - Survey and progress," *Journal of Optoelectronics and Advanced Materials*, vol. 5, no. 1, pp. 23-34, 2003.

- [15] D. Thornburg, "Physical properties of the  $As_2(Se, Te)_3$  glasses," *Journal of Electronic Materials*, vol. 2, no. 4, pp. 495-532, 1973.
- [16] M. Shurgalin, V. N. Fuflyigin, and E. G. Anderson, "The structural heterogeneity and optical properties in chalcogenide glass films," *Journal of Physics D: Applied Physics*, vol. 38, pp. 4037-4047, 2005.
- [17] P. G. Le Comber, "Present and future applications of amorphous silicon and its alloys," *Journal of Non-Crystalline Solids*, vol. 155, no. 1-3, pp. 1-13, 1989.
- [18] Z. Remeš, "Study of defects and microstructure of amorphous and microcrystalline silicon thin films and polycrystalline diamond using optical methods," *Ph. D. Thesis*, Charles University, Prague, 1999.
- [19] W. E. Spear and P. G. Le Comber, "Substitutional doping of amorphous silicon," *Solid State Communications*, vol. 88, no. 11-12, pp. 1015-1018, 1993.
- [20] A. J. Harris, R. S. Walker, and R. Sneddon, "Current-voltage characteristics of amorphous silicon p-n junctions," *Journal of Applied Physics*, vol. 51, no. 8, pp. 4287-4290, 1980.
- [21] P. G. Le Comber and W. E. Spear, "Electronic transport in amorphous silicon film," *Physical Review Letters*, vol. 25, no. 8, pp. 509-511, 1970.
- [22] H. Fritzsche, "Evidence for compositional heterogeneities in hydrogenated amorphous silicon nitride films," *Applied Physics Letters*, vol. 65, no. 22, pp. 2824-2826, 1994.
- [23] S. O. Kasap, *Principles of Electrical Engineering Material and Devices*. Boston, Massachusetts: Irwin McGraw-Hill, 1997.
- [24] E. O. Johnson, "Electronic displays," *Display devices*, pp. 233-246, 1980.
- [25] K. Morigaki, "Physics of amorphous semiconductors," World Scientific, Imperial College Press, 1999.
- [26] W. B. Jackson, S. M. Kelso, C. C. Tsai, J. W. Allen, and S.-J. Oh, "Energy dependence of the optical matrix element in hydrogenated amorphous and crystalline silicon," *Physical Review B*, vol. 31, no. 8, pp. 5187-5198, 1985.
- [27] R. H. Klazes, M. H. L. M. van den Broek, J. Bezemer, and S. Radelaar, "Determination of the optical bandgap of amorphous silicon," *Philosophical Magazine B*, vol. 45, no. 4, pp. 377-383, 1982.
- [28] S. John, C. Soukoulis, M. H. Cohen, and E. N. Economou, "Theory of electron band tails and the Urbach optical-absorption edge," *Physical Review Letters*, vol. 57, no. 14, pp. 1777-1780, 1986.

- [29] S. K. O’Leary, S. Zukotynski, and J. M. Perz, “Hydrogen-induced quantum confinement in amorphous silicon,” *Journal of Applied Physics*, vol. 78, no. 6, pp. 4282-4284, 1995.
- [30] J. Tauc, R. Grigorovici, and A. Vancu, “Optical properties and electronic structure of amorphous germanium,” *Physica Status Solidi*, vol. 15, no. 2, pp. 627-637, 1966.
- [31] W.-C. Chen, B. J. Feldman, J. Bajaj, F.-M. Tong, and G. K. Wong, “Thermalization gap excitation photoluminescence and optical absorption in amorphous silicon-hydrogen alloys,” *Solid State Communications*, vol. 38, no. 5, pp. 357-363, 1981.
- [32] D. Redfield, “Energy-band tails and the optical absorption edge; The case of a-Si:H,” *Solid State Communications*, vol. 44, no. 9, pp. 1347-1349, 1982.
- [33] G. D. Cody, in *Hydrogenated Amorphous Silicon*, vol. 21B of *Semiconductors and Semimetals*, edited by J. I. Pankove (Academic, New York, 1984), pp. 11-82, 1984.
- [34] S. K. O’Leary, S. R. Johnson, and P. K. Lim, “The relationship between the distribution of electronic states and the optical absorption spectrum of an amorphous semiconductor: An empirical analysis,” *Journal of Applied Physics*, vol. 82, no. 7, pp. 3334-3340, 1997.
- [35] L. Jiao, I. Chen, R. W. Collins, C. R. Wronski, and N. Hata, “An improved analysis for band edge optical absorption spectra in hydrogenated amorphous silicon from optical and photoconductivity measurements,” *Applied Physics Letters*, vol. 72, no. 9, pp.1057-1059, 1998.
- [36] S. K. O’Leary, “An analytical density of states and joint density of states analysis of amorphous semiconductors,” *Journal of Applied Physics*, vol. 96, no. 7, pp. 3680-3686, 2004.
- [37] S. M. Malik and S. K. O’Leary, “Optical transitions in hydrogenated amorphous silicon,” *Applied Physics Letters*, vol. 80, no. 5, pp. 790-792, 2002.
- [38] S. K. O’Leary and S. M. Malik, “A simplified joint density of states analysis of hydrogenated amorphous silicon,” *Journal of Applied Physics*, vol. 92, no. 8, pp. 4276-4282, 2002.

---

## CHAPTER 2

---

# The sensitivity of the optical response of hydrogenated amorphous silicon to variations in the conduction band tail breadth

*A version of this paper was published in Solid State Communications.*

*“Reprinted with permission from Thevaril, J.J. and O’Leary, S.K., The role that conduction band tail states play in determining the optical response of hydrogenated amorphous silicon, vol. 151, no. 7, pp. 730-733, Copyright [2011].”*

The following equations, introduced in this chapter, were introduced previously in this thesis:

Eq. (2.1)  $\Rightarrow$  Eq. (1.13)

Eq. (2.2)  $\Rightarrow$  Eq. (1.10)

Eq. (2.3)  $\Rightarrow$  Eq. (1.31)

Eq. (2.4)  $\Rightarrow$  Eq. (1.32)

Eq. (2.5)  $\Rightarrow$  Eq. (1.29)

Eq. (2.6)  $\Rightarrow$  Eq. (1.30)

Eq. (2.7)  $\Rightarrow$  Eq. (1.34)

## 2.1 Introduction

The optical response of hydrogenated amorphous silicon (a-Si:H) has been a focus for intensive investigation for many years [1–10]. Insights into this response have been gleaned through the development of models for the spectral dependence of the imaginary part of dielectric function associated with a-Si:H,  $\epsilon_2(\hbar\omega)$ . Such models serve two useful functions: 1) they provide a theoretical framework for the purposes of materials characterization, and 2) they allow for the quantitative prediction of device performance [11]. For the specific case of a-Si:H, Jackson *et al.* [12] suggest that

$$\epsilon_2(\hbar\omega) = 4.3 \times 10^{-45} \mathcal{R}^2(\hbar\omega) J(\hbar\omega), \quad (2.1)$$

where  $\mathcal{R}^2(\hbar\omega)$ , the normalized dipole matrix element squared average, is in units of  $\text{\AA}^2$ , and  $J(\hbar\omega)$ , the joint density of states (JDOS) function, is in units of  $\text{cm}^{-6}\text{eV}^{-1}$ .

At zero temperature,

$$J(\hbar\omega) \equiv \int_{-\infty}^{\infty} N_v(E) N_c(E + \hbar\omega) dE, \quad (2.2)$$

where  $N_v(E)$  and  $N_c(E)$  denote the valence band and conduction band density of states (DOS) functions, respectively,  $N_v(E) \Delta E$  and  $N_c(E) \Delta E$  representing the number of one-electron valence band and one-electron conduction band electronic states, between energies  $[E, E + \Delta E]$ , per unit volume.

Many of the empirical models that have been proposed for the spectral dependence of  $\epsilon_2(\hbar\omega)$  are themselves built upon empirical models for  $N_v(E)$  and  $N_c(E)$  [13]. Such models include that proposed by Tauc *et al.* [14] in 1966, Chen *et al.* [15] in 1981, Redfield [16] in 1982, Cody [17] in 1984, O’Leary *et al.* [18] in 1997, Jiao *et al.* [19] in 1998, O’Leary and Malik [20] in 2002, and O’Leary [21] in 2004. The empirical

model of O’Leary and Malik [20], reported in 2002, employs a simplified empirical model for  $N_v(E)$  and  $N_c(E)$  associated with a-Si:H, one that neglects the conduction band tail (CBT) electronic states; the valence band tail (VBT) electronic states were accounted for, however. It was shown that the resultant spectral dependence of  $\epsilon_2(\hbar\omega)$  agrees with that of experiment. In this paper, we aim to justify this neglect of the CBT states by O’Leary and Malik [20] for the case of a-Si:H, noting that while O’Leary and Malik [20] employ their simplified empirical model in order to fit some a-Si:H experimental data, an explicit justification for the neglect of the CBT states was not provided. The spectral dependence of the JDOS function,  $J(\hbar\omega)$ , provides the basis for our justification, as the optical response of a-Si:H is mostly shaped by the spectral dependence of the JDOS function,  $J(\hbar\omega)$ , the spectral dependence of  $\mathcal{R}^2(\hbar\omega)$  playing a relatively minor role [12, 22].

This paper is organized in the following manner. In Section 2.2, an analytical framework for our analysis is presented. In particular, an empirical model for the DOS functions is introduced and nominal a-Si:H modeling parameters are assigned. Then, in Section 2.3, we employ this empirical model for DOS functions in order to evaluate the corresponding JDOS function,  $J(\hbar\omega)$ . For the purposes of this analysis, we focus on examining the sensitivity of the JDOS function to variations in the conduction band tail breadth. Finally, the conclusions of our study are reported in Section 2.4.

## 2.2 Analytical framework

We cast our analysis within the framework of a general empirical model for the DOS functions,  $N_v(E)$  and  $N_c(E)$ , that captures the basic expected features. For the case of a-Si:H, there is general consensus that  $N_v(E)$  and  $N_c(E)$  exhibit square-root functional dependencies in the band regions and exponential functional dependencies

in the tail regions. Following O'Leary [21], we thus set

$$N_v(E) = N_{vo} \begin{cases} \sqrt{E_v - E_{vT}} \exp\left(\frac{E_{vT} - E_v}{\gamma_v}\right) \exp\left(\frac{E_v - E}{\gamma_v}\right), & E > E_{vT} \\ \sqrt{E_v - E}, & E \leq E_{vT} \end{cases}, \quad (2.3)$$

and

$$N_c(E) = N_{co} \begin{cases} \sqrt{E - E_c}, & E \geq E_{cT} \\ \sqrt{E_{cT} - E_c} \exp\left(\frac{E_c - E_{cT}}{\gamma_c}\right) \exp\left(\frac{E - E_c}{\gamma_c}\right), & E < E_{cT} \end{cases}, \quad (2.4)$$

where  $N_{vo}$  and  $N_{co}$  denote the valence band and conduction band DOS prefactors, respectively,  $E_v$  and  $E_c$  represent the valence band and conduction band band edges,  $\gamma_v$  and  $\gamma_c$  are the breadths of the valence band and conduction band tails,  $E_{vT}$  and  $E_{cT}$  being the critical energies at which the exponential and square-root distributions interface; it should be noted that this model implicitly requires that  $E_v - E_{vT} \geq 0$  and  $E_{cT} - E_c \geq 0$ . It is noted that this general empirical model for the DOS functions includes valence band band (VBB) states, VBT states, conduction band band (CBB) states, and CBT states. We further note that there are eight independent modeling parameters in this model, i.e.,  $N_{vo}$ ,  $N_{co}$ ,  $E_v$ ,  $E_c$ ,  $\gamma_v$ ,  $\gamma_c$ ,  $E_{vT}$ , and  $E_{cT}$ .<sup>1</sup> It is clear, from Eqs. (2.3) and (2.4), that both  $N_v(E)$  and  $N_c(E)$  are continuous functions of energy, i.e.,  $N_v(E_{vT}^-) = N_v(E_{vT}^+)$  and  $N_c(E_{cT}^-) = N_c(E_{cT}^+)$ .

In order to further narrow the scope of our analysis, we set  $E_{vT}$  to  $E_v - \gamma_v/2$  and

---

<sup>1</sup>Given that the valence band and conduction band band energies,  $E_v$  and  $E_c$ , respectively, are relative quantities, the number of truly independent modeling parameters for the general empirical DOS model, i.e., Eqs. (2.3) and (2.4), is actually seven.

set  $E_{c_T}$  to  $E_c + \gamma_c/2$ . With these settings, Eq. (2.3) reduces to

$$N_v(E) = N_{vo} \begin{cases} \sqrt{\frac{\gamma_v}{2}} \exp\left(-\frac{1}{2}\right) \exp\left(\frac{E_v - E}{\gamma_v}\right), & E > E_v - \frac{\gamma_v}{2} \\ \sqrt{E_v - E}, & E \leq E_v - \frac{\gamma_v}{2} \end{cases}, \quad (2.5)$$

and Eq. (2.4) reduces to

$$N_c(E) = N_{co} \begin{cases} \sqrt{E - E_c}, & E \geq E_c + \frac{\gamma_c}{2} \\ \sqrt{\frac{\gamma_c}{2}} \exp\left(-\frac{1}{2}\right) \exp\left(\frac{E - E_c}{\gamma_c}\right), & E < E_c + \frac{\gamma_c}{2} \end{cases}, \quad (2.6)$$

where now the number of independent modeling parameters has been reduced to six, i.e.,  $N_{vo}$ ,  $N_{co}$ ,  $E_v$ ,  $E_c$ ,  $\gamma_v$ , and  $\gamma_c$ .<sup>2</sup> We note that now the DOS functions,  $N_v(E)$  and  $N_c(E)$ , in addition to being continuous functions of energy, have derivatives that are continuous functions of energy when  $\gamma_v$  and  $\gamma_c$  are non-zero. We also note that for the special case that  $\gamma_c \rightarrow 0$ ,

$$N_c(E) \rightarrow N_{co} \begin{cases} \sqrt{E - E_c}, & E \geq E_c \\ 0, & E < E_c \end{cases}, \quad (2.7)$$

which is in accord with the simplified empirical DOS model of O'Leary and Malik [20], i.e., the CBT states are neglected. This empirical model for the DOS functions,  $N_v(E)$  and  $N_c(E)$ , i.e., Eqs. (2.5) and (2.6), forms the framework for our analysis. For the nominal a-Si:H modeling parameters,  $N_{vo} = N_{co} = 2 \times 10^{22} \text{ cm}^{-3} \text{ eV}^{-3/2}$ ,  $E_v = 0.0 \text{ eV}$ ,

---

<sup>2</sup>For this special case of the general empirical DOS model, i.e., Eqs. (2.5) and (2.6), the number of truly independent modeling parameters is actually five.

$E_c = 1.7$  eV,  $\gamma_v = 50$  meV, and  $\gamma_c = 27$  meV, the corresponding DOS functions are as depicted in Figure 2.1, these modeling parameter selections being representative of a-Si:H [13, 19–27]. These nominal a-Si:H modeling parameter selections, employed for the purposes of this analysis, are tabulated in Table 2.1.

**Table 2.1:** The nominal a-Si:H modeling parameter selections employed for the purposes of this analysis. These modeling parameters relate to Eqs. (2.5) and (2.6).

parameter (units)	value
$N_{vo}$ ( $\text{cm}^{-3}\text{eV}^{-3/2}$ )	$2 \times 10^{22}$
$N_{co}$ ( $\text{cm}^{-3}\text{eV}^{-3/2}$ )	$2 \times 10^{22}$
$E_v$ (eV)	0.0
$E_c$ (eV)	1.7
$\gamma_v$ (meV)	50
$\gamma_c$ (meV)	27

## 2.3 JDOS evaluation and analysis

We now evaluate the JDOS function,  $J(\hbar\omega)$ , corresponding to our empirical model for the DOS functions, i.e., with  $N_v(E)$  and  $N_c(E)$  as set in Eqs. (2.5) and (2.6), respectively. For the purposes of this analysis, we examine the sensitivity of this JDOS function to variations in the conduction band tail breadth,  $\gamma_c$ , the valence band tail breadth,  $\gamma_v$ , being fixed at its nominal a-Si:H value, i.e., 50 meV. The other modeling parameters are also set to their nominal a-Si:H values, i.e.,  $N_{vo} = N_{co} = 2 \times 10^{22} \text{ cm}^{-3}\text{eV}^{-3/2}$  and  $E_g \equiv E_c - E_v = 1.7$  eV;  $E_g$  may be referred to as the energy gap [21]. In Figure 2.2, we plot the spectral dependencies of the resultant JDOS functions,  $J(\hbar\omega)$ , for the  $\gamma_c$  selections 0, 35, and 50 meV. We note that in all cases, two regions of behavior are observed: 1) for  $\hbar\omega$  less than the band gap, the JDOS function exhibits an exponential functional dependence, and 2) for  $\hbar\omega$  greater than the band gap, the JDOS function exhibits an algebraic functional dependence. We also

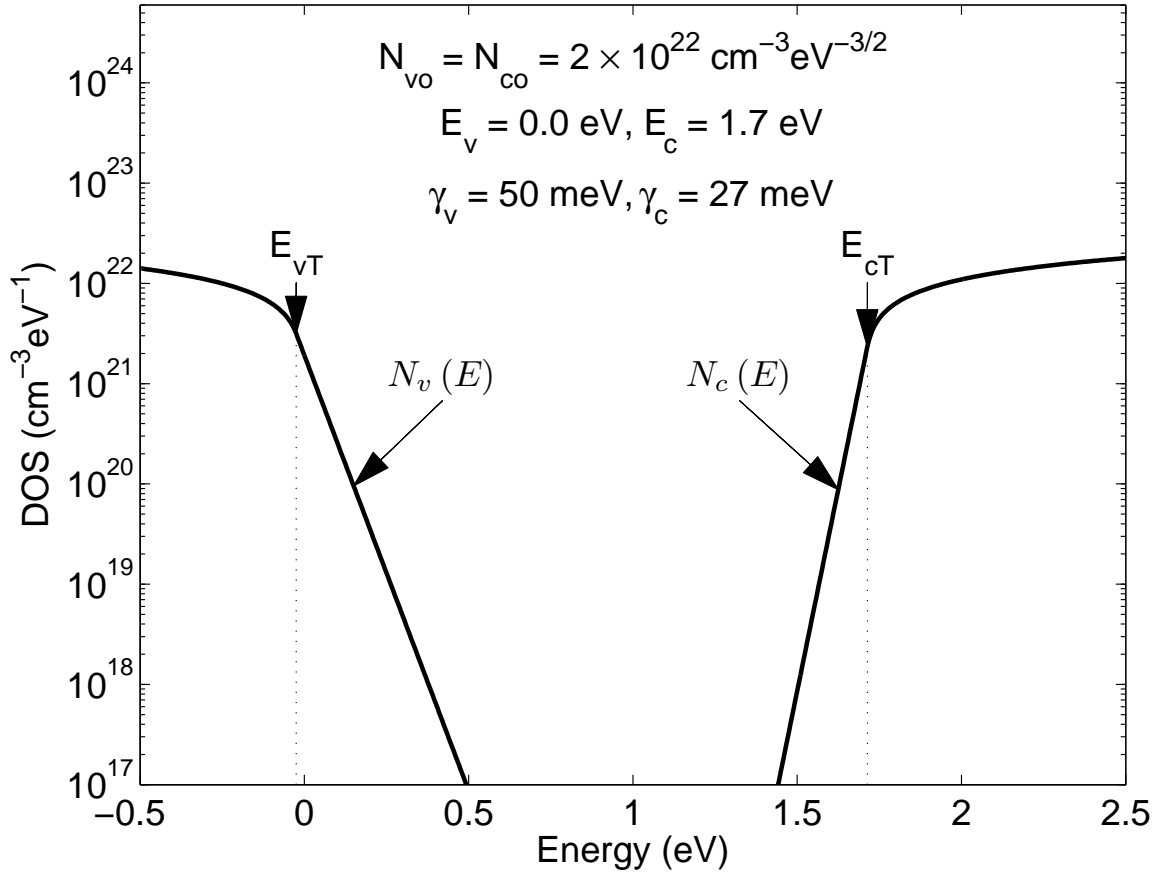


**Figure 2.1:** The valence band and conduction band DOS functions associated with a-Si:H. The valence band DOS function,  $N_v(E)$ , specified in Eq. (2.5), is determined assuming the nominal a-Si:H parameter selections  $N_{vo} = 2 \times 10^{22} \text{ cm}^{-3} \text{ eV}^{-3/2}$ ,  $E_v = 0.0 \text{ eV}$ , and  $\gamma_v = 50 \text{ meV}$ . The conduction band DOS function,  $N_c(E)$ , specified in Eq. (2.6), is determined assuming the nominal a-Si:H parameter selections  $N_{co} = 2 \times 10^{22} \text{ cm}^{-3} \text{ eV}^{-3/2}$ ,  $E_c = 1.7 \text{ eV}$ , and  $\gamma_c = 27 \text{ meV}$ . Only differences between the energies  $E_v$  and  $E_c$  will impact upon the obtained JDOS results. The critical points at which the band states and tail states interface,  $E_{vT}$  and  $E_{cT}$ , are clearly marked with the dotted lines and the arrows.

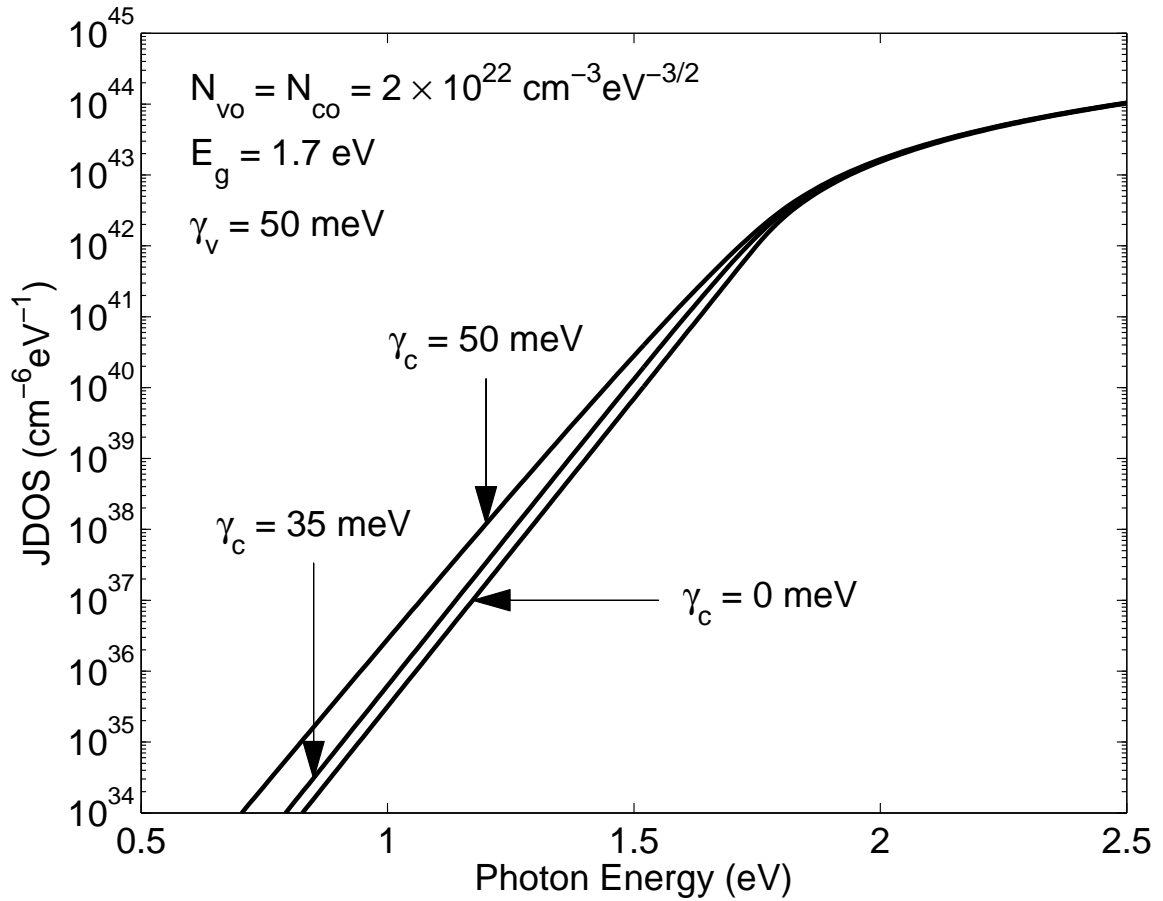


**Figure 2.2:** The JDOS function,  $J(\hbar\omega)$ , associated with a-Si:H, determined through an evaluation of Eq. (2.2), for various selections of  $\gamma_c$ . For all cases,  $N_{vo}$ ,  $N_{co}$ ,  $E_v$ ,  $E_c$ , and  $\gamma_v$  are held at their nominal a-Si:H values, i.e.,  $N_{vo} = N_{co} = 2 \times 10^{22} \text{ cm}^{-3} \text{ eV}^{-3/2}$ ,  $E_g \equiv E_c - E_v = 1.7 \text{ eV}$ , and  $\gamma_v = 50 \text{ meV}$ .

note that while the result corresponding to the  $\gamma_c = 0$  meV case, which corresponds to the simplified empirical DOS model of O’Leary and Malik [20], forms a lower bound, the result corresponding to the  $\gamma_c = 50$  meV case forms an upper bound, the result corresponding to the  $\gamma_c = 35$  meV case being sandwiched in between these bounds.

In order to further quantitatively examine the spectral dependence of the JDOS function, we follow the spirit of the analysis of Orapunt and O’Leary [28] and define the tail breadth as being the reciprocal of the logarithmic derivative of the JDOS function, i.e.,

$$E_o(\hbar\omega) \equiv \left[ \frac{d \ln [J(\hbar\omega)]}{d\hbar\omega} \right]^{-1}, \quad (2.8)$$

where we note that  $E_o$ , as defined, is a continuous function of the photon energy,  $\hbar\omega$ ; for an exact exponential tail, this tail breadth, as defined, corresponds to a single number, the exponential breadth, but any deviations from an exact exponential dependence will lead to a spectral dependence of  $E_o$ . For the same nominal a-Si:H modeling parameter selections employed in Figure 2.2, i.e.,  $N_{vo} = N_{co} = 2 \times 10^{22} \text{ cm}^{-3} \text{ eV}^{-3/2}$ ,  $E_g \equiv E_c - E_v = 1.7 \text{ eV}$ , and  $\gamma_v = 50 \text{ meV}$ , we plot the spectral dependence of  $E_o$  on the photon energy,  $\hbar\omega$ , for the three selections of  $\gamma_c$  considered in Figure 2.2, i.e., 0, 35, and 50 meV, in Figure 2.3. We note that for the case of  $\gamma_c$  set to 0 meV, that  $E_o$  remains fixed at 50 meV, i.e.,  $\gamma_v$ , until  $\hbar\omega$  exceeds  $E_c - E_{v_T}$ , beyond which it monotonically increases, this monotonic increase corresponding to the transition between the exponential and algebraic regions of the JDOS function, as was previously observed by Orapunt and O’Leary [28]. For the case of  $\gamma_c$  set to 35 meV, it is seen that while  $E_o$  asymptotically approaches 50 meV for low photon energies, it is also observed that for higher photon energies it increases monotonically with the photon energy, the transition between the exponential and algebraic regions being less abrupt than for the case of  $\gamma_c$  set to 0 meV. An even gentler transition between these regions

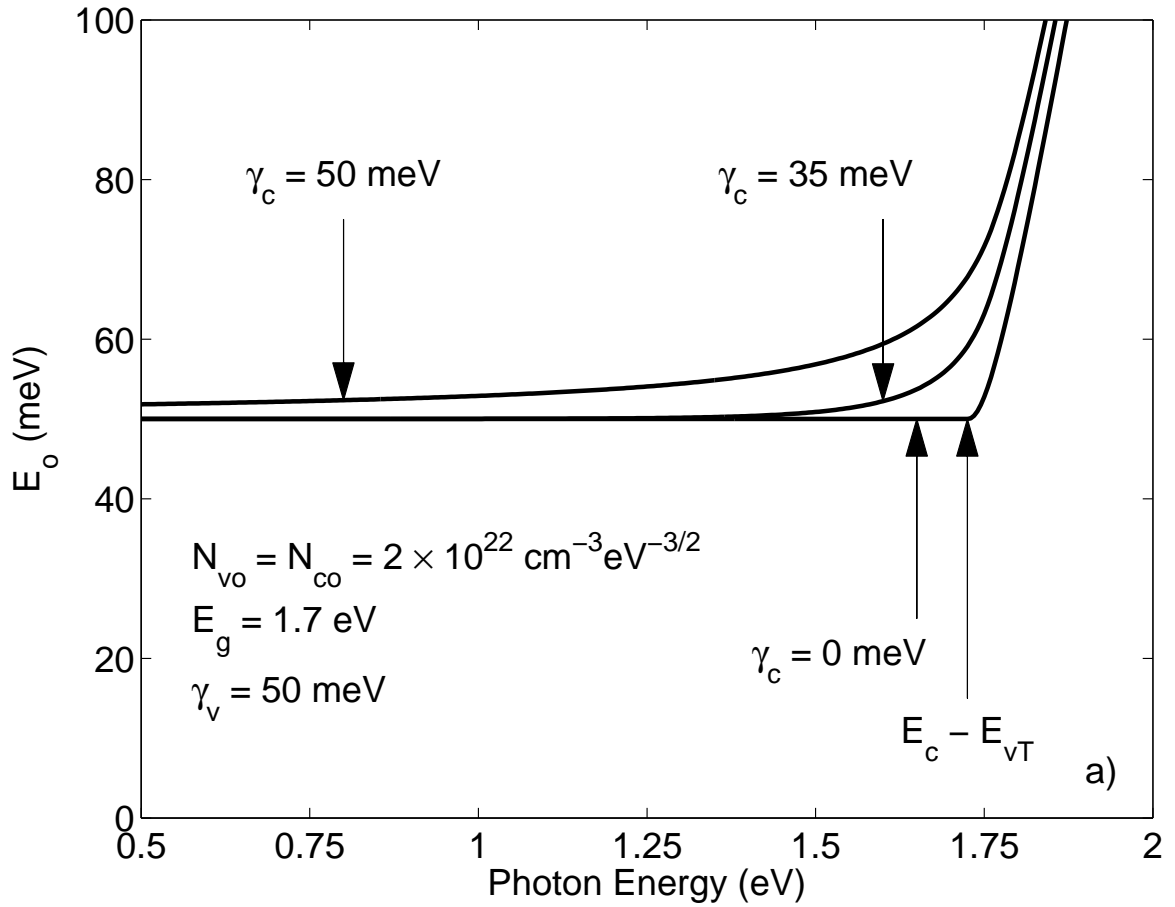


**Figure 2.3:** The dependence of  $E_o$ , as defined in Eq. (2.8), on the photon energy,  $\hbar\omega$ , for a number of selections of  $\gamma_c$ . For all cases,  $N_{vo}$ ,  $N_{co}$ ,  $E_v$ ,  $E_c$ , and  $\gamma_v$  are held at their nominal a-Si:H values, i.e.,  $N_{vo} = N_{co} = 2 \times 10^{22} \text{ cm}^{-3} \text{ eV}^{-3/2}$ ,  $E_g \equiv E_c - E_v = 1.7 \text{ eV}$ , and  $\gamma_v = 50 \text{ meV}$ .

is observed for the case of  $\gamma_c$  set to 50 meV.

We continue our analysis by examining the dependence of  $E_o$  on  $\gamma_c$  for a fixed value of the photon energy,  $\hbar\omega$ . In particular, for the nominal a-Si:H parameter selections, i.e.,  $N_{vo} = N_{co} = 2 \times 10^{22} \text{ cm}^{-3} \text{ eV}^{-3/2}$  and  $E_g \equiv E_c - E_v = 1.7 \text{ eV}$ , setting  $\gamma_v$  to 50 meV and  $\hbar\omega$  to 1 eV, we examine the dependence of  $E_o$  on  $\gamma_c$ . We plot this dependence in Figure 2.4. We note that  $E_o$  is essentially equal to 50 meV, i.e.,  $\gamma_v$ , until  $\gamma_c$  exceeds  $\gamma_v$ , beyond which  $E_o$  seems to asymptotically approach  $\gamma_c$ . This observation, and the symmetry in the JDOS function, suggests that an approximate analytical expression for  $E_o$  may be obtained by setting

$$E_o \simeq \max.(\gamma_v, \gamma_c). \quad (2.9)$$

We plot this approximate analytical expression for  $E_o$  in Figure 2.4 along with the corresponding exact result, noting that only when  $\gamma_v$  and  $\gamma_c$  are of comparable values that there is any noticeable deviation between the approximate and exact results. This suggests that when  $\gamma_c$  is less than  $\gamma_v$  that the use of a model for the DOS functions that neglects the presence of the CBT states, such as that devised by O'Leary and Malik [20], is justified in the characterization of the optical response.

For the specific case of a-Si:H, we note that the conduction band tail is narrower than the valence band tail. In Figure 2.5, for example, we plot experimentally determined values of  $\gamma_v$  and  $\gamma_c$  corresponding to a-Si:H. Experimental results from Sherman *et al.* [29], Tiedje *et al.* [30], and Winer and Ley [31], are employed for the purposes of this analysis. We also plot the  $\gamma_v$  and  $\gamma_c$  values obtained by O'Leary [13] through a fit with some a-Si:H  $\epsilon_2(\hbar\omega)$  experimental data. We note that in all cases the valence band tail breadth,  $\gamma_v$ , exceeds the corresponding conduction band tail breadth,  $\gamma_c$ , and in most cases by a considerably margin. This clearly demonstrates

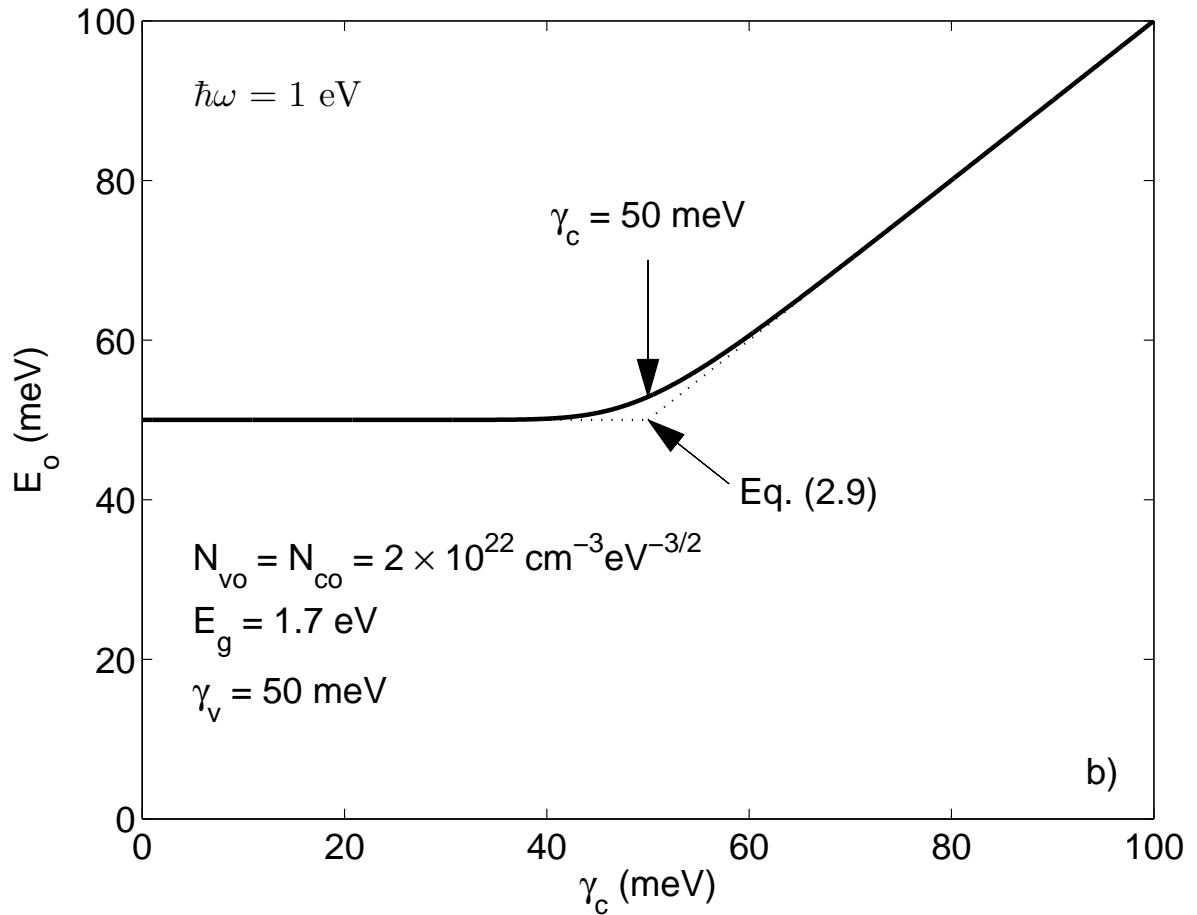


**Figure 2.4:** The dependence of  $E_o$ , as defined in Eq. (2.8), on the conduction band tail breadth,  $\gamma_c$ , for the photon energy,  $\hbar\omega$ , set to 1 eV. For all cases,  $N_{vo}$ ,  $N_{co}$ ,  $E_v$ ,  $E_c$ , and  $\gamma_v$  are held at their nominal a-Si:H values, i.e.,  $N_{vo} = N_{co} = 2 \times 10^{22} \text{ cm}^{-3} \text{ eV}^{-3/2}$ ,  $E_g \equiv E_c - E_v = 1.7$  eV, and  $\gamma_v = 50$  meV. The approximate analytical expression for  $E_o$ , i.e., Eq. (2.9), is also depicted with the dotted line.

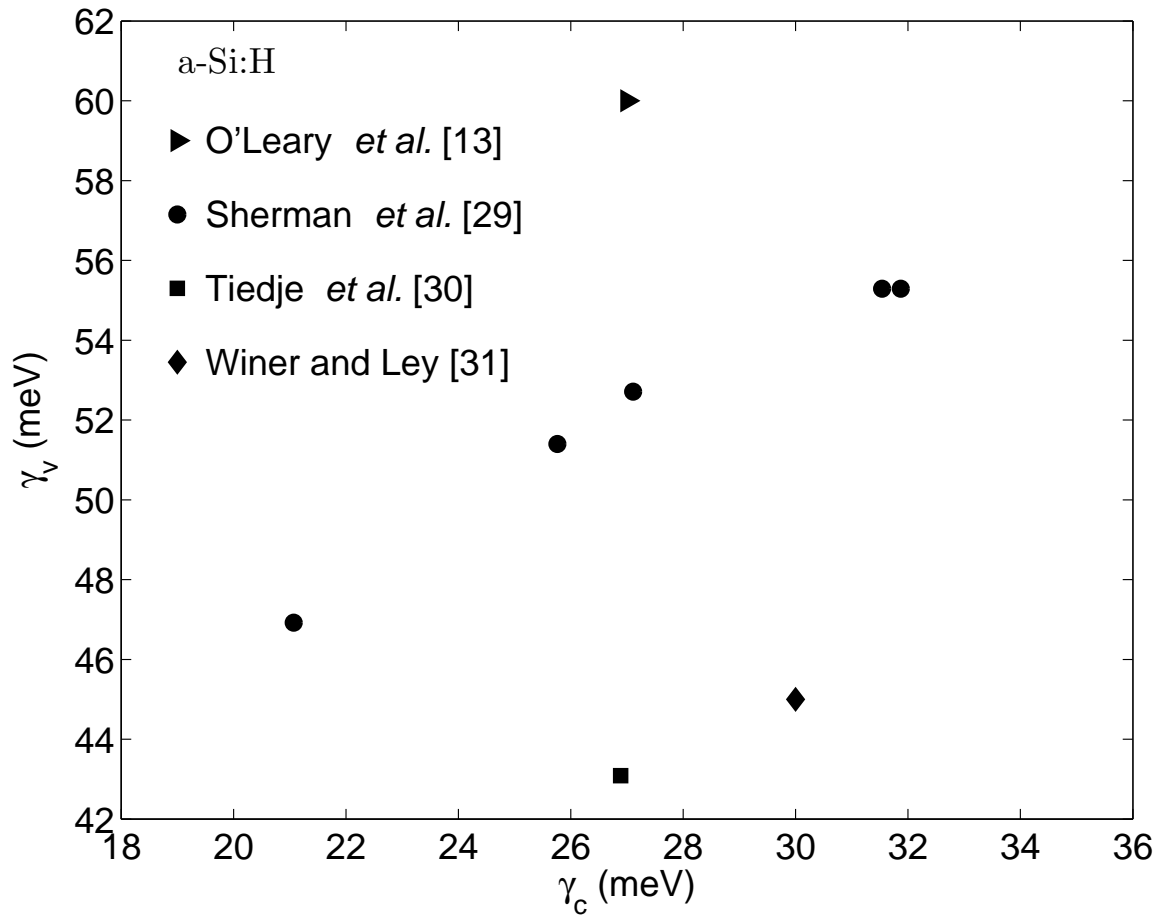


**Figure 2.5:** The dependence of  $\gamma_v$  on  $\gamma_c$ . Results from the experiments of Sherman *et al.* [29], Tiedje *et al.* [30], and Winer and Ley [31], are depicted. Results obtained from the modeling analysis of O'Leary [13] are also shown.

that, as far as the determination of the optical response is concerned, that the neglect of the CBT states is justified for the case of a-Si:H. This justifies the use of the simplified empirical DOS model of O’Leary and Malik [20] for the analysis of the optical response of this material.

## 2.4 Conclusion

In conclusion, through the use of a general empirical model for the DOS functions, one that considers VBB, VBT, CBB, and CBT states, we examined the sensitivity of the JDOS function to variations in the conduction band tail breadth,  $\gamma_c$ , all other parameters being held fixed at the nominal a-Si:H values. We found that when the conduction band tail is narrower than the valence band tail, its role in shaping the corresponding spectral dependence of the JDOS function is relatively minor. This justifies the use of a simplified empirical model for the DOS functions that neglects the presence of the CBT states, such as that devised by O’Leary and Malik [20], in the characterization of the optical response. Experimental data corresponding to a-Si:H, demonstrating that  $\gamma_c$  is less than  $\gamma_v$ , is presented, thereby justifying the use of this simplified empirical DOS model for the analysis of the optical response of this material.

**Acknowledgements:** The authors gratefully acknowledge financial support from the Natural Sciences and Engineering Research Council of Canada. The use of equipment granted from the Canada Foundation for Innovation and equipment loaned from the Canadian Microelectronics Corporation is also acknowledged.

## References

- [1] M. H. Brodsky, R. S. Title, K. Weiser, and G. D. Pettit, "Structural, optical, and electrical properties of amorphous silicon films," *Physical Review B*, vol. 1, no. 6, pp. 2632-2641, 1970.
- [2] E. C. Freeman and W. Paul, "Optical constants of rf sputtered hydrogenated amorphous Si," *Physical Review B*, vol. 20, no. 2, pp. 716-728, 1979.
- [3] T. Datta and J. A. Woollam, "Generalized model for the optical absorption edge in a-Si:H," *Physical Review B*, vol. 39, no. 3, pp. 1953-1954, 1989.
- [4] S. K. O'Leary, S. Zukotynski, and J. M. Perz, "Semiclassical density-of-states and optical-absorption analysis of amorphous semiconductors," *Physical Review B*, vol. 51, no. 7, pp. 4143-4149, 1995.
- [5] S. K. O'Leary, S. Zukotynski, and J. M. Perz, "Optical absorption in amorphous semiconductors," *Physical Review B*, vol. 52, no. 11, pp. 7795-7797, 1995.
- [6] S. K. O'Leary, "Optical absorption, disorder, and the disorderless limit in amorphous semiconductors," *Applied Physics Letters*, vol. 72, no. 11, pp. 1332-1334, 1998.
- [7] B. J. Fogal, S. K. O'Leary, D. J. Lockwood, J.-M. Baribeau, M. Noël, and J. C. Zwinkels, "Disorder and the optical properties of amorphous silicon grown by molecular beam epitaxy," *Solid State Communications*, vol. 120, no. 11, pp. 429-434, 2001.
- [8] S. K. O'Leary, B. J. Fogal, D. J. Lockwood, J.-M. Baribeau, M. Noël, and J. C. Zwinkels, "Optical dispersion relationships in amorphous silicon grown by molecular beam epitaxy," *Journal of Non-Crystalline Solids*, vol. 290, no. 1, pp. 57-63, 2001.
- [9] D. J. Lockwood, J.-M. Baribeau, M. Noël, J. C. Zwinkels, B. J. Fogal, and S. K. O'Leary, "Optical absorption in an amorphous silicon superlattice grown by molecular beam epitaxy," *Solid State Communications*, vol. 122, no. 5, pp. 271-275, 2002.
- [10] L.-L. Tay, D. J. Lockwood, J.-M. Baribeau, M. Noël, J. C. Zwinkels, F. Orapunt, and S. K. O'Leary, "Influence of growth temperature on order within silicon films grown by ultrahigh-vacuum evaporation on silica," *Applied Physics Letters*, vol. 88, no. 12, pp. 121920-1-3, 2006.
- [11] A. S. Ferlauto, G. M. Ferreira, J. M. Pearce, C. R. Wronski, R. W. Collins, X. Deng, and G. Ganguly, "Analytical model for the optical functions of amorphous semiconductors from the near-infrared to ultraviolet: Applications in thin film photovoltaics," *Journal of Applied Physics*, vol. 92, no. 5, pp. 2424-2436, 2002.

- [12] W. B. Jackson, S. M. Kelso, C. C. Tsai, J. W. Allen, and S.-J. Oh, “Energy dependence of the optical matrix element in hydrogenated amorphous and crystalline silicon,” *Physical Review B*, vol. 31, no. 8, pp. 5187-5198, 1985.
- [13] S. K. O’Leary, “An empirical density of states and joint density of states analysis of hydrogenated amorphous silicon: a review,” *Journal of Materials Science: Materials in electronics*, vol. 15, pp. 401-410, 2004.
- [14] J. Tauc, R. Grigorovici, and A. Vancu, “Optical properties and electronic structure of amorphous germanium,” *Physica Status Solidi*, vol. 15, no. 2, pp. 627-637, 1966.
- [15] W.-C. Chen, B. J. Feldman, J. Bajaj, F.-M. Tong, and G. K. Wong, “Thermalization gap excitation photoluminescence and optical absorption in amorphous silicon-hydrogen alloys,” *Solid State Communications*, vol. 38, no. 5, pp. 357-363, 1981.
- [16] D. Redfield, “Energy-band tails and the optical absorption edge; The case of a-Si:H,” *Solid State Communications*, vol. 44, no. 9, pp. 1347-1349, 1982.
- [17] G. D. Cody, in *Hydrogenated Amorphous Silicon*, vol. 21B of *Semiconductors and Semimetals*, edited by J. I. Pankove (Academic, New York, 1984), pp. 11-82, 1984.
- [18] S. K. O’Leary, S. R. Johnson, and P. K. Lim, “The relationship between the distribution of electronic states and the optical absorption spectrum of an amorphous semiconductor: An empirical analysis,” *Journal of Applied Physics*, vol. 82, no. 7, pp. 3334-3340, 1997.
- [19] L. Jiao, I. Chen, R. W. Collins, C. R. Wronski, and N. Hata, “An improved analysis for band edge optical absorption spectra in hydrogenated amorphous silicon from optical and photoconductivity measurements,” *Applied Physics Letters*, vol. 72, no. 9, pp. 1057-1059, 1998.
- [20] S. K. O’Leary and S. M. Malik, “A simplified joint density of states analysis of hydrogenated amorphous silicon,” *Journal of Applied Physics*, vol. 92, no. 8, pp. 4276-4282, 2002.
- [21] S. K. O’Leary, “An analytical density of states and joint density of states analysis of amorphous semiconductors,” *Journal of Applied Physics*, vol. 96, no. 7, pp. 3680-3686, 2004.
- [22] S. K. O’Leary, “Spectral dependence of the squared average optical transition matrix element associated with hydrogenated amorphous silicon,” *Applied Physics Letters*, vol. 82, no. 17, pp. 2784-2786, 2003.

- [23] S. M. Malik and S. K. O’Leary, “Optical transitions in hydrogenated amorphous silicon,” *Applied Physics Letters*, vol. 80, no. 5, pp. 790-792, 2002.
- [24] S. M. Malik and S. K. O’Leary, “Deviations from square-root distributions of electronic states in hydrogenated amorphous silicon and their impact upon the resultant optical properties,” *Journal of Non-Crystalline Solids*, vol. 336, no. 1, pp. 64-70, 2004.
- [25] S. M. Malik and S. K. O’Leary, “An analysis of the distributions of electronic states associated with hydrogenated amorphous silicon,” *Journal of Materials Science: Materials in Electronics*, vol. 16, no. 3, pp. 177-181, 2005.
- [26] T. M. Mok and S. K. O’Leary, “The dependence of the Tauc and Cody optical gaps associated with hydrogenated amorphous silicon on the film thickness: *al* experimental limitations and the impact of curvature in the Tauc and Cody plots,” *Journal of Applied Physics*, vol. 102, no. 11, pp. 113525-1-9, 2007.
- [27] F. Orapunt and S. K. O’Leary, “Optical transitions and the mobility edge in amorphous semiconductors: A joint density of states analysis,” *Journal of Applied Physics*, vol. 104, no. 7, pp. 073513-1-6, 2008.
- [28] F. Orapunt and S. K. O’Leary, “A quantitative characterization of the optical absorption spectrum associated with hydrogenated amorphous silicon,” *Journal of Materials Science: Materials in Electronics*, vol. 20, no. 10, pp. 1033-1038, 2009.
- [29] S. Sherman, S. Wagner, and R. A. Gottscho, “Correlation between the valence- and conduction-band-tail energies in hydrogenated amorphous silicon,” *Applied Physics Letters*, vol. 69, no. 21, pp. 3242-3244, 1996.
- [30] T. Tiedje, J. M. Cebulka, D. L. Morel, and B. Abeles, “Evidence for exponential band tails in amorphous silicon hydride,” *Applied Review Letters*, vol. 46, no. 21, pp. 1425-1428, 1981.
- [31] K. Winer and L. Ley, “Surface states and the exponential valence-band tail in a-Si:H,” *Physical Review B*, vol. 36, no. 11, pp. 6072-6078, 1987.

---

## CHAPTER 3

---

# A dimensionless joint density of states formalism for the quantitative characterization of the optical response of hydrogenated amorphous silicon

*A version of this paper was published in the Journal of Applied Physics and is reproduced with permission from the American Institute of Physics.*

*“Reprinted with permission from Thevaril, J.J. and O’Leary, S.K., A dimensionless joint density of states formalism for the quantitative characterization of the optical response of hydrogenated amorphous silicon, vol. 107, no. 8, pp. 083105-1-6, Copyright [2010], American Institute of Physics.”*

The following equations, introduced in this chapter, were introduced previously in this thesis:

Eq. (3.1)  $\Rightarrow$  Eq. (1.13)

Eq. (3.2)  $\Rightarrow$  Eq. (1.10)

Eq. (3.3)  $\Rightarrow$  Eq. (1.37)

Eq. (3.4)  $\Rightarrow$  Eq. (1.38)

Eq. (3.5)  $\Rightarrow$  Eq. (1.33)

### 3.1 Introduction

Models for the spectral dependence of the imaginary part of the dielectric function associated with hydrogenated amorphous silicon (a-Si:H),  $\epsilon_2(\hbar\omega)$ , serve two useful functions: 1) they provide a theoretical framework for the purposes of materials characterization, and 2) they allow for the quantitative prediction of device performance [1]. For the specific case of a-Si:H, Jackson *et al.* [2] suggest that

$$\epsilon_2(\hbar\omega) = 4.3 \times 10^{-45} \mathcal{R}^2(\hbar\omega) J(\hbar\omega), \quad (3.1)$$

where  $\mathcal{R}^2(\hbar\omega)$ , the normalized dipole matrix element squared average, is in units of  $\text{\AA}^2$ , and  $J(\hbar\omega)$ , the joint density of states (JDOS) function, is in units of  $\text{cm}^{-6}\text{eV}^{-1}$ . At zero temperature,

$$J(\hbar\omega) \equiv \int_{-\infty}^{\infty} N_v(E) N_c(E + \hbar\omega) dE, \quad (3.2)$$

where  $N_v(E)$  and  $N_c(E)$  denote the valence band and conduction band density of states (DOS) functions, respectively,  $N_v(E) \Delta E$  and  $N_c(E) \Delta E$  representing the number of one-electron valence band and one-electron conduction band electronic states, between energies  $[E, E + \Delta E]$ , per unit volume [3].<sup>1</sup> Many of the empirical models that have been proposed for the spectral dependence of  $\epsilon_2(\hbar\omega)$  are themselves built upon empirical models for  $N_v(E)$  and  $N_c(E)$  [4]. Such models include that proposed by Tauc *et al.* [5] in 1966, Chen *et al.* [6] in 1981, Redfield [7] in 1982, Cody [8] in 1984, O'Leary *et al.* [9] in 1997, Jiao *et al.* [10] in 1998, O'Leary and

---

<sup>1</sup>The JDOS function,  $J(\hbar\omega)$ , as defined in Eq. (3.2), is in accord with the formalism of Jackson *et al.* [2], which was specifically introduced for the case of amorphous semiconductors; Eq. (6) of Jackson *et al.* [2] is Eq. (3.2) of this paper. It should not be confused with the JDOS function that is often used in the analysis of crystalline semiconductors, as has been pointed out by Singh and Shimakawa [3].

Malik [11] in 2002, and O’Leary [12] in 2004.

In 2002, O’Leary and Malik [11] proposed a simplified empirical model for  $N_v(E)$  and  $N_c(E)$  associated with a-Si:H, one that neglects the conduction band tail electronic states; the valence band tail electronic states were accounted for, however. It was shown that the resultant spectral dependence of  $\epsilon_2(\hbar\omega)$  agrees with that of experiment. In this paper, we aim to further simplify this empirical model for the DOS functions, reducing the number of independent modeling parameters from the six of the simplified model of O’Leary and Malik [11] to five. In doing so, we aim to provide a more elementary and effective platform for the determination of the underlying modeling parameters from experiment; the reduction in the number of independent modeling parameters restricts the parameter space that must be probed when extracting the underlying modeling parameters from the results of experiment, thereby simplifying matters. In addition, we find that we are able to cast our analysis into a dimensionless JDOS framework. We justify our simplification by demonstrating, for reasonable a-Si:H modeling parameter selections, that the JDOS spectrum obtained using our further simplified model is very similar to that determined using the more general model of O’Leary and Malik [11]. We then show that this further simplified model is as effective as its predecessor in capturing the results of experiment. Finally, we demonstrate the utility of our dimensionless JDOS formalism, using it for the purposes of performing a critical comparative analysis of three different a-Si:H optical absorption data sets.

This paper is organized in the following manner. In Section 3.2, an empirical model for the DOS functions associated with a-Si:H will be presented, this model forming the basis for our subsequent analysis. Then, in Section 3.3, we employ this model in order to compute the JDOS function,  $J(\hbar\omega)$ , casting our results into a dimensionless format. The demonstration that our formalism is as effective as its

predecessor in capturing the results of experiment is provided in Section 3.4, the focus of our analysis being the spectral dependence of the imaginary part of the dielectric function,  $\epsilon_2(\hbar\omega)$ , corresponding to a-Si:H. In Section 3.5, we employ our dimensionless JDOS formalism in order to perform a critical comparative analysis of three different a-Si:H optical absorption data sets. Finally, conclusions are drawn in Section 3.6.

## 3.2 Modeling the distribution of electronic states

For the case of a-Si:H, there is general consensus that  $N_v(E)$  and  $N_c(E)$  exhibit square-root functional dependencies in the band regions and exponential functional dependencies in the tail regions. Noting, for the specific case of a-Si:H, that the conduction band tail is considerably narrower than the valence band tail, O’Leary and Malik [11] proposed a simplified empirical model for the DOS functions that neglects conduction band tail electronic states. Building upon the earlier work of O’Leary *et al.* [9] and Jiao *et al.* [10], O’Leary and Malik [11] set

$$N_v(E) = N_{vo} \begin{cases} \sqrt{E_v - E_{vT}} \exp\left(\frac{E_{vT} - E_v}{\gamma_v}\right) \exp\left(\frac{E_v - E}{\gamma_v}\right), & E > E_{vT} \\ \sqrt{E_v - E}, & E \leq E_{vT} \end{cases}, \quad (3.3)$$

and

$$N_c(E) = N_{co} \begin{cases} \sqrt{E - E_c}, & E \geq E_c \\ 0, & E < E_c \end{cases}, \quad (3.4)$$

where  $N_{vo}$  and  $N_{co}$  denote the valence band and conduction band DOS prefactors, respectively,  $E_v$  and  $E_c$  represent the valence band and conduction band band edges,  $\gamma_v$  is the breadth of the valence band tail, and  $E_{vT}$  is the critical energy at which

the exponential and square-root distributions interface; this model implicitly requires that  $E_v - E_{v_T} > 0$ . Note that there are six independent modeling parameters in this model, i.e.,  $N_{vo}$ ,  $N_{co}$ ,  $E_v$ ,  $E_c$ ,  $\gamma_v$ , and  $E_{v_T}$ .<sup>2</sup> It is clear, from Eqs. (3.3) and (3.4), that  $N_v(E)$  and  $N_c(E)$  are continuous functions of energy, i.e.,  $N_v(E_{v_T}^-) = N_v(E_{v_T}^+)$  and  $N_c(E_c^-) = N_c(E_c^+)$ .

We can further simplify Eq. (3.3) by assuming that the derivative of  $N_v(E)$  is continuous at energy  $E_{v_T}$ , i.e.,  $N'_v(E_{v_T}^-) = N'_v(E_{v_T}^+)$ ; thus both  $N_v(E)$  and its derivative are continuous functions of energy. This will only occur if  $E_{v_T} = E_v - \frac{1}{2}\gamma_v$ . We note that under this condition, the number of independent modeling parameters is now reduced by one, i.e., the independent modeling parameters are now  $N_{vo}$ ,  $N_{co}$ ,  $E_v$ ,  $E_c$ , and  $\gamma_v$ .<sup>3</sup> In Figure 3.1, we plot the valence band DOS function,  $N_v(E)$ , as set in Eq. (3.3) with  $E_{v_T}$  set to  $E_v - \frac{1}{2}\gamma_v$ , for a number of selections of the valence band tail breadth,  $\gamma_v$ , for the nominal valence band modeling parameter selections  $N_{vo} = 2 \times 10^{22} \text{ cm}^{-3}\text{eV}^{-3/2}$  and  $E_v = 0 \text{ eV}$ . We note that as  $\gamma_v \rightarrow 0$ , that the valence band DOS function reduces to a square-root distribution, i.e., it reduces to the empirical DOS model of Tauc *et al.* [5]. That is,

$$N_v(E) \rightarrow N_{vo} \begin{cases} 0, & E > E_v \\ \sqrt{E_v - E}, & E \leq E_v \end{cases}. \quad (3.5)$$

---

<sup>2</sup>Given that the valence band and conduction band energies,  $E_v$  and  $E_c$ , respectively, are relative quantities, the number of truly independent modeling parameters in the simplified empirical DOS model of O'Leary and Malik [11], i.e., Eqs. (3.3) and (3.4), is five.

<sup>3</sup>For this further simplified empirical DOS model, i.e., Eqs. (3.3) and (3.4) with  $E_{v_T}$  set to  $E_v - \frac{1}{2}\gamma_v$ , the number of truly independent modeling parameters is four.

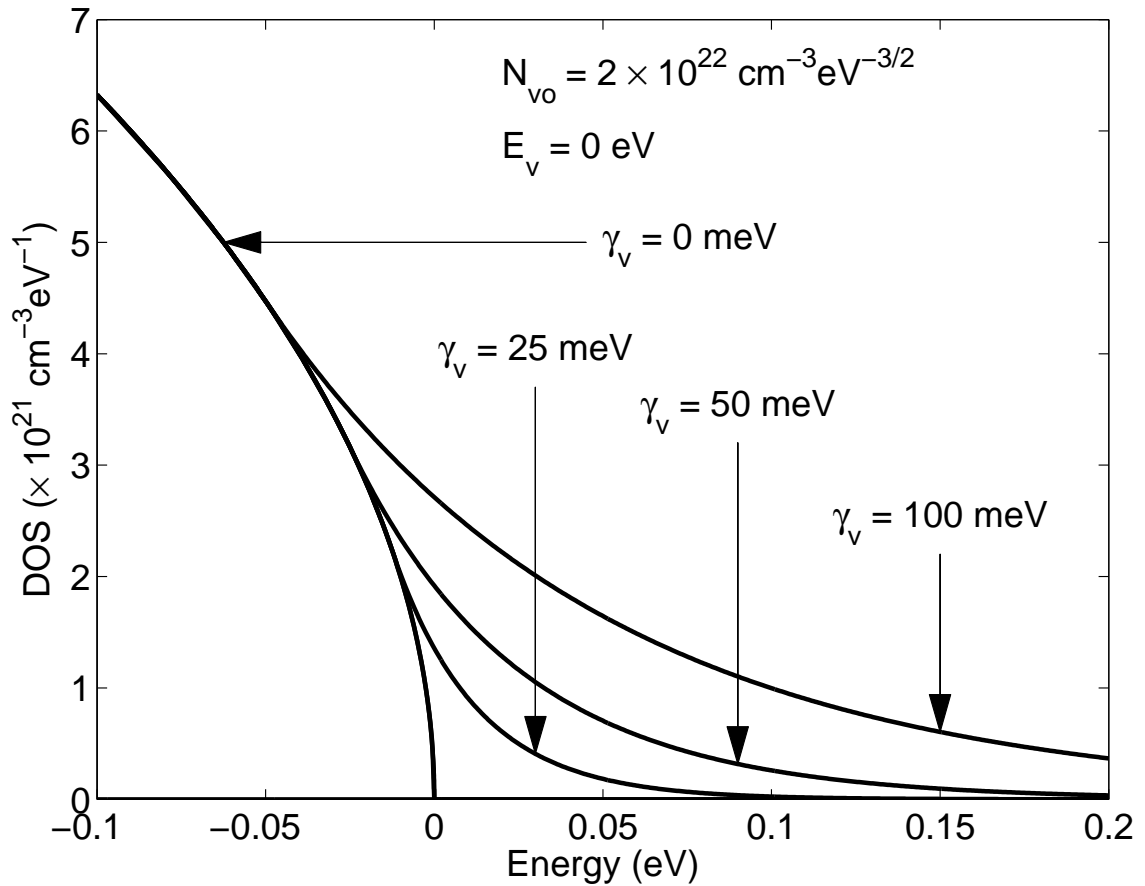


**Figure 3.1:** The valence band DOS function,  $N_v(E)$ , for a number of selections of  $\gamma_v$ . This function, specified in Eq. (3.3) with  $E_{vT}$  set to  $E_v - \frac{1}{2}\gamma_v$ , is evaluated assuming the nominal modeling parameter selections  $N_{vo} = 2 \times 10^{22} \text{ cm}^{-3} \text{ eV}^{-3/2}$  and  $E_v = 0 \text{ eV}$  for all cases. The abscissa axis represents the energy,  $E$ , while the ordinate axis depicts the corresponding valence band DOS value.

### 3.3 JDOS formalism

We now evaluate the JDOS function,  $J(\hbar\omega)$ , corresponding to our further simplified empirical DOS model, i.e., with  $N_v(E)$  and  $N_c(E)$  as set in Eqs. (3.3) and (3.4), respectively, with  $E_{v_T}$  set to  $E_v - \frac{1}{2}\gamma_v$ . From Eqs. (3.2), (3.3), and (3.4), with  $E_{v_T}$  set to  $E_v - \frac{1}{2}\gamma_v$ , it may be shown that

$$J(\hbar\omega) = N_{vo}N_{co}\gamma_v^2 \mathcal{J}\left(\frac{\hbar\omega - E_g}{\gamma_v}\right), \quad (3.6)$$

where the energy gap,  $E_g \equiv E_c - E_v$ , and the dimensionless JDOS function

$$\mathcal{J}(z) \equiv \begin{cases} z^2 \Xi\left(\frac{z - \frac{1}{2}}{z}\right) + \frac{1}{\sqrt{2}} \exp\left(z - \frac{1}{2}\right) \mathcal{Y}\left(z - \frac{1}{2}\right), & z \geq \frac{1}{2} \\ \frac{1}{\sqrt{2}} \exp\left(z - \frac{1}{2}\right) \mathcal{Y}(0), & z < \frac{1}{2} \end{cases}, \quad (3.7)$$

where  $\Xi(\cdot)$  and  $\mathcal{Y}(\cdot)$  are as defined in O'Leary and Malik [11], i.e.,

$$\Xi(z) \equiv \int_0^z \sqrt{x} \sqrt{1-x} dx, \quad (3.8)$$

and

$$\mathcal{Y}(z) \equiv \int_z^\infty \sqrt{x} \exp(-x) dx; \quad (3.9)$$

O'Leary and Malik [11] demonstrated that

$$\Xi(z) = \frac{1}{4} \sin^{-1}(\sqrt{z}) - \frac{1}{4} \sqrt{z} \sqrt{1-z} [1 - 2z], \quad (3.10)$$

and

$$\mathcal{Y}(z) = \sqrt{z} \exp(-z) + \frac{\sqrt{\pi}}{2} \operatorname{erfc}(\sqrt{z}), \quad (3.11)$$

where the complimentary error function

$$\operatorname{erfc}(z) \equiv \frac{2}{\sqrt{\pi}} \int_z^{\infty} \exp(-u^2) du. \quad (3.12)$$

This dimensionless JDOS function,  $\mathcal{J}(z)$ , offers a dimensionless framework for the evaluation of the JDOS function,  $J(\hbar\omega)$ . We plot this dimensionless JDOS function, as a function of its argument, in Figure 3.2. Note that while there may be five independent modeling parameters, the JDOS function itself is a function of only four independent modeling parameters, i.e.,  $N_{vo}$ ,  $N_{co}$ ,  $E_g$ , and  $\gamma_v$ .<sup>4</sup>

In order to assess the impact of setting  $E_{v_T} = E_v - \frac{1}{2}\gamma_v$ , within the framework of the simplified model of O’Leary and Malik [11], we examine the sensitivity of the JDOS function to variations in the selection of  $E_{v_T}$ . The nominal modeling parameter selections  $N_{vo} = N_{co} = 2 \times 10^{22} \text{ cm}^{-3} \text{ eV}^{-3/2}$ ,  $E_g = 1.7 \text{ eV}$ , and  $\gamma_v = 50 \text{ meV}$  are adopted for the purposes of this analysis, these modeling parameter selections being representative of a-Si:H [4, 10, 11, 13–16]. In Figure 3.3, we plot the resultant JDOS spectra, corresponding to a number of  $E_{v_T}$  selections, these  $E_{v_T}$  selections spanning the range of values found for a-Si:H; in fitting some a-Si:H experimental data, O’Leary [4] found that  $E_{v_T} = E_v - 4.3 \text{ meV}$  (for  $\gamma_v = 60 \text{ meV}$ ), i.e.,  $E_{v_T} = E_v - 0.07\gamma_v$ , while Jiao *et al.* [10] found that  $E_{v_T} = E_v - 35 \text{ meV}$  (for  $\gamma_v = 50 \text{ meV}$ ), i.e.,  $E_{v_T} = E_v - 0.7\gamma_v$ . We observe, for all selections of  $E_{v_T}$  considered, that the JDOS result corresponding to setting  $E_{v_T} = E_v - \frac{1}{2}\gamma_v$  forms an upper bound to all of the other JDOS functions; we considered a large number of  $E_{v_T}$  selections, not just the ones represented in Figure 3.3, and found this to be the case for all the selections we made. We find only minor differences in the JDOS functions corresponding to these  $E_{v_T}$  selections. Quantitatively, the JDOS function corresponding to  $E_{v_T}$  set to

---

<sup>4</sup>For this further simplified empirical DOS model, i.e., Eqs. (3.3) and (3.4) with  $E_{v_T}$  set to  $E_v - \frac{1}{2}\gamma_v$ , the number of truly independent modeling parameters is four.

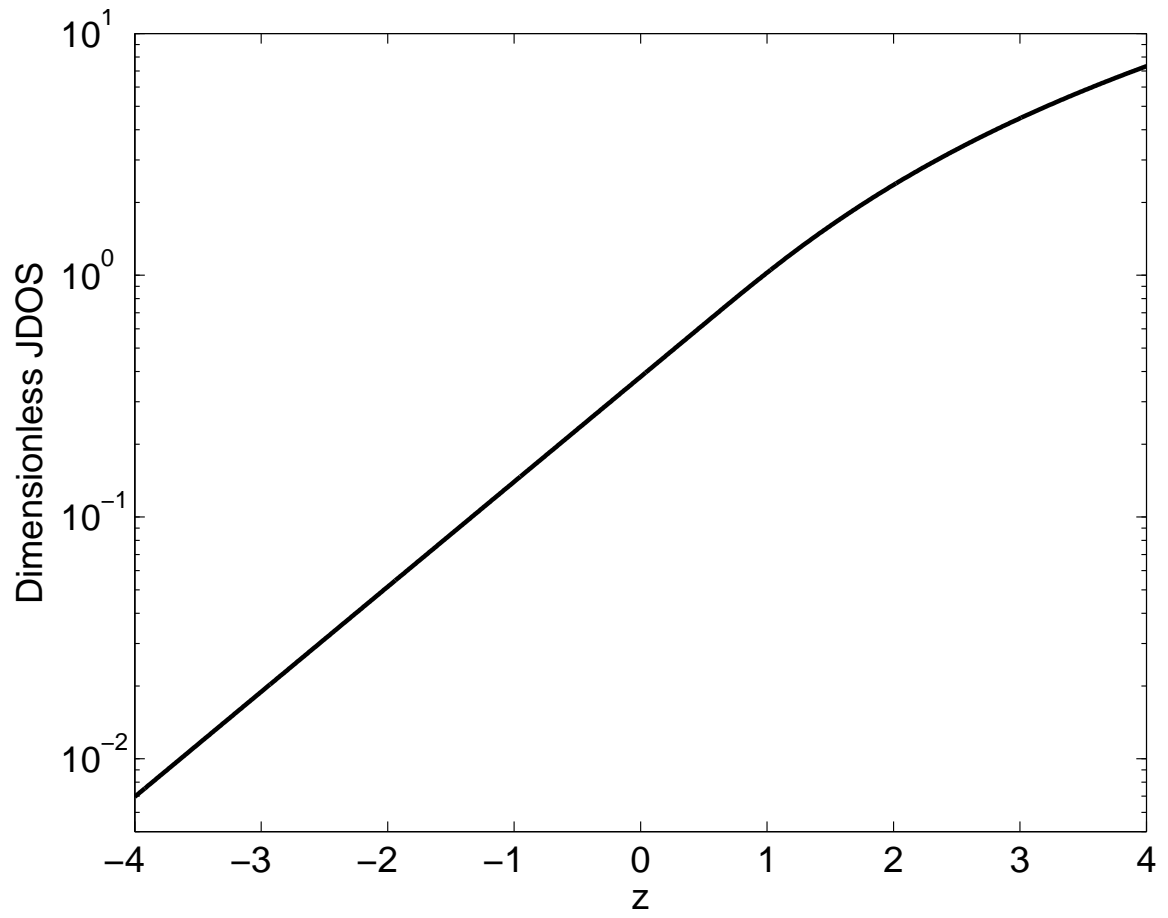


**Figure 3.2:** The dimensionless JDOS function,  $\mathcal{J}(z)$ , plotted as a function of  $z$ .

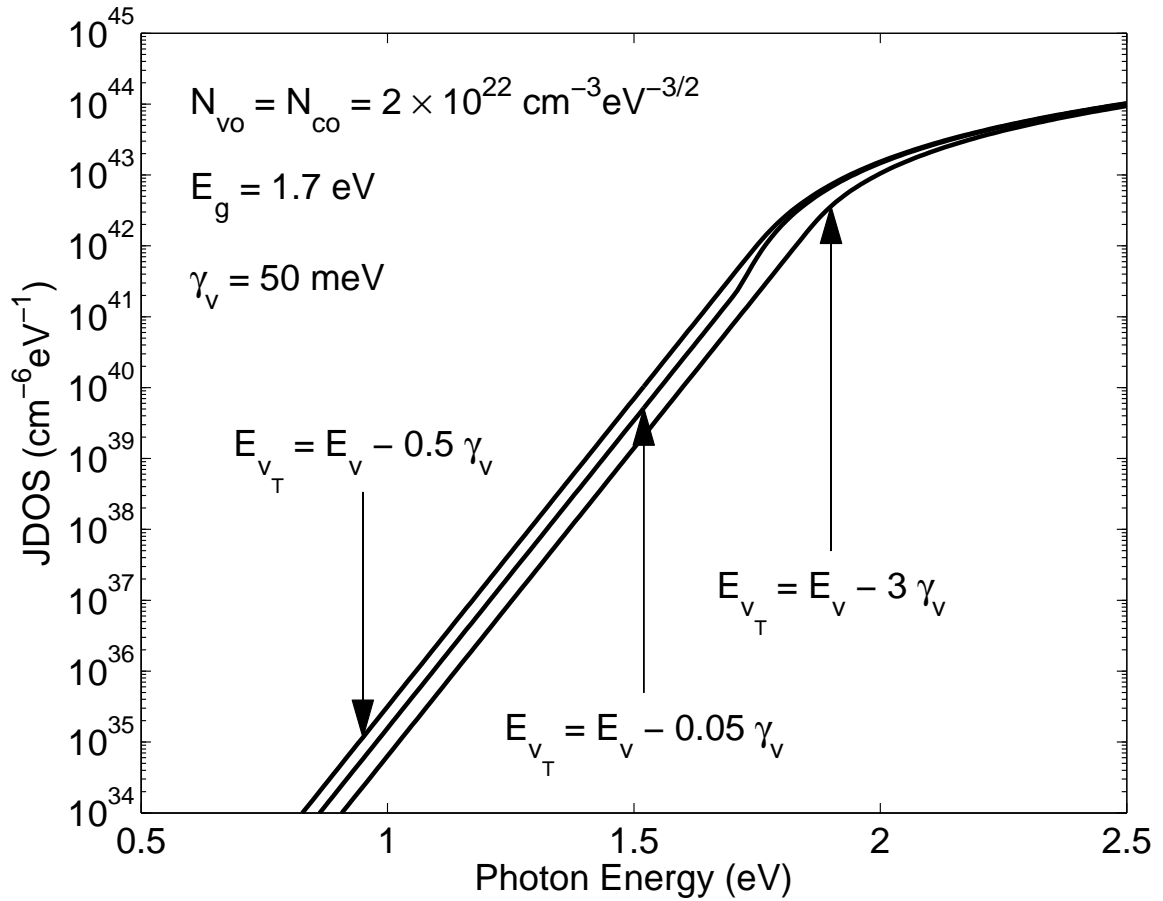


**Figure 3.3:** The sensitivity of the JDOS function,  $J(\hbar\omega)$ , to variations in the critical energy at which the exponential and square-root valence band distributions interface,  $E_{v_T}$ . All other modeling parameters are set to their nominal values for all cases, i.e.,  $N_{vo} = N_{co} = 2 \times 10^{22} \text{ cm}^{-3} \text{ eV}^{-3/2}$ ,  $E_g = 1.7 \text{ eV}$ , and  $\gamma_v = 50 \text{ meV}$ .

$E_v - 0.05\gamma_v$  is only a factor of 2 below that corresponding to  $E_{v_T}$  set to  $E_v - \frac{1}{2}\gamma_v$  in the low  $\hbar\omega$  limit, i.e., when the difference is greatest. The JDOS function corresponding to  $E_{v_T}$  set to  $E_v - 3\gamma_v$  is only a factor of 5 below that corresponding to  $E_{v_T}$  set to  $E_v - \frac{1}{2}\gamma_v$  in the low  $\hbar\omega$  limit. In light of the fact that these JDOS functions change over many orders of magnitude, these differences in the JDOS functions are relatively minor. As a result, we conclude that, for reasonable a-Si:H modeling parameter selections, setting  $E_{v_T}$  to  $E_v - \frac{1}{2}\gamma_v$  will lead to JDOS results that are very similar to those produced through other selections of  $E_{v_T}$ .

### 3.4 The imaginary part of the dielectric function

We now determine the spectral dependence of the imaginary part of the dielectric function,  $\epsilon_2(\hbar\omega)$ , using our dimensionless JDOS formalism. For the purposes of this analysis, we employ Eq. (3.1) in conjunction with an elementary model for  $\mathcal{R}^2(\hbar\omega)$ . Jackson *et al.* [2] performed a series of experiments that aimed to determine the spectral dependence of  $\mathcal{R}^2(\hbar\omega)$  for the case of a-Si:H. Empirically, for a broad range of photon energies, Jackson *et al.* [2] found that

$$\mathcal{R}^2(\hbar\omega) = R_o^2 \begin{cases} \left(\frac{E_d}{\hbar\omega}\right)^5, & \hbar\omega \geq E_d \\ 1, & \hbar\omega < E_d \end{cases}, \quad (3.13)$$

where the characteristic energy,  $E_d = 3.4$  eV, and the prefactor,  $R_o^2 = 10 \text{ \AA}^2$ . Using Eqs. (3.1) and (3.13), for the a-Si:H modeling parameter selections  $N_{vo} = N_{co} = 2.38 \times 10^{22} \text{ cm}^{-3} \text{ eV}^{-3/2}$ ,  $E_g = 1.68$  eV, and  $\gamma_v = 48$  meV, we plot the resultant spectral dependence of the imaginary part of the dielectric function,  $\epsilon_2(\hbar\omega)$ , in Figure 3.4. The corresponding experimental data of Jackson *et al.* [2] is also depicted. It is clear that

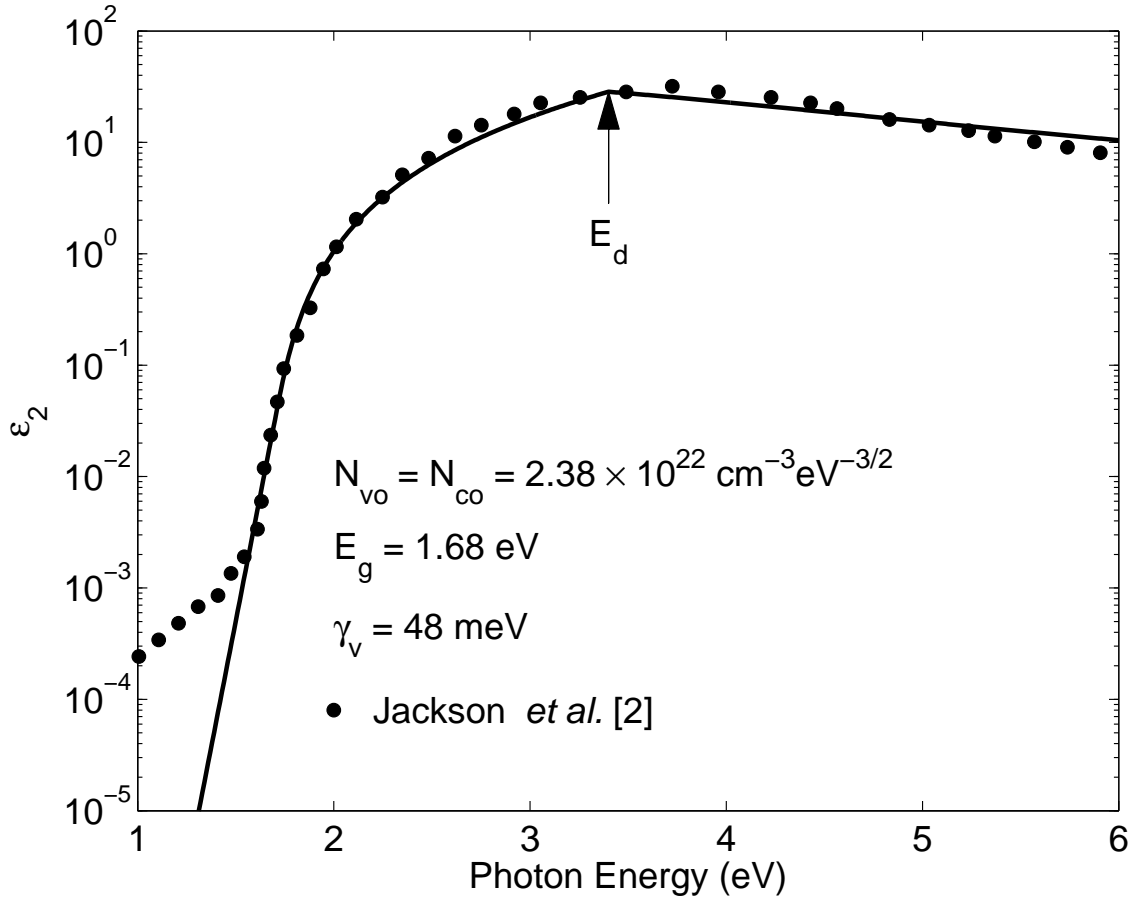


**Figure 3.4:** The imaginary part of the dielectric function corresponding to a-Si:H. The experimental data of Jackson *et al.* [2] is depicted with the solid points. Our calculated result is indicated with the solid line. The characteristic energy,  $E_d$ , is indicated with the arrow. We assume that  $N_{vo} = N_{co} = 2.38 \times 10^{22} \text{ cm}^{-3} \text{ eV}^{-3/2}$ ,  $E_g = 1.68 \text{ eV}$ ,  $\gamma_v = 48 \text{ meV}$ ,  $R_o^2 = 10 \text{ \AA}^2$ , and  $E_d = 3.4 \text{ eV}$  for the purposes of this analysis. We see that there is almost complete agreement between our model and the experimental results of Jackson *et al.* [2], except for  $\hbar\omega < 1.4 \text{ eV}$ .

our modeling result for the imaginary part of the dielectric function is in satisfactory agreement with the experimental data of Jackson *et al.* [2], except for  $\hbar\omega < 1.4$  eV. This discrepancy may be attributable to the neglect of the conduction band tail states in our formalism which then neglects the low energy transitions occurring between the valence band tail states and the conduction band tail states.

### 3.5 The utility of the dimensionless JDOS formalism

It is well known that the optical absorption spectrum associated with a-Si:H exhibits a variety of features that hint at the presence of band states and tail states within the underlying DOS functions. Unfortunately, thus far it has proven difficult to quantitatively compare different spectra owing to differences in the energy gap and the optical absorption tail breadth. We view our dimensionless JDOS formalism as providing a remedy for this conundrum, it being an energy gap and tail breadth independent platform for the critical comparison of disparate optical absorption spectra. In this analysis, we employ our dimensionless JDOS formalism in order to critically compare three distinct a-Si:H optical absorption data sets, each of these optical absorption data sets corresponding to a different a-Si:H sample. Through a process of rescaling, we recast the experimental data sets into a dimensionless form, one that is compliant with the form of our dimensionless JDOS function,  $\mathcal{J}(z)$ , i.e., Eq. (3.7). From the differences between the rescaled experimental results, energy gap and tail breadth independent differences between the experimental results will be rendered transparent.

The experimental optical absorption data sets that are considered correspond to: 1) a sample prepared by Cody *et al.* [17, 18] (this experimental data set corresponds

to the  $T_H = 293$  K data set depicted in Figure 1 of Cody *et al.* [18]), 2) a sample prepared by Reměš [19] (this experimental data set corresponds to the standard GD-a data set depicted in Figure 5.2 of Reměš [19]), and 3) a sample prepared by Viturro and Weiser [20] (this experimental data set corresponds to the  $C_H = 1$  % data set depicted in Figure 4 of Viturro and Weiser [20]). Details, on the means of sample preparation and on the approaches taken whereby these optical absorption spectra are experimentally determined, are provided in the literature [17–20]. The three optical absorption spectra are depicted in Figure 3.5. Noting that the optical absorption spectrum

$$\alpha(\hbar\omega) = \frac{\omega}{n(\hbar\omega)c} \epsilon_2(\hbar\omega), \quad (3.14)$$

where  $n(\hbar\omega)$  denotes the spectral dependence of the refractive index and  $c$  represents the speed of light in a vacuum, it is seen, from Eqs. (3.1), (3.6), and (3.14), that

$$\alpha(\hbar\omega) = 4.3 \times 10^{-45} \frac{\omega}{n(\hbar\omega)c} \mathcal{R}^2(\hbar\omega) N_{vo} N_{co} \gamma_v^2 \mathcal{J}\left(\frac{\hbar\omega - E_g}{\gamma_v}\right). \quad (3.15)$$

For the purposes of this analysis, we assume that the band parameters are not influenced by the tail breadths. Thus, borrowing from the a-Si:H analysis presented in Section 3.4, we set  $N_{vo} = N_{co} = 2.38 \times 10^{22} \text{ cm}^{-3} \text{ eV}^{-3/2}$  for all cases. The spectral dependence of the refractive index,  $n(\hbar\omega)$ , is determined by fitting a tenth-order polynomial to the experimental results of Klazes *et al.* [21] (the experimental data considered corresponds to that presented in Figure 4 of Klazes *et al.* [21]); this approach was used previously by Mok and O’Leary [22], the deviations from this model for  $n(\hbar\omega)$  not being expected to be significant. We find that the selections 1)  $\gamma_v = 68.9$  meV and  $E_g = 1.73$  eV, 2)  $\gamma_v = 91.2$  meV and  $E_g = 1.57$  eV, and 3)  $\gamma_v = 193$  meV and  $E_g = 1.53$  eV, lead to reasonably satisfactory agreement with the a-Si:H optical absorption data sets corresponding to Cody *et al.* [18], Reměš [19], and Viturro and

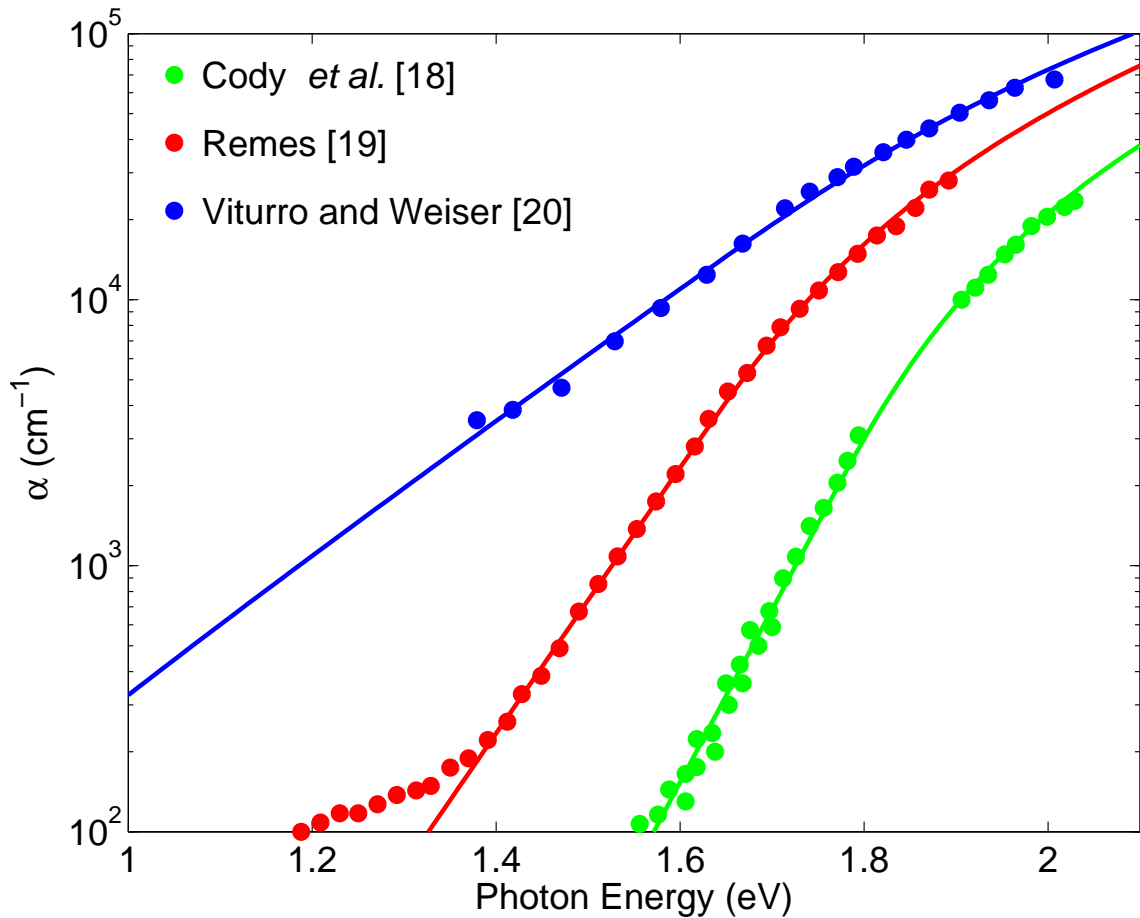


**Figure 3.5:** Three a-Si:H optical absorption data sets plotted as a function of the photon energy. The data sets considered include that corresponding to Cody *et al.* [18] (the  $T_H = 293$  K data set depicted in Figure 1 of Cody *et al.* [18]), plotted with the solid green points, Remeš [19] (the standard GD-a data set depicted in Figure 5.2 of Remeš [19]), plotted with the solid red points, and Viturro and Weiser [20] (the  $C_H = 1\%$  data set depicted in Figure 4 of Viturro and Weiser [20]), plotted with the blue solid points. The optical absorption spectral dependencies obtained through our theoretical analysis, for the cases of  $\gamma_v = 68.9$  meV and  $E_g = 1.73$  eV,  $\gamma_v = 91.2$  meV and  $E_g = 1.57$  eV, and  $\gamma_v = 193$  meV and  $E_g = 1.53$  eV, are depicted using the green, red, and blue solid lines, respectively, these parameter selections being made in order to fit the theoretical results with the experimental data of Cody *et al.* [18], Remeš [19], and Viturro and Weiser [20], respectively; for all cases, we set  $N_{vo} = N_{co} = 2.38 \times 10^{22} \text{ cm}^{-3} \text{ eV}^{-3/2}$ . The online version is depicted in color.

Weiser [20], respectively. We see that there is almost complete agreement between our model and the experimental results, except for the experimental results of Reměs [19] for  $\hbar\omega < 1.4$  eV.

In an effort to critically compare these disparate optical absorption spectra, each with its own distinct tail breadth and energy gap, we present a rescaled version of these experimental data sets in Figure 3.6. For the ordinate axis, this rescaling is performed by dividing each experimental value by  $4.3 \times 10^{-45} \frac{\omega}{n(\hbar\omega)c} \mathcal{R}^2(\hbar\omega) N_{vo} N_{co} \gamma_v^2$ . For the abscissa axis, this rescaling is performed by subtracting  $E_g$  from the photon energy and then dividing the resultant number by  $\gamma_v$ , i.e., plotting  $\frac{\hbar\omega - E_g}{\gamma_v}$ . The dimensionless JDOS function,  $\mathcal{J}(z)$ , as specified in Eq. (3.7), is also plotted. We see that, for the most part at least, these curves are almost completely coincident. This suggests that there is a universal character associated with the optical absorption spectrum of a-Si:H [23].<sup>5</sup> The deviations that occur at low values of  $z$  for the case of the experimental data set of Reměs [19] are attributable to the  $\hbar\omega < 1.4$  eV deviations observed in Figure 3.5. The slight deviations that are observed for high values of  $z$  might be related to uncertainty in the spectral dependence of the refractive index,  $n(\hbar\omega)$ , our polynomial fit to the experimental data of Klazes *et al.* [21] being subject to uncertainties; there is no guarantee, of course, that the spectral dependence of  $n(\hbar\omega)$  found by Klazes *et al.* [21] applies exactly for all a-Si:H samples. Further analysis would be required in order to draw any stronger conclusion, however.

## 3.6 Conclusions

In conclusion, we have simplified the empirical model of O’Leary and Malik [11] for the DOS functions associated with a-Si:H, the number of independent

---

<sup>5</sup>This universality can be exploited in order to distinguish between the various regions of the optical absorption spectrum. The approach of Orapunt and O’Leary [23] can be used for the purposes of such an analysis.

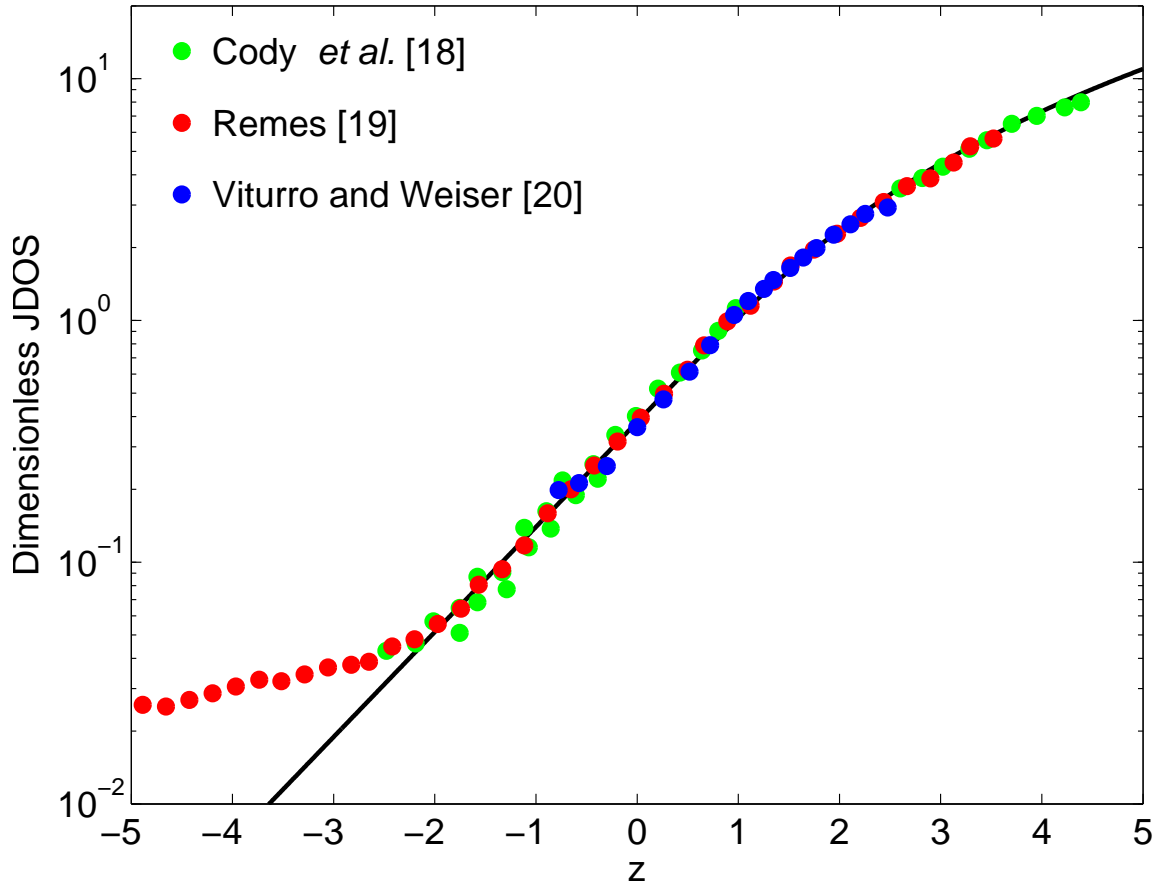


**Figure 3.6:** The rescaled a-Si:H optical absorption data sets and the dimensionless JDOS function,  $\mathcal{J}(z)$ , plotted as a function of the independent variable,  $z$ . The data sets considered include that corresponding to Cody *et al.* [18] (the  $T_H = 293$  K data set depicted in Figure 1 of Cody *et al.* [18]), plotted with the solid green points, Remeš [19] (the standard GD-a data set depicted in Figure 5.2 of Remeš [19]), plotted with the solid red points, and Viturro and Weiser [20] (the  $C_H = 1\%$  data set depicted in Figure 4 of Viturro and Weiser [20]), plotted with the blue solid points. The dimensionless JDOS function,  $\mathcal{J}(z)$ , plotted as a function of  $z$ , is also shown with the solid black line. The online version is depicted in color.

modeling parameters being reduced in the process. We have cast our JDOS evaluations into a dimensionless form, this formalism providing an elementary and effective platform for the determination of the underlying modeling parameters from experiment. We then justified our simplification by showing, for reasonable a-Si:H modeling parameter selections, that our JDOS results are very similar to those determined using the more general approach of O’Leary and Malik [11]. We also showed that this simplified model is as effective as its predecessor in capturing the results of experiment. Finally, we demonstrated the utility of our dimensionless JDOS formalism, using it for the purposes of performing a critical comparative analysis of three different a-Si:H optical absorption data sets.

**Acknowledgements:** The authors gratefully acknowledge financial support from the Natural Sciences and Engineering Research Council of Canada. The use of equipment granted from the Canada Foundation for Innovation and equipment loaned from the Canadian Microelectronics Corporation is also acknowledged.

## References

- [1] A. S. Ferlauto, G. M. Ferreira, J. M. Pearce, C. R. Wronski, R. W. Collins, X. Deng, and G. Ganguly, “Analytical model for the optical functions of amorphous semiconductors from the near-infrared to ultraviolet: Applications in thin film photovoltaics,” *Journal of Applied Physics*, vol. 92, no. 5, pp. 2424-2436, 2002.
- [2] W. B. Jackson, S. M. Kelso, C. C. Tsai, J. W. Allen, and S.-J. Oh, “Energy dependence of the optical matrix element in hydrogenated amorphous and crystalline silicon,” *Physical Review B*, vol. 31, no. 8, pp. 5187-5198, 1985.
- [3] J. Singh and K. Shimakawa, *Advances in Amorphous Semiconductors*, Taylor and Francis, London, 2003.
- [4] S. K. O’Leary, “An empirical density of states and joint density of states analysis of hydrogenated amorphous silicon: a review,” *Journal of Materials Science: Materials in electronics*, vol. 15, pp. 401-410, 2004.
- [5] J. Tauc, R. Grigorovici, and A. Vancu, “Optical properties and electronic structure of amorphous germanium,” *Physica Status Solidi*, vol. 15, no. 2, pp. 627-637, 1966.
- [6] W.-C. Chen, B. J. Feldman, J. Bajaj, F.-M. Tong, and G. K. Wong, “Thermalization gap excitation photoluminescence and optical absorption in amorphous silicon-hydrogen alloys,” *Solid State Communications*, vol. 38, no. 5, pp. 357-363, 1981.
- [7] D. Redfield, “Energy-band tails and the optical absorption edge; The case of a-Si:H,” *Solid State Communications*, vol. 44, no. 9, pp. 1347-1349, 1982.
- [8] G. D. Cody, in *Hydrogenated Amorphous Silicon*, vol. 21B of *Semiconductors and Semimetals*, edited by J. I. Pankove (Academic, New York, 1984), pp. 11-82, 1984.
- [9] S. K. O’Leary, S. R. Johnson, and P. K. Lim, “The relationship between the distribution of electronic states and the optical absorption spectrum of an amorphous semiconductor: an empirical analysis,” *Journal of Applied Physics*, vol. 82, no. 7, pp. 3334-3340, 1997.
- [10] L. Jiao, I. Chen, R. W. Collins, C. R. Wronski, and N. Hata, “An improved analysis for band edge optical absorption spectra in hydrogenated amorphous silicon from optical and photoconductivity measurements,” *Applied Physics Letters*, vol. 72, no. 9, pp. 1057-1059, 1998.
- [11] S. K. O’Leary and S. M. Malik, “A simplified joint density of states analysis of hydrogenated amorphous silicon,” *Journal of Applied Physics*, vol. 92, no. 8, pp. 4276-4282, 2002.

- [12] S. K. O’Leary, “An analytical density of states and joint density of states analysis of amorphous semiconductors,” *Journal of Applied Physics*, vol. 96, no. 7, pp. 3680-3686, 2004.
- [13] S. M. Malik and S. K. O’Leary, “Optical transitions in hydrogenated amorphous silicon,” *Applied Physics Letters*, vol. 80, no. 5, pp. 790-792, 2002.
- [14] S. K. O’Leary, “Spectral dependence of the squared average optical transition matrix element associated with hydrogenated amorphous silicon,” *Applied Physics Letters*, vol. 82, no. 17, pp. 2784-2786, 2003.
- [15] S. M. Malik and S. K. O’Leary, “Deviations from square-root distributions of electronic states in hydrogenated amorphous silicon and their impact upon the resultant optical properties,” *Journal of Non-Crystalline Solids*, vol. 336, no. 1, pp. 64-70, 2004.
- [16] S. M. Malik and S. K. O’Leary, “An analysis of the distributions of electronic states associated with hydrogenated amorphous silicon,” *Journal of Materials Science: Materials in Electronics*, vol. 16, no. 3, pp. 177-181, 2005.
- [17] G. D. Cody, C. R. Wronski, B. Abeles, R. B. Stephens, and B. Brooks, “Optical characterization of amorphous silicon hydride films,” *Solar Cells*, vol. 2, no. 3, pp. 227-243, 1980.
- [18] G. D. Cody, T. Tiedje, B. Abeles, B. Brooks, and Y. Goldstein, “Disorder and the optical-absorption edge of hydrogenated amorphous silicon,” *Physical Review Letters*, vol. 47, no. 20, pp. 1480-1483, 1981.
- [19] Z. Remeš, “Study of defects and microstructure of amorphous and microcrystalline silicon thin films and polycrystalline diamond using optical methods,” *Ph. D. Thesis*, Charles University, Prague, 1999.
- [20] R. E. Viturro and K. Weiser, “Some properties of hydrogenated amorphous silicon produced by direct reaction of silicon and hydrogen atoms,” *Philosophical Magazine B*, vol. 53, no. 2, pp. 93-103, 1986.
- [21] R. H. Klazes, M. H. L. M. van den Broek, J. Bezemer, and S. Radelaar, “Determination of the optical bandgap of amorphous silicon,” *Philosophical Magazine B*, vol. 45, no. 4, pp. 377-383, 1982.
- [22] T. M. Mok and S. K. O’Leary, “The dependence of the Tauc and Cody optical gaps associated with hydrogenated amorphous silicon on the film thickness: all experimental limitations and the impact of curvature in the Tauc and Cody plots,” *Journal of Applied Physics*, vol. 102, no. 11, pp. 113525-1-9, 2007.

- [23] F. Orapunt and S. K. O'Leary, "A quantitative characterization of the optical absorption spectrum associated with hydrogenated amorphous silicon," *Journal of Materials Science: Materials in Electronics*, vol. 20, no. 10, pp. 1033-1038, 2009.

---

---

## CHAPTER 4

---

# A universal feature in the optical absorption spectrum associated with hydrogenated amorphous silicon: A dimensionless joint density of states analysis

*A version of this manuscript was submitted to the Journal of Applied Physics. It is co-authored with my supervisor, Dr. S. K. O'Leary.*

The following equations, introduced in this chapter, were introduced previously in this thesis:

Eq. (4.1)  $\Rightarrow$  Eq. (1.14)

Eq. (4.2)  $\Rightarrow$  Eq. (1.13)

Eq. (4.3)  $\Rightarrow$  Eq. (3.6)

## 4.1 Introduction

Hydrogenated amorphous silicon (a-Si:H) possesses a number of interesting material properties that have made it an attractive electronic material for a wide variety of large area electron device applications [1, 2]. Current applications for this material run the gamut from solar cells [3] to thin film transistors [4], and new applications are emerging with each passing year. As optical response is a key requirement for many of the device applications implemented or envisaged for this material, the optical properties of a-Si:H, and the other forms of thin-film silicon, have been the focus of intense interest for many years. Accordingly, a number of theoretical [5–14] and experimental [15–25] investigations into the spectral dependence of the optical functions associated with this class of materials have been performed. As a consequence of this body of work, the optical response of a-Si:H, and many of the other forms of thin film silicon, are now thought to be relatively well understood.

Recently, Thevaril and O’Leary [26] developed an empirical model for the spectral dependence of the optical functions associated with a-Si:H that stemmed from an earlier analysis of O’Leary and Malik [12]; the analysis of Thevaril and O’Leary [26] actually represents a simplification of the empirical model of O’Leary and Malik [12] with a reduced number of independent modeling parameters, this reduction in the number of parameters being shown to be justified for the specific case of a-Si:H. The resultant joint density of states (JDOS) formalism, which allows for the quantitative characterization of the optical response associated with this material, was shown to provide an elementary and effective platform for the determination of the underlying modeling parameters from experiment. Its dimensionless character permits the identification of energy gap and tail breadth independent differences between disparate experimental a-Si:H optical absorption data sets.

An interesting aspect of the analysis of Thevaril and O’Leary [26] is that it hints at a universal feature in the optical absorption spectrum associated with a-Si:H. Through a process of rescaling, recasting the three experimental a-Si:H optical absorption data sets that were considered into a dimensionless form, Thevaril and O’Leary [26] find, for the most part at least, that the rescaled experimental data curves are almost completely coincident. In a field often characterized by disjoint, fragmented, and disparate results, the convergence of the rescaled experimental results represents a rather surprising finding. In this paper, through an examination of a much larger number of experimental a-Si:H optical absorption data sets, we will critically examine whether or not this universal feature is generally present in the optical absorption spectrum associated with this material.

This paper is organized in the following manner. In Section 4.2, we will briefly present our dimensionless JDOS formalism whereby we will model the spectral dependence of the optical absorption coefficient associated with a-Si:H. Then, in Section 4.3, we analyze experimental data corresponding to Cody *et al.* [17]. Experimental data corresponding to Viturro and Weiser [27] and Remeš [28] is then examined in Section 4.4. A critical comparative analysis of all of the experimental data considered in this analysis is then featured in Section 4.5. Finally, our conclusions are presented in Section 4.6.

## 4.2 Modeling the optical response of a-Si:H

For the purposes of this analysis, we follow the approach of Thevaril and O’Leary [26] in modeling the spectral dependence of the optical absorption coefficient,  $\alpha(\hbar\omega)$ . We start by noting that

$$\alpha(\hbar\omega) = \frac{\omega}{n(\hbar\omega)c} \epsilon_2(\hbar\omega), \quad (4.1)$$

where  $n(\hbar\omega)$  denotes the spectral dependence of the index of refraction,  $c$  represents the speed of light in a vacuum, and  $\epsilon_2(\hbar\omega)$  is the imaginary part of the dielectric function. The spectral dependence of  $n(\hbar\omega)$  is determined by fitting a tenth-order polynomial to the experimental results of Klazes *et al.* [29]; this approach was previously employed by Mok and O’Leary [30]. For the specific case of a-Si:H, Jackson *et al.* [18] find that

$$\epsilon_2(\hbar\omega) = 4.3 \times 10^{-45} \mathcal{R}^2(\hbar\omega) J(\hbar\omega), \quad (4.2)$$

where  $J(\hbar\omega)$ , the JDOS function, is in units of  $\text{cm}^{-6}\text{eV}^{-1}$ , and  $\mathcal{R}^2(\hbar\omega)$ , the normalized dipole matrix element squared average, is in units of  $\text{\AA}^2$ . Assuming square-root distributions of valence band and conduction band band states, and an exponential distribution of valence band tail states, i.e., neglecting the presence of tail states associated with the conduction band, Thevaril and O’Leary [26] find that

$$J(\hbar\omega) = N_{vo}N_{co}\gamma_v^2 \mathcal{J}\left(\frac{\hbar\omega - E_g}{\gamma_v}\right), \quad (4.3)$$

where  $N_{vo}$  and  $N_{co}$  denote the valence band and conduction band DOS prefactors, respectively,  $\gamma_v$  represents the breadth of the valence band tail,  $E_g \equiv E_c - E_v$  is the energy gap, where  $E_v$  and  $E_c$  represent the valence band and conduction band band edges, and  $\mathcal{J}(\cdot)$  is the dimensionless JDOS function, defined in Eq. (7) of Thevaril and O’Leary [26]. Eqs. (4.1), (4.2), and (4.3) form the basis for our subsequent analysis.

It should be noted that our modeling of the spectral dependence of the optical absorption spectrum associated with a-Si:H,  $\alpha(\hbar\omega)$ , ignores defect absorption. Defect absorption, attributable to the presence of distributions of electronic states deep within the gap region, is often exhibited by this semiconductor and many of the other forms of thin-film silicon. The defects that lead to such distributions correspond to departures from the continuous random network structure characteristic of an ‘ideal’

amorphous semiconductor [1]. We are aiming to explore the scaling relationships that are present within the optical absorption spectrum associated with a-Si:H. As defective forms of thin-film silicon are defective in so many different ways, for the purposes of this analysis we will focus on the regions of the optical absorption spectrum that are not influenced by defect absorption.

### 4.3 The experimental data of Cody *et al.*

The experimental a-Si:H optical absorption data sets first considered in this analysis are those of Cody *et al.* [17]. In particular, ten optical absorption data sets from Cody *et al.* [17] are considered. Seven of these data sets correspond to a a-Si:H film from which hydrogen was evolved in a stepwise manner through isochronal heating in a vacuum (the heating temperatures considered,  $T_H$ , are 293 K (calibration), 500, 525, 550, 575, 600, and 625 C), the remaining three data sets corresponding to a similarly prepared a-Si:H film measured at three different temperatures (the measurement temperatures considered,  $T_M$ , are 12.7, 151, and 293 K). Plasma enhanced chemical vapor deposition was employed in order to fabricate the films. The optical absorption spectra were determined through optical transmission measurements [31, 32]. The ten experimental a-Si:H optical absorption data sets of Cody *et al.* [17] are depicted in Figure 4.1.

We will now fit our model for the spectral dependence of  $\alpha(\hbar\omega)$ , i.e., Eqs. (4.1), (4.2), and (4.3), to the experimental data sets of Cody *et al.* [17]. For the purposes of this analysis, we follow Thevaril and O’Leary [26] and assume that the band parameters,  $N_{vo}$ , and  $N_{co}$ , are not influenced by the valence band tail breadth,  $\gamma_v$ . Following Thevaril and O’Leary [26], we thus set  $N_{vo} = N_{co} = 2.38 \times 10^{22} \text{ cm}^{-3} \text{ eV}^{-3/2}$  for all cases, noting that this value is representative of a-Si:H [33–38]. Following Jackson *et al.* [18], we set  $\mathcal{R}^2(\hbar\omega)$  to  $10 \text{ \AA}^2$  for all cases, noting that Jackson *et al.* [18] find that

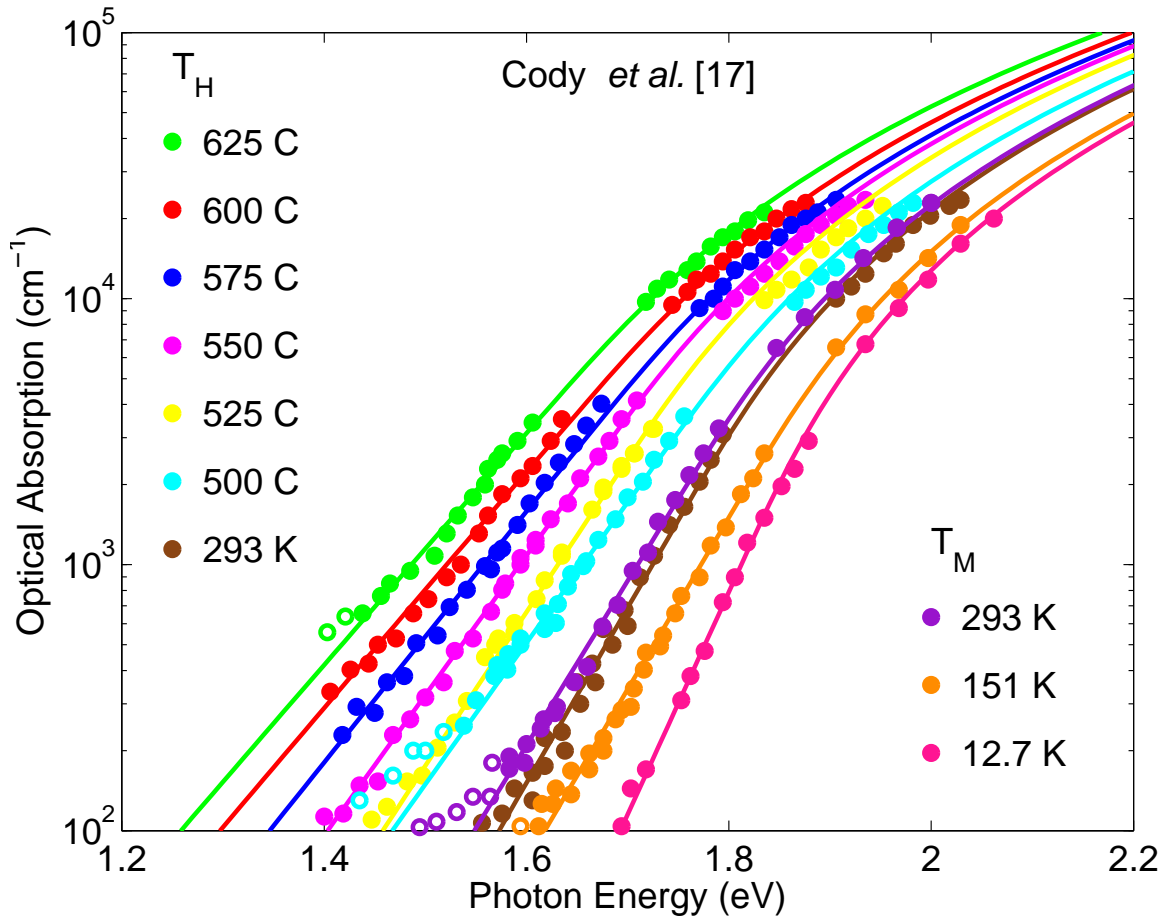


**Figure 4.1:** The experimental a-Si:H optical absorption data sets of Cody *et al.* [17] and the corresponding fits. The experimental data itself is represented with the solid and open colored points. The solid colored points correspond to experimental data that is not believed to be influenced by defect absorption while the open colored points correspond to experimental data that is believed to be influenced by defect absorption. The color scheme is indicated in the legend within the figure. The identification of each data set borrows directly from the classification scheme employed by Cody *et al.* [17]; see Figure 1 of Cody *et al.* [17]. The fits to these experimental data sets are depicted with the corresponding colored lines. The model parameter selections for these fits, i.e., the corresponding  $\gamma_v$  and  $E_g$  values, are indicated in Table 4.1. The online version of this figure is depicted in color.

$\mathcal{R}^2(\hbar\omega)$  exhibits little spectral variation over the range of  $\hbar\omega$  considered. Thus, our analysis reduces to the determination of  $\gamma_v$  and  $E_g$  corresponding to each experimental a-Si:H optical absorption data set of Cody *et al.* [17]. We find that the parameter selections for  $\gamma_v$  and  $E_g$  tabulated in Table 4.1 lead to reasonably satisfactory agreement with the experimental a-Si:H optical absorption data sets of Cody *et al.* [17].

**Table 4.1:** The model parameter selections corresponding to the fits to the experimental a-Si:H optical absorption data sets of Cody *et al.* [17] depicted in Figure 4.1. The number of excluded data points and the presence of a difference between the experimental results and the corresponding fits, for each data set considered, are also indicated.

Data set	$\gamma_v$ (meV)	$E_g$ (eV)	no. of excluded points	slight high $\hbar\omega$ differences
$T_H = 293$ K	67.9	1.724		yes
$T_H = 500$ C	85.2	1.691	5	yes
$T_H = 525$ C	78.1	1.649		yes
$T_H = 550$ C	86.3	1.629		yes
$T_H = 575$ C	96.8	1.618		
$T_H = 600$ C	103.2	1.597		
$T_H = 625$ C	105.3	1.566	2	
$T_M = 12.7$ K	52.9	1.787		
$T_M = 151$ K	68.9	1.775	1	
$T_M = 293$ K	72.4	1.718	6	

Discrepancies between our modeling results and those of experiment are found, however. In the high absorption region, for the most part at least, we note very little deviation from our theoretical fit other than the usual scatter characteristic of experimental data. We do note, however, some deviation for the  $T_H = 293$  K,  $T_H = 500$ ,  $T_H = 525$ , and  $T_H = 550$  C data sets; for these cases, for higher values of  $\hbar\omega$ , i.e.,  $\hbar\omega > 1.8$  eV, the theoretical results increase at a slightly greater rate than the experimental results of Cody *et al.* [17] leading to a slight gap between the experimental

results and that of the corresponding fits. Variations in the spectral dependencies of  $\mathcal{R}^2(\hbar\omega)$  and  $n(\hbar\omega)$  are the most likely causes for these deviations; the experimental measurements of  $\mathcal{R}^2(\hbar\omega)$  performed by Jackson *et al.* [18] are subject to a considerable amount of uncertainty in this range of  $\hbar\omega$  as both  $J(\hbar\omega)$  and  $\epsilon_2(\hbar\omega)$  are changing by many orders of magnitude [39]. The low absorption region is more problematic, however. A distinctive flaring in the low absorption region of the spectrum is observed for many of the data sets of Cody *et al.* [17]. Roxlo *et al.* [32] suggest that this spectral behavior of the optical absorption spectrum is the characteristic signature corresponding to the onset of defect absorption. Roxlo *et al.* [32] further point out that the limitations of the optical transmission measurements preclude the accurate determination of the optical absorption coefficient for low levels of absorption, i.e., for  $\alpha(\hbar\omega)$  less than  $5 \times 10^2 \text{ cm}^{-1}$ . On the basis of these considerations, we believe that we have sufficient probable cause to reject the flaring low absorption components of these data sets for the purposes of our analysis on the grounds that they have likely been influenced by defect absorption. The rejected data is clearly depicted in Figure 4.1.

In an effort to critically compare these disparate optical absorption spectra, each with its own distinct tail breadth and energy gap, we present a rescaled version of these experimental data sets in Figure 4.2. For the ordinate axis, this rescaling is performed by dividing each experimental value by  $4.3 \times 10^{-45} \frac{\omega}{n(\hbar\omega)c} \mathcal{R}^2(\hbar\omega) N_{vo} N_{co} \gamma_v^2$ . For the abscissa axis, this rescaling is performed by substrating  $E_g$  from the photon energy and then dividing the resultant quantity by  $\gamma_v$ , i.e., plotting  $\frac{\hbar\omega - E_g}{\gamma_v}$ . This casts the experimental data sets of Cody *et al.* [17] into a form that is compliant with the form of the dimensionless JDOS function,  $\mathcal{J}(\cdot)$ , specified in Eq. (7) of Thevaril and O'Leary [26]. This dimensionless JDOS function is also plotted in Figure 4.2. We see that, for the most part at least, ignoring the defect absorption influenced data, that

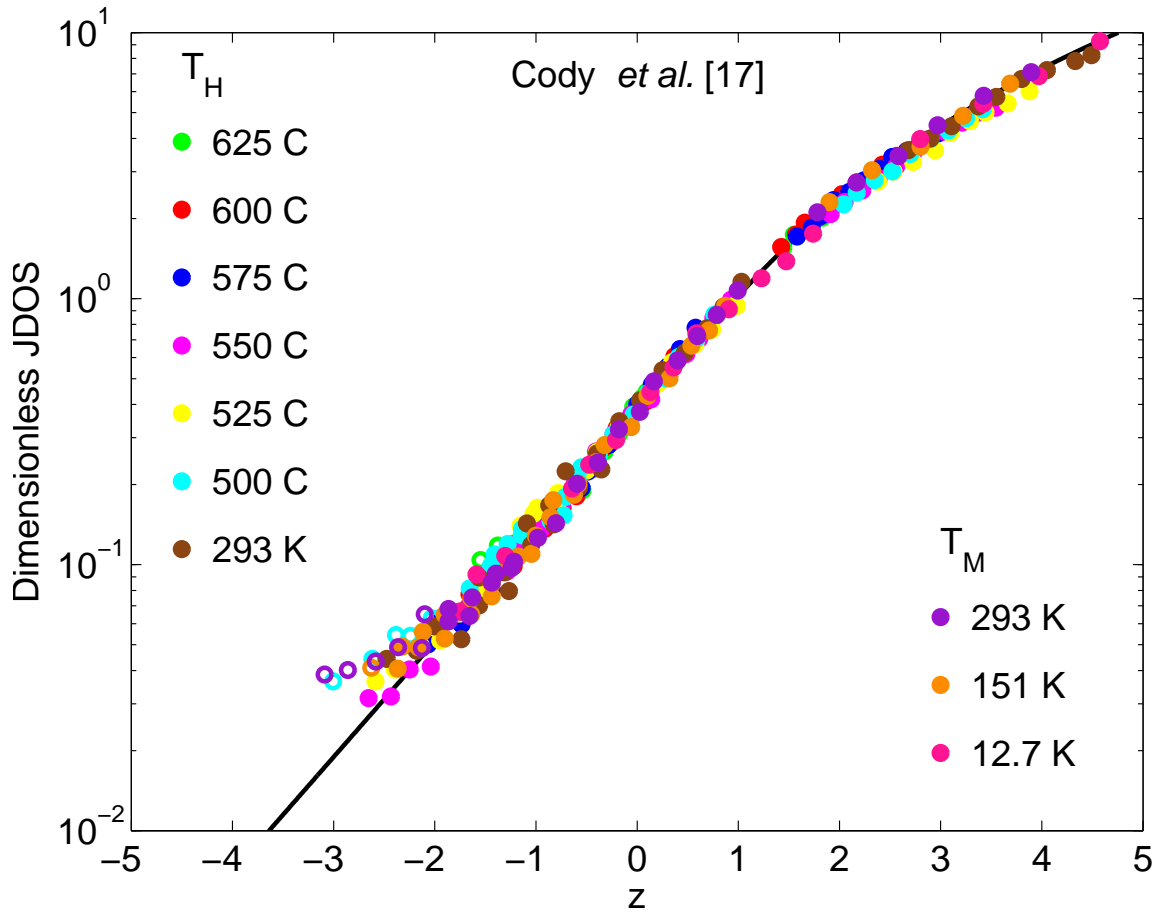


**Figure 4.2:** The rescaled experimental a-Si:H optical absorption data sets of Cody *et al.* [17] and the dimensionless JDOS function,  $\mathcal{J}(z)$ , plotted as a function of the independent variable,  $z$ . The rescaled experimental data is represented with the solid and open colored points. The solid colored points correspond to rescaled experimental data that is not believed to be influenced by defect absorption while the open colored points correspond to rescaled experimental data that is believed to be influenced by defect absorption. The color scheme is indicated in the legend within the figure. The identification of each data set borrows directly from the classification scheme employed by Cody *et al.* [17]; see Figure 1 of Cody *et al.* [17]. The dimensionless JDOS function,  $\mathcal{J}(z)$ , plotted as a function of  $z$ , is also shown with the solid black line. The online version of this figure is depicted in color.

these curves are almost completely coincident with the dimensionless JDOS function,  $\mathcal{J}(\cdot)$ , for the ten experimental a-Si:H optical absorption data sets of Cody *et al.* [17].

## 4.4 The experimental data of Viturro and Weiser and the experimental data of Remeš

We now consider the experimental a-Si:H optical absorption data sets of Viturro and Weiser [27]. In total, ten optical absorption data sets from Viturro and Weiser [27] are considered. These data sets correspond to a-Si:H films whose hydrogen concentrations,  $C_H$ , are found to be 1.0, 2.0, 4.0, 4.7, 5.5, 6.0, 6.3, 6.8, 7.5, and 8.5 % (atomic percent). A direct synthesis reaction between silicon and hydrogen atoms was employed in order to fabricate the films. The optical absorption spectra were determined through reflection and transmission measurements. The ten experimental a-Si:H optical absorption data sets of Viturro and Weiser [27] are depicted in Figure 4.3.

We now fit our model for the spectral dependence of  $\alpha(\hbar\omega)$ , i.e., Eqs. (4.1), (4.2), and (4.3), to the experimental data sets of Viturro and Weiser [27]. As with the data of Cody *et al.* [17], we set  $N_{vo} = N_{co} = 2.38 \times 10^{22} \text{ cm}^{-3} \text{ eV}^{-3/2}$  and  $\mathcal{R}^2(\hbar\omega) = 10 \text{ \AA}^2$  for all cases. We find that the parameter selections for  $\gamma_v$  and  $E_g$  tabulated in Table 4.2 lead to reasonably satisfactory agreement with the a-Si:H optical absorption data sets of Viturro and Weiser [27]. Unlike the case of Cody *et al.* [17], very few discrepancies between our modeling results and those of experiment are found; we do find, however, the same slight gap between the experimental results and that of the corresponding fit as that found for some of the data sets of Cody *et al.* [17] for higher values of  $\hbar\omega$ , i.e.,  $\hbar\omega > 1.8 \text{ eV}$ , for most of the data sets of Viturro and Weiser [27], this most likely arising as a consequence of variations in the spectral dependencies of

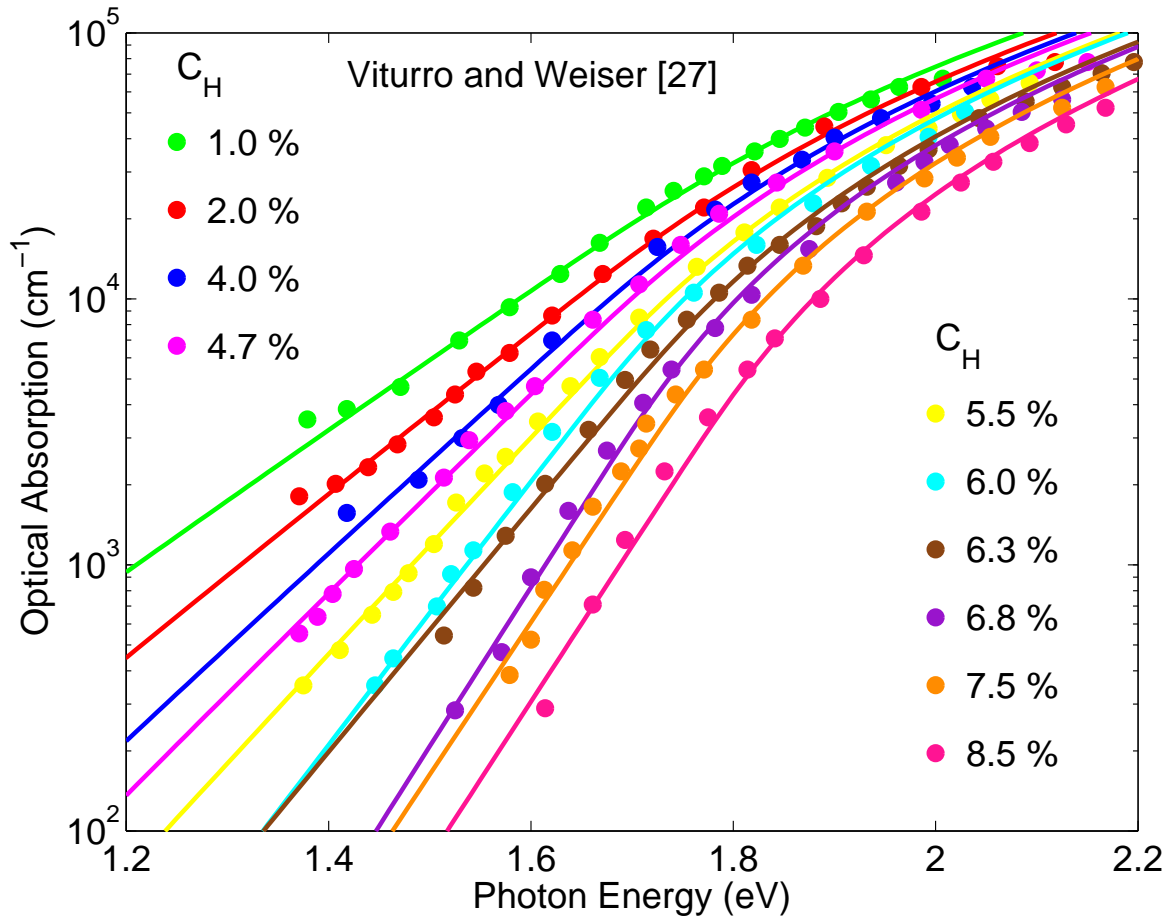


**Figure 4.3:** The experimental a-Si:H optical absorption data sets of Viturro and Weiser [27] and the corresponding fits. The experimental data itself is represented with the solid points; for the case of Viturro and Weiser [27] there are no experimental points that are believed to be influenced by defect absorption. The color scheme is indicated in the legend within the figure. The identification of each data set borrows directly from the classification scheme employed by Viturro and Weiser [27]; see Figure 4 of Viturro and Weiser [27]. The fits to these experimental data sets are depicted with the corresponding colored lines. The model parameter selections for these fits, i.e., the corresponding  $\gamma_v$  and  $E_g$  values, are indicated in Table 4.2. The online version of this figure is depicted in color.

$\mathcal{R}^2(\hbar\omega)$  and  $n(\hbar\omega)$ . As a consequence, when we plot the rescaled experimental data using the same rescaling procedure as that employed for the analysis of the experimental data of Cody *et al.* [17], we find that it is almost completely coincident with the dimensionless JDOS function,  $\mathcal{J}(\cdot)$ ; see Figure 4.4.

**Table 4.2:** The model parameter selections corresponding to the fits to the experimental a-Si:H optical absorption data sets of Viturro and Weiser [27] depicted in Figure 4.3. The number of excluded data points and the presence of a difference between the experimental results and the corresponding fits, for each data set considered, are also indicated.

Data set	$\gamma_v$ (meV)	$E_g$ (eV)	no. of excluded points	slight high $\hbar\omega$ differences
$C_H = 1.0$ %	182.1	1.516		yes
$C_H = 2.0$ %	155.8	1.537		yes
$C_H = 4.0$ %	134.2	1.547		
$C_H = 4.7$ %	123.7	1.558		yes
$C_H = 5.5$ %	113.2	1.584		yes
$C_H = 6.0$ %	92.1	1.584		
$C_H = 6.3$ %	99.9	1.622		yes
$C_M = 6.8$ %	75.5	1.626		yes
$C_M = 7.5$ %	78.9	1.658		
$C_M = 8.5$ %	76.8	1.705		

We now consider the experimental a-Si:H optical absorption data sets of Remeš [28]. In total, eleven optical absorption data sets from Remeš [28] are considered. These data sets correspond to six a-Si:H films produced through hot wire deposition (HW39, HW48, HW70, HW91, HW129, and HW132), three a-Si:H films produced through plasma enhanced chemical vapor deposition, one of which has been annealed (standard GD, standard GD-a, and GD500), and two of the a-Si:H films produced through very high frequency plasma enhanced chemical vapor deposition (VHF-GD (50%) and VHF-GD (10%)). The optical absorption spectra were determined through a

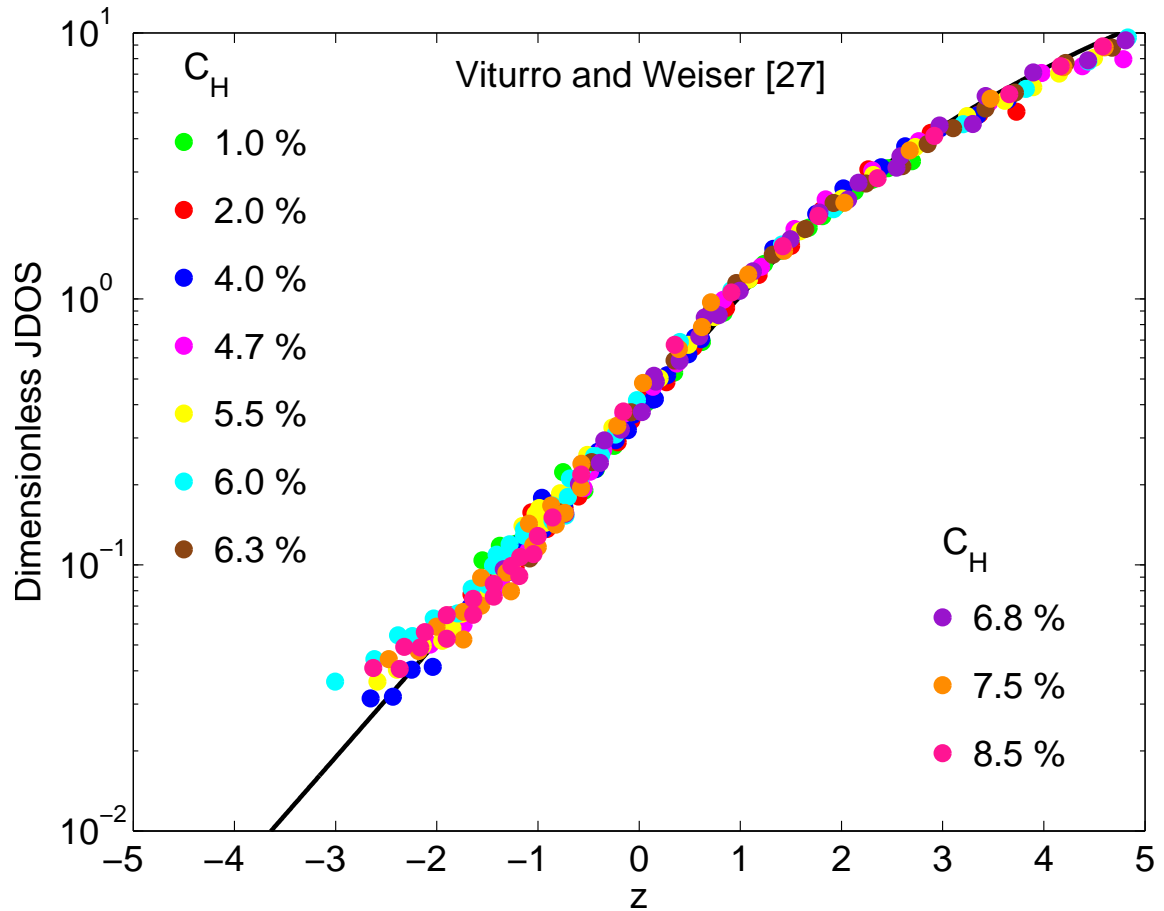


**Figure 4.4:** The rescaled experimental a-Si:H optical absorption data sets of Viturro and Weiser [27] and the dimensionless JDOS function,  $\mathcal{J}(z)$ , plotted as a function of the independent variable,  $z$ . The rescaled experimental data itself is represented with the solid points; for the case of Viturro and Weiser [27] there are no experimental points that are believed to be contaminated with defect absorption. The color scheme is indicated in the legend within the figure. The identification of each data set borrows directly from the classification scheme employed by Viturro and Weiser [27]; see Figure 4 of Viturro and Weiser [27]. The dimensionless JDOS function,  $\mathcal{J}(z)$ , plotted as a function of  $z$ , is also shown with the solid black line. The online version of this figure is depicted in color.

combination of reflection and transmission measurements and constant photocurrent measurements. The eleven experimental a-Si:H optical absorption data sets of Remeš [28] are depicted in Figure 4.5; in the interests of providing a fair comparison with the results of Cody *et al.* [17] and Viturro and Weiser [27], we only consider experimental data with optical absorption values excess of  $10^2 \text{ cm}^{-1}$ . As the optical absorption spectrum corresponding to the HW70 a-Si:H film seems somewhat distinct from that of the other films in the high absorption region, i.e., the curvature seems to be different when compared with the other optical absorption spectra, we will not consider it in our analysis of the experimental a-Si:H optical absorption data sets of Remeš [28]. This could arise as a consequence of this particular film's composition; see, for example, the analysis of Jun *et al.* [40]. Further study of the nature of this HW70 film would be required in order to draw a more definitive conclusion on this issue.

We now fit our model for the spectral dependence of  $\alpha(\hbar\omega)$ , i.e., Eqs. (4.1), (4.2), and (4.3), to the experimental data sets of Remeš [28]. As with the data of Cody *et al.* [17] and Viturro and Weiser [27], we set  $N_{vo} = N_{co} = 2.38 \times 10^{22} \text{ cm}^{-3} \text{ eV}^{-3/2}$  and  $\mathcal{R}^2(\hbar\omega) = 10 \text{ \AA}^2$  for all cases. We find that the parameter selections for  $\gamma_v$  and  $E_g$  tabulated in Table 4.3 lead to reasonably satisfactory agreement with the a-Si:H optical absorption data sets of Remeš [28]; except, of course, for the HW70 film, as has already been mentioned. As with the case of Viturro and Weiser [27], and unlike the case of Cody *et al.* [17], very few discrepancies between our modeling results and those of experiment are found. As a consequence, when we plot the rescaled experimental data using the same rescaling procedure as that employed for the analysis of the experimental data of Cody *et al.* [17] and Viturro and Weiser [27], we find that they are almost completely coincident with the dimensionless JDOS function,  $\mathcal{J}(\cdot)$ ; see Figure 4.6.

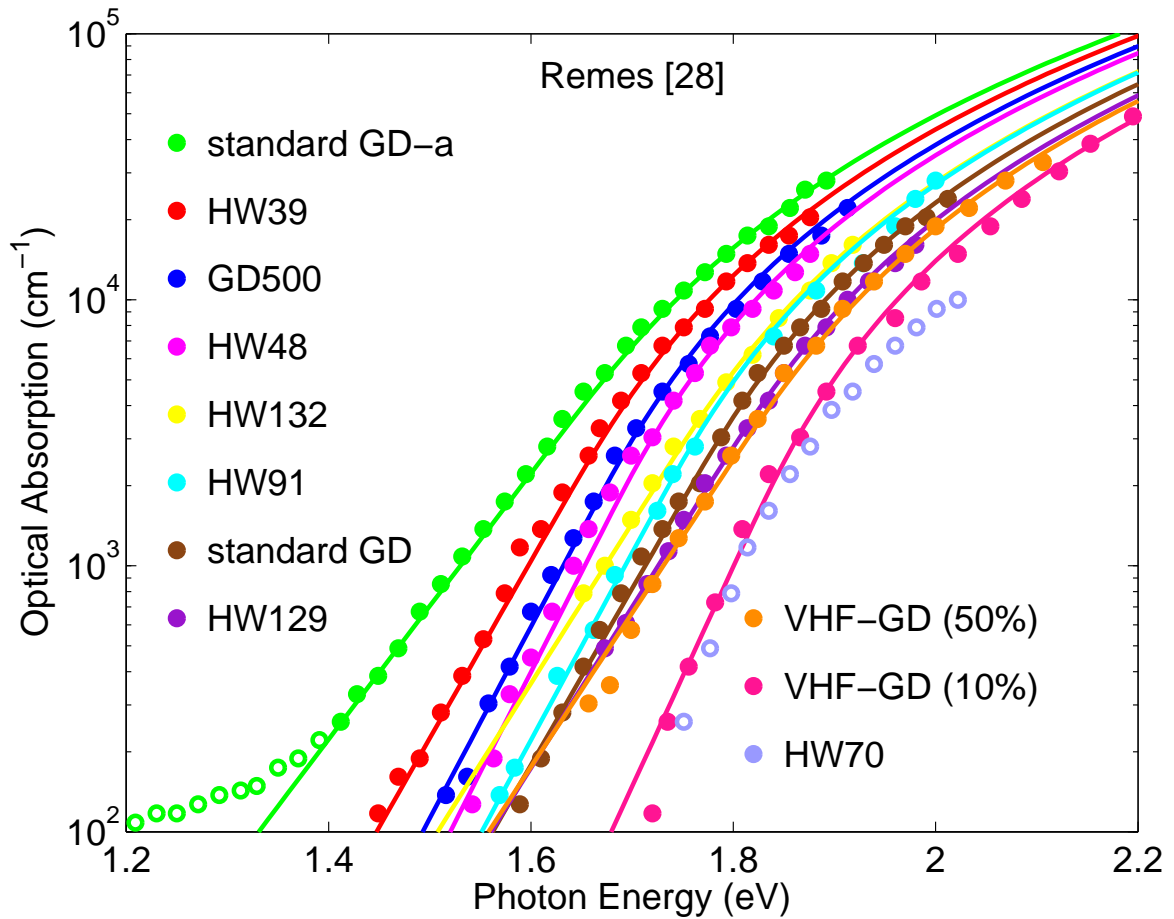


**Figure 4.5:** The experimental a-Si:H optical absorption data sets of Remeš [28] and the corresponding fits. The experimental data itself is represented with the solid points; for the case of Remeš [28] there are no experimental points that are believed to be contaminated with defect absorption. The HW70 a-Si:H film of Remeš [28] is not considered as it exhibits a spectral variation that is distinct from the other spectra for high values of  $\hbar\omega$ ; it is depicted with the open points. The color scheme is indicated in the legend within the figure. The identification of each data set borrows directly from the classification scheme employed by Remeš [28]; see Figure 5.2 of Remeš [28]. The fits to these experimental data sets are depicted with the corresponding colored lines. The model parameter selections for these fits, i.e., the corresponding  $\gamma_v$  and  $E_g$  values, are indicated in Table 4.3. The online version of this figure is depicted in color.

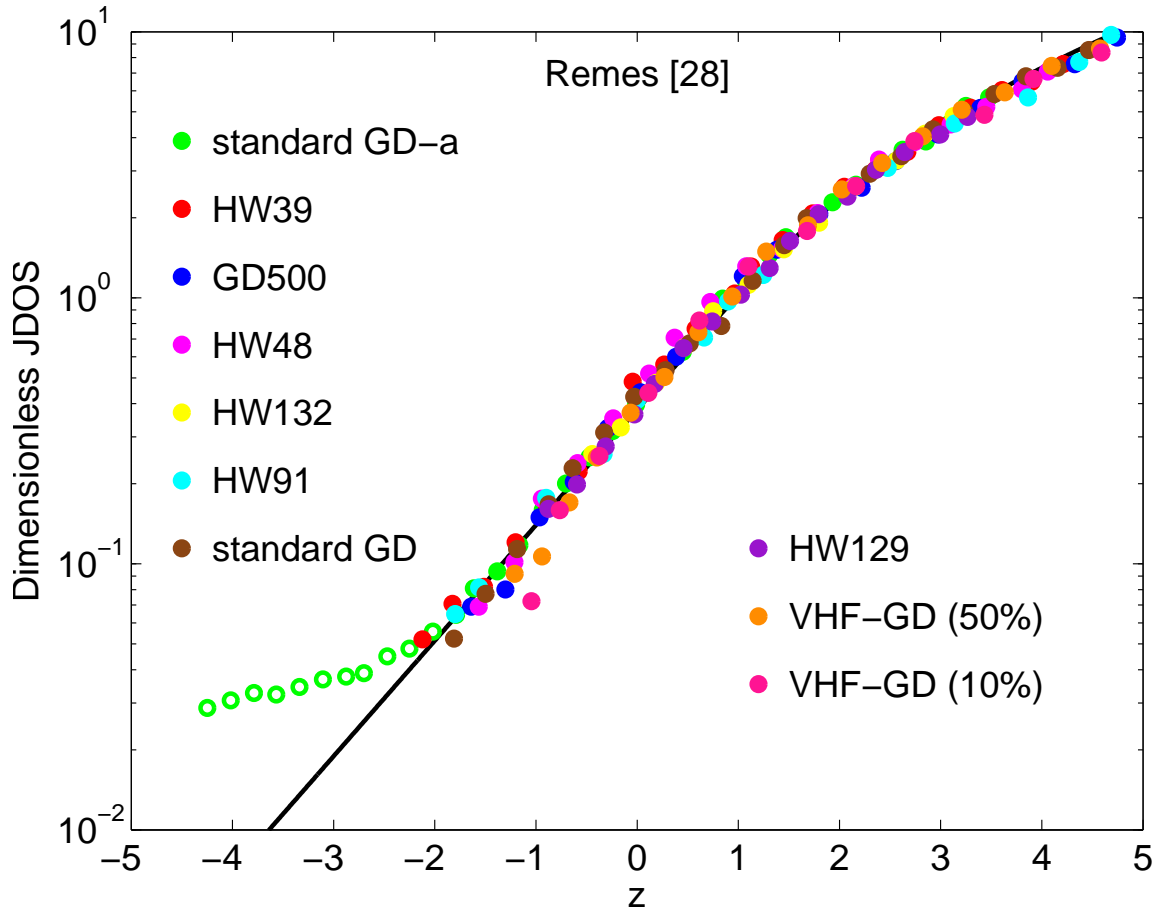


**Figure 4.6:** The rescaled experimental a-Si:H optical absorption data sets of Remeš [28] and the dimensionless JDOS function,  $\mathcal{J}(z)$ , plotted as a function of the independent variable,  $z$ . The rescaled experimental data itself is represented with the solid colored points; for the case of Remeš [28] there are no experimental points that are believed to be influenced by defect absorption. The HW70 a-Si:H film of Remeš [28] is not considered as it has not been fit to our dimensionless JDOS formalism, i.e., Eqs. (4.1), (4.2), and (4.3). The color scheme is indicated in the legend within the figure. The identification of each data set borrows directly from the classification scheme employed by Remeš [28]; see Figure 5.2 of Remeš [28]. The dimensionless JDOS function,  $\mathcal{J}(z)$ , plotted as a function of  $z$ , is also shown with the solid black line. The online version of this figure is depicted in color.

**Table 4.3:** The model parameter selections corresponding to the fits to the experimental a-Si:H optical absorption data sets of Remeš [28] depicted in Figure 4.5. The number of excluded data points and the presence of a difference between the experimental results and the corresponding fits, for each data set considered, are also indicated.

Data set	$\gamma_v$ (meV)	$E_g$ (eV)	no. of excluded points	slight high $\hbar\omega$ differences
HW39	67.4	1.592		
HW48	59.4	1.635		
HW70			all points	
HW91	63.4	1.683		
HW129	74.1	1.738		
HW132	74.5	1.685		
standard GD	67.4	1.711		
standard GD-a	91.1	1.575	11	
GD500	62.2	1.618		
VHF-GD (50%)	77.6	1.751		
VHF-GD (10%)	53.6	1.776		

## 4.5 Critical comparative analysis

In order to more properly gauge how close the experimental data actually is to our theoretical fits, and therefore, when the scaling factors are taken into account, how close the rescaled experimental data is to the dimensionless JDOS function,  $\mathcal{J}(\cdot)$ , in Figure 4.7, for each experimental point in the experimental a-Si:H optical absorption data sets of Cody *et al.* [17] we plot the ratio of the optical absorption experimental value,  $\alpha_{\text{expt}}$ , with the corresponding fit value,  $\alpha_{\text{fit}}$ ; the corresponding fit value,  $\alpha_{\text{fit}}$ , is determined using the fit at exactly the same value of  $\hbar\omega$  as the experimental data point. In light of the fact that these fits were determined over many orders of magnitude, the fact that so many data points in Figure 4.7 crowd so closely

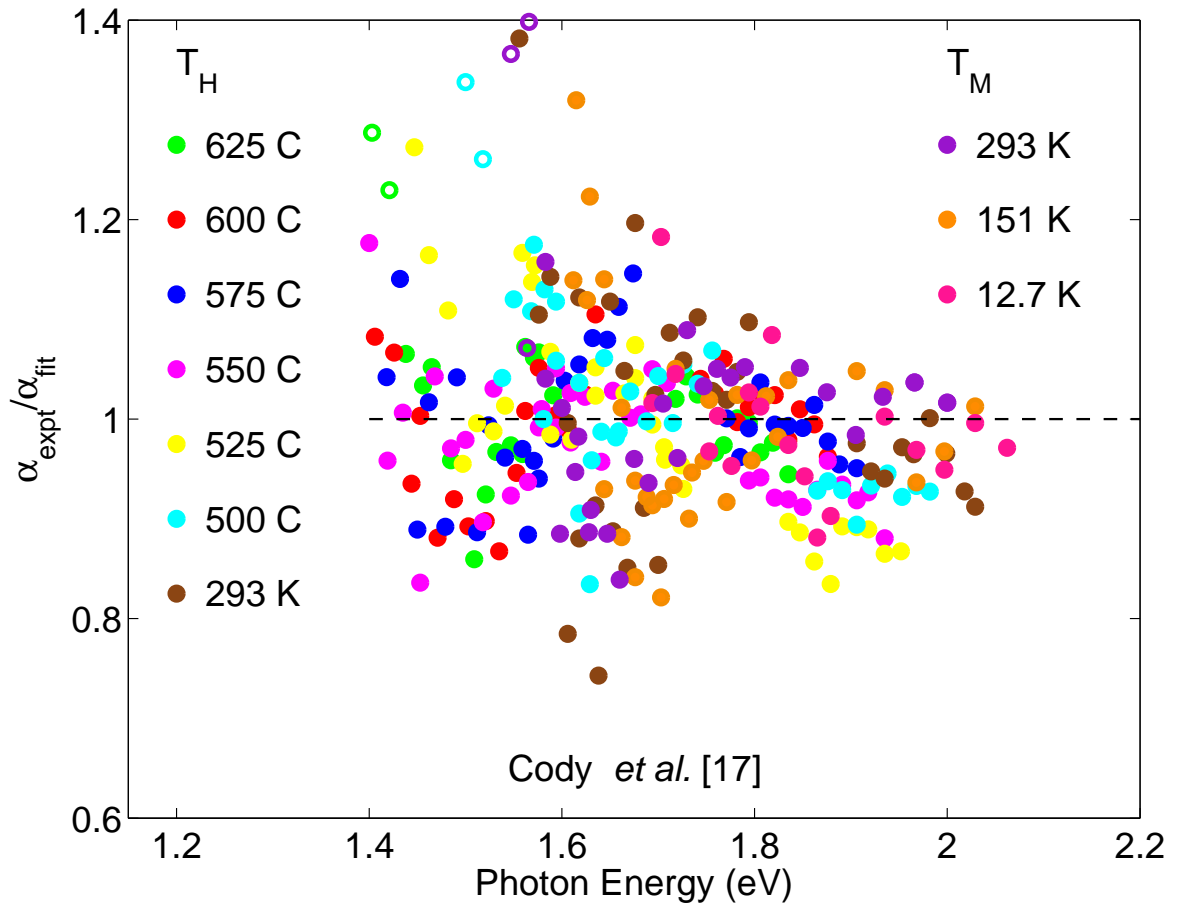


**Figure 4.7:** Deviations between the experimental results and the corresponding fits as determined through a ratio of the experimental and fit results for the experimental a-Si:H optical absorption data sets of Cody *et al.* [17]. The ordinate values for this plot are obtained by dividing each experimental value,  $\alpha_{\text{expt}}$ , by the corresponding fit value,  $\alpha_{\text{fit}}$ , the abscissa axis being the corresponding photon energy,  $\hbar\omega$ . The online version of this figure is depicted in color.

about unity is interesting, particular when one considers that our fits were determined by selecting only two parameters,  $\gamma_v$  and  $E_g$ , corresponding to each data set. We note that the variations about unity become larger for lower photon energies. This probably arises as a consequence of the increasing importance of defect absorption for lower values of photon energy. The fact that instrumentation limits are approached for lower values of photon energy may also account for these increasingly intense variations. Similar results, corresponding to Viturro and Weiser [27] and Remeš [28], are depicted in Figure 4.8 and Figure 4.9, respectively. It should be noted that for high photon energies, the results of Viturro and Weiser [27] seem to monotonically decrease below unity in a consistent fashion as the photon energy increases. This may hint at variations in the matrix element that are not accounted for by simply setting  $\mathcal{R}^2(\hbar\omega)$  to  $10 \text{ \AA}^2$ , as was suggested earlier.

In an effort to further quantitatively assess the tightness of our fits to the experimental data, we introduce the factor  $\beta$ , which provides a measure of the stray between the experimental and fit values. For each experimental data point, we examine whether or not the experimental optical absorption value,  $\alpha_{\text{expt}}$ , lies between  $\frac{1}{\beta}\alpha_{\text{fit}}$  and  $\beta\alpha_{\text{fit}}$ , i.e., whether  $\frac{1}{\beta}\alpha_{\text{fit}} \leq \alpha_{\text{expt}} \leq \beta\alpha_{\text{fit}}$ ; of course, the quantity  $\beta$  must exceed unity. In Figure 4.10, we plot all of the experimental data points corresponding to Cody *et al.* [17], Viturro and Weiser [27], and Remeš [28]; the data points that have already been excluded on the grounds that they are influenced by defect absorption are not considered. It is seen that for  $\beta$  set to 1.1, around 73 % of the experimental data points lie between  $\frac{1}{\beta}\alpha_{\text{fit}}$  and  $\beta\alpha_{\text{fit}}$ . Plotting the fraction of the experimental points between  $\frac{1}{\beta}\alpha_{\text{fit}}$  and  $\beta\alpha_{\text{fit}}$  as a function of  $\beta$  in Figure 4.11, we see results corresponding to the experimental results of Cody *et al.* [17], Viturro and Weiser [27], and Remeš [28]. We see that the fraction of included experimental points monotonically increases with  $\beta$ . For all cases, in excess of 70 % of the considered experimental data

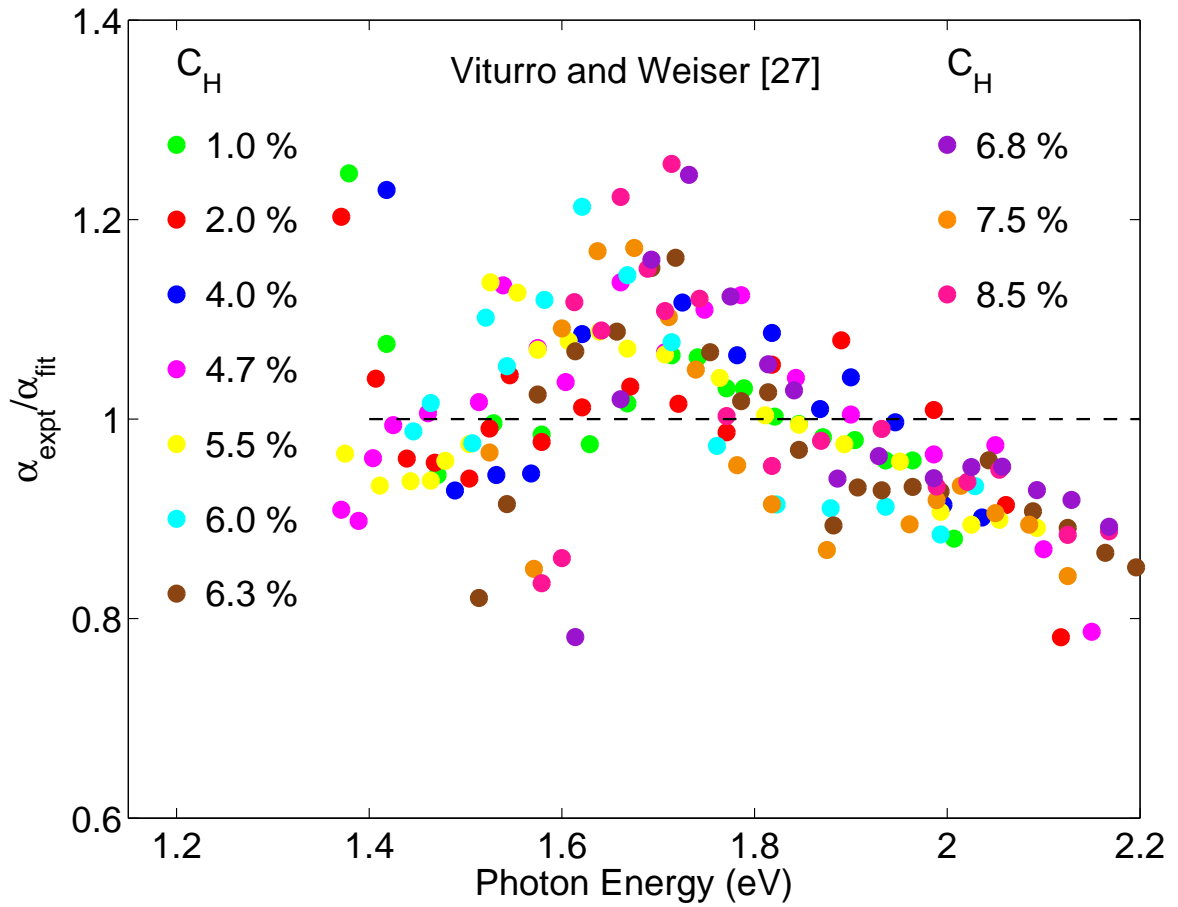


**Figure 4.8:** Deviations between the experimental results and the corresponding fits as determined through a ratio of the experimental and fit results for the experimental a-Si:H optical absorption data sets of Viturro and Weiser [27]. The ordinate values for this plot are obtained by dividing each experimental value,  $\alpha_{\text{expt}}$ , by the corresponding fit value,  $\alpha_{\text{fit}}$ , the abscissa axis being the corresponding photon energy,  $\hbar\omega$ . The online version of this figure is depicted in color.

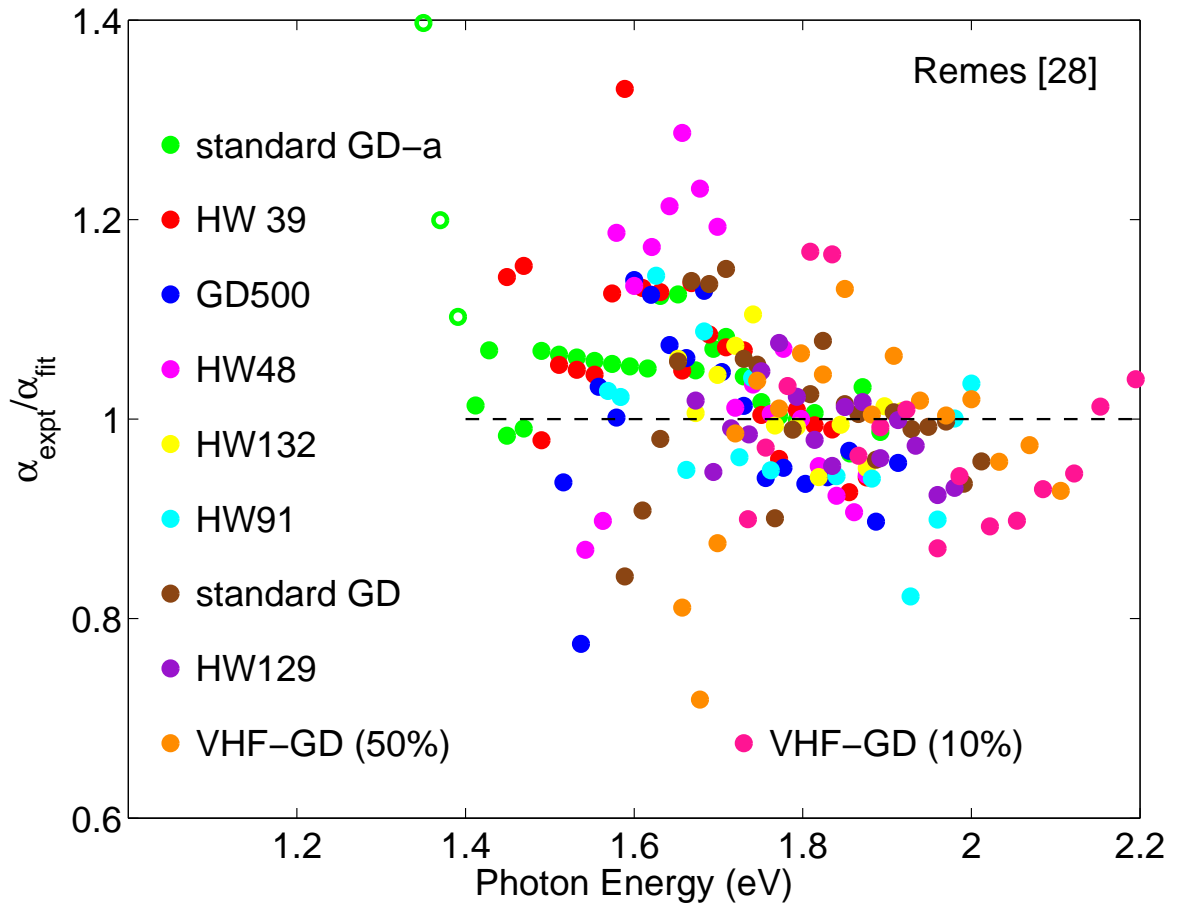


**Figure 4.9:** Deviations between the experimental results and the corresponding fits as determined through a ratio of the experimental and fit results for the experimental a-Si:H optical absorption data sets of Remes [28]. The ordinate values for this plot are obtained by dividing each experimental value,  $\alpha_{\text{expt}}$ , by the corresponding fit value,  $\alpha_{\text{fit}}$ , the abscissa axis being the corresponding photon energy,  $\hbar\omega$ . The online version of this figure is depicted in color.

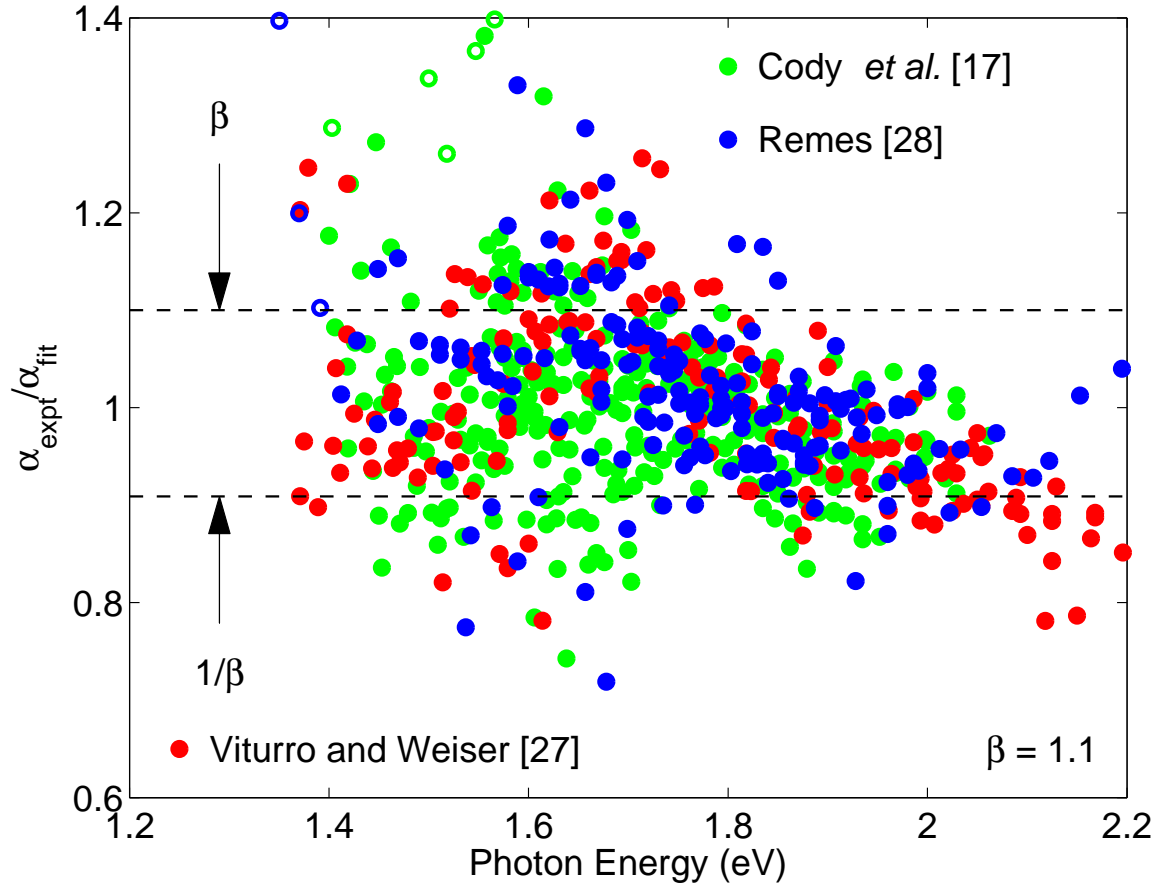


**Figure 4.10:** Deviations between the experimental results and the corresponding fits as determined through a ratio of the experimental and fit results for the experimental a-Si:H optical absorption data sets of Cody *et al.* [17], Viturro and Weiser [27], and Remeš [28]. The ordinate values for this plot are obtained by dividing each experimental value,  $\alpha_{\text{expt}}$ , by the corresponding fit value,  $\alpha_{\text{fit}}$ , the abscissa axis being the corresponding photon energy,  $\hbar\omega$ . For the optical absorption values not influenced by defect absorption, 219 of the 290 experimental points of Cody *et al.* [17], 117 of the 176 experimental points of Viturro and Weiser [27], and 136 of the 181 experimental points of Remeš [28], lie between  $\frac{1}{\beta}\alpha_{\text{fit}}$  and  $\beta\alpha_{\text{fit}}$ , for the specific case of  $\beta$  set to 1.1.

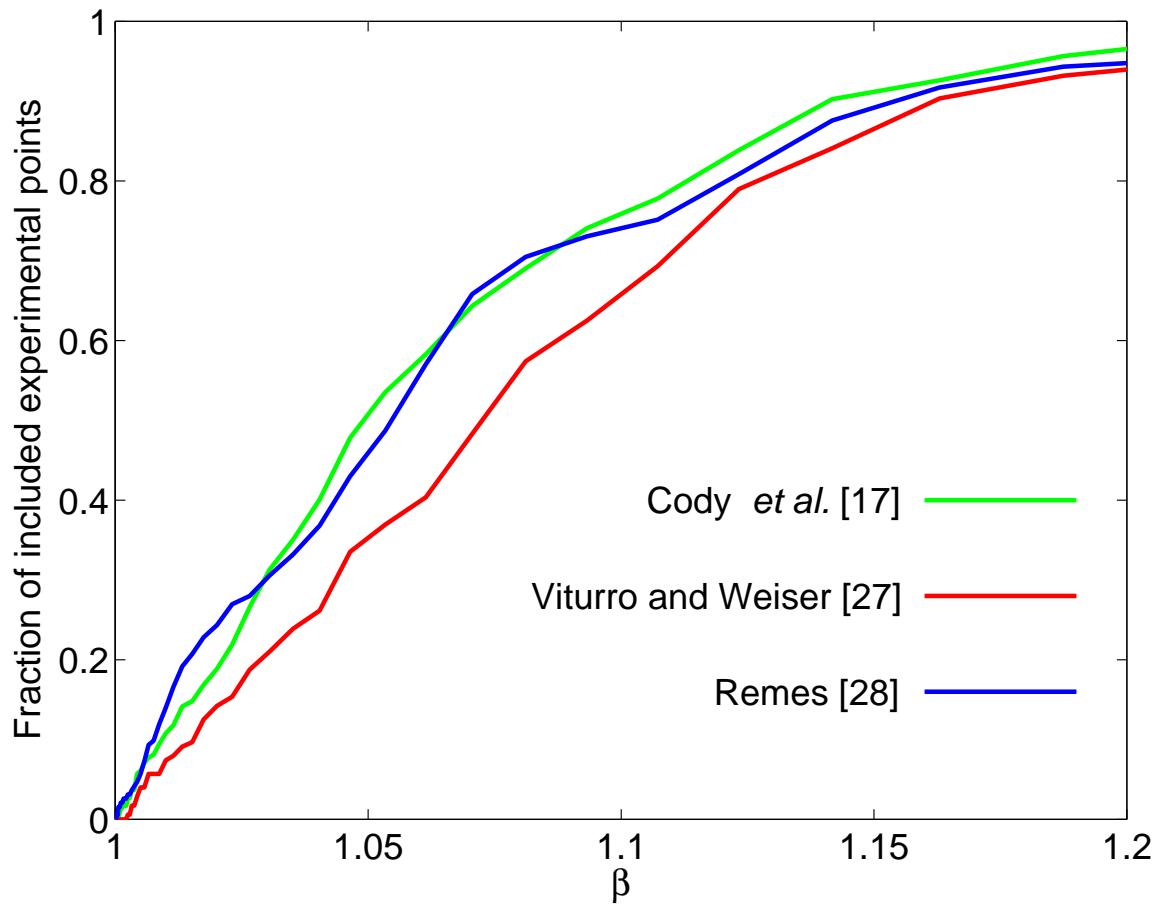


**Figure 4.11:** The fraction of the experimental points between  $\frac{1}{\beta}\alpha_{\text{fit}}$  and  $\beta\alpha_{\text{fit}}$  as a function of  $\beta$ . The data sets of Cody *et al.* [17], Viturro and Weiser [27], and Remeš [28] are considered in this analysis.

points are included for  $\beta$  set to 1.11. This provides compelling evidence in favor of the presence of a universal feature in the optical absorption spectrum associated with a-Si:H. In light of the fact that the a-Si:H optical absorption data sets are drawn from a variety of different forms of a-Si:H, this universal character seems to transcend the exact nature of the material considered.

## 4.6 Conclusions

Using a dimensionless JDOS formalism for the quantitative characterization of the optical response associated with a-Si:H, a critical comparative analysis of a large number of disparate optical absorption data sets is considered. When these data sets are cast into this dimensionless framework, we observe a trend that is almost completely coincident for all of the data sets considered. This suggests that there is a universal character associated with the optical absorption spectrum associated with a-Si:H.

**Acknowledgements:** The authors gratefully acknowledge financial support from the Natural Sciences and Engineering Research Council of Canada.

## References

- [1] R. A. Street, *Hydrogenated Amorphous Silicon*, Cambridge University Press, New York, 1991.
- [2] R. A. Street, Editor, *Technology and Applications of Amorphous Silicon*. New York, New York: Springer-Verlag, 2000.
- [3] L. K. Wagner and J. C. Grossman, “Microscopic description of light induced defects in amorphous silicon solar cells,” *Physical Review Letters*, vol. 101, no. 26, pp. 265501-1-3, 2008.
- [4] W.-S. Lee, G. W. Neudeck, J. Choi, and S. Luan, “A model for the temperature-dependent saturated  $I_D$ - $V_D$  characteristics of an a-Si:H thin-film transistor,” *IEEE Transactions on Electron Devices*, vol. 38, no. 9, pp. 2070-2074, 1991.
- [5] F. Stern, “Optical absorption edge of compensated germanium,” *Physical Review B*, vol. 3, no. 10, pp. 3559-3560, 1971.
- [6] S. John, C. Soukoulis, M. H. Cohen, and E. N. Economou, “Theory of electron band tails and the Urbach optical-absorption edge,” *Physical Review Letters*, vol. 57, no. 14, pp. 1777-1780, 1986.
- [7] S. John, M. Y. Chou, M. H. Cohen, and C. M. Soukoulis, “Density of states for an electron in a correlated Gaussian random potential: theory of the Urbach tail,” *Physical Review B*, vol. 37, no. 12, pp. 6963-6976, 1988.
- [8] S. K. O’Leary, S. Zukotynski, and J. M. Perz, “Semiclassical density-of-states and optical-absorption analysis of amorphous semiconductors,” *Physical Review B*, vol. 51, no. 7, pp. 4143-4149, 1995.
- [9] S. K. O’Leary, S. Zukotynski, and J. M. Perz, “Optical absorption in amorphous semiconductors,” *Physical Review B*, vol. 52, no. 11, pp. 7795-7797, 1995.
- [10] S. K. O’Leary, S. R. Johnson, and P. K. Lim, “The relationship between the distribution of electronic states and the optical absorption spectrum of an amorphous semiconductor: an empirical analysis,” *Journal of Applied Physics*, vol. 82, no. 7, pp. 3334-3340, 1997.
- [11] A. S. Ferlauto, G. M. Ferreira, J. M. Pearce, C. R. Wronski, R. W. Collins, X. Deng, and G. Ganguly, “Analytical model for the optical functions of amorphous semiconductors from the near-infrared to ultraviolet: Applications in thin film photovoltaics,” *Journal of Applied Physics*, vol. 92, no. 5, pp. 2424-2436, 2002.
- [12] S. K. O’Leary and S. M. Malik, “A simplified joint density of states analysis of hydrogenated amorphous silicon,” *Journal of Applied Physics*, vol. 92, no. 8, pp. 4276-4282, 2002.

- [13] S. K. O’Leary, “An analytical density of states and joint density of states analysis of amorphous semiconductors,” *Journal of Applied Physics*, vol. 96, no. 7, pp. 3680-3686, 2004.
- [14] E. Malainho, M. I. Vasilevskiy, P. Alpuim, and S. A. Filonovich, “Dielectric function of hydrogenated amorphous silicon near the optical absorption edge,” *Journal of Applied Physics*, vol. 106, no. 7, pp. 073110-1-9, 2009.
- [15] M. H. Brodsky, R. S. Title, K. Weiser, and G. D. Pettit, “Structural, optical, and electrical properties of amorphous silicon films,” *Physical Review B*, vol. 1, no. 6, pp. 2632-2641, 1970.
- [16] E. C. Freeman and W. Paul, “Optical constants of rf sputtered hydrogenated amorphous Si,” *Physical Review B*, vol. 20, no. 2, pp. 716-728, 1979.
- [17] G. D. Cody, T. Tiedje, B. Abeles, B. Brooks, and Y. Goldstein, “Disorder and the optical-absorption edge of hydrogenated amorphous silicon,” *Physical Review Letters*, vol. 47, no. 20, pp. 1480-1483, 1981.
- [18] W. B. Jackson, S. M. Kelso, C. C. Tsai, J. W. Allen, and S.-J. Oh, “Energy dependence of the optical matrix element in hydrogenated amorphous and crystalline silicon,” *Physical Review B*, vol. 31, no. 8, pp. 5187-5198, 1985.
- [19] R. V. Kruzelecky, C. Ukah, D. Racansky, S. Zukotynski, and J. M. Perz, “Interband optical absorption in amorphous silicon,” *Journal of Non-Crystalline Solids*, vol. 103, no. 2-3, pp. 234-249, 1988.
- [20] H. V. Nguyen, Y. Lu, S. Kim, M. Wakagi, and R. W. Collins, “Optical properties of ultrathin crystalline and amorphous silicon films,” *Physical Review Letters*, vol. 74, no. 19, pp. 3880-3883, 1995.
- [21] A. Kondilis, “Imperfections and optical absorption in glow-discharge a-Si:H films: A study in the visible and near-infrared region,” *Physical Review B*, vol. 62, no. 15, pp. 10526-10534, 2000.
- [22] B. J. Fogal, S. K. O’Leary, D. J. Lockwood, J.-M. Baribeau, M. Noël, and J. C. Zwinkels, “Disorder and the optical properties of amorphous silicon grown by molecular beam epitaxy,” *Solid State Communications*, vol. 120, no. 11, pp. 429-434, 2001.
- [23] S. K. O’Leary, B. J. Fogal, D. J. Lockwood, J.-M. Baribeau, M. Noël, and J. C. Zwinkels, “Optical dispersion relationships in amorphous silicon grown by molecular beam epitaxy,” *Journal of Non-Crystalline Solids*, vol. 290, no. 1, pp. 57-63, 2001.

- [24] D. J. Lockwood, J.-M. Baribeau, M. Noël, J. C. Zwinkels, B. J. Fogal, and S. K. O’Leary, “Optical absorption in an amorphous silicon superlattice grown by molecular beam epitaxy,” *Solid State Communications*, vol. 122, no. 5, pp. 271-275, 2002.
- [25] L.-L. Tay, D. J. Lockwood, J.-M. Baribeau, M. Noël, J. C. Zwinkels, F. Orapunt, and S. K. O’Leary, “Influence of growth temperature on order within silicon films grown by ultrahigh-vacuum evaporation on silica,” *Applied Physics Letters*, vol. 88, no. 12, pp. 121920-1-3, 2006.
- [26] J. J. Thevaril and S. K. O’Leary, “A dimensionless joint density of states formalism for the quantitative characterization of the optical response of hydrogenated amorphous silicon,” *Journal of Applied Physics*, vol. 107, no. 8, pp. 083105-1-6, 2010.
- [27] R. E. Viturro and K. Weiser, “Some properties of hydrogenated amorphous silicon produced by direct reaction of silicon and hydrogen atoms,” *Philosophical Magazine B*, vol. 53, no. 2, pp. 93-103, 1986.
- [28] Z. Remeš, “Study of defects and microstructure of amorphous and microcrystalline silicon thin films and polycrystalline diamond using optical methods,” *Ph. D. Thesis*, Charles University, Prague, 1999.
- [29] R. H. Klazes, M. H. L. M. van den Broek, J. Bezemer, and S. Radelaar, “Determination of the optical bandgap of amorphous silicon,” *Philosophical Magazine B*, vol. 45, no. 4, pp. 377-383, 1982.
- [30] T. M. Mok and S. K. O’Leary, “The dependence of the Tauc and Cody optical gaps associated with hydrogenated amorphous silicon on the film thickness: all experimental limitations and the impact of curvature in the Tauc and Cody plots,” *Journal of Applied Physics*, vol. 102, no. 11, pp. 113525-1-9, 2007.
- [31] G. D. Cody, C. R. Wronski, B. Abeles, R. B. Stephens, and B. Brooks, “Optical characterization of amorphous silicon hydride films,” *Solar Cells*, vol. 2, no. 3, pp. 227-243, 1980.
- [32] C. B. Roxlo, B. Abeles, C. R. Wronski, G. D. Cody, and T. Tiedje, “Comment on the optical absorption edge in a-Si:H,” *Solid State Communications*, vol. 47, no. 12, pp. 985-987, 1983.
- [33] L. Jiao, I. Chen, R. W. Collins, C. R. Wronski, and N. Hata, “An improved analysis for band edge optical absorption spectra in hydrogenated amorphous silicon from optical and photoconductivity measurements,” *Applied Physics Letters*, vol. 72, no. 9, pp. 1057-1059, 1998.

- [34] S. M. Malik and S. K. O’Leary, “An analysis of the distributions of electronic states associated with hydrogenated amorphous silicon,” *Journal of Materials Science: Materials in Electronics*, vol. 16, no. 3, pp. 177-181, 2005.
- [35] S. K. O’Leary, “An empirical density of states and joint density of states analysis of hydrogenated amorphous silicon: a review,” *Journal of Materials Science: Materials in electronics*, vol. 15, pp. 401-410, 2004.
- [36] S. M. Malik and S. K. O’Leary, “Optical transitions in hydrogenated amorphous silicon,” *Applied Physics Letters*, vol. 80, no. 5, pp. 790-792, 2002.
- [37] S. M. Malik and S. K. O’Leary, “Deviations from square-root distributions of electronic states in hydrogenated amorphous silicon and their impact upon the resultant optical properties,” *Journal of Non-Crystalline Solids*, vol. 336, no. 1, pp. 64-70, 2004.
- [38] F. Orapunt and S. K. O’Leary, “A quantitative characterization of the optical absorption spectrum associated with hydrogenated amorphous silicon,” *Journal of Materials Science: Materials in Electronics*, vol. 20, no. 10, pp. 1033-1038, 2009.
- [39] S. K. O’Leary, “Spectral dependence of the squared average optical transition matrix element associated with hydrogenated amorphous silicon,” *Applied Physics Letters*, vol. 82, no. 17, pp. 2784-2786, 2003.
- [40] K. H. Jun, R. Carius, and H. Stiebig, “Optical characteristics of intrinsic microcrystalline silicon,” *Physical Review B*, vol. 66, no. 11, pp. 11530-1-11, 2002.

---

## CHAPTER 5

---

# Defect absorption and optical transitions in hydrogenated amorphous silicon

*A version of this paper was published in Solid State Communications.*

*“Reprinted with permission from Thevaril, J.J. and O’Leary, S.K., Defect absorption and optical transitions in hydrogenated amorphous silicon, vol. 150, no. 37-38, pp. 1851-1855, Copyright [2010].”*

The following equations, introduced in this chapter, were introduced previously in this thesis:

Eq. (5.1)  $\Rightarrow$  Eq. (1.13)

Eq. (5.2)  $\Rightarrow$  Eq. (1.10)

Eq. (5.3)  $\Rightarrow$  Eq. (1.31)

Eq. (5.4)  $\Rightarrow$  Eq. (1.32)

Eq. (5.7)  $\Rightarrow$  Eq. (1.14)

## 5.1 Introduction

The optical response of hydrogenated amorphous silicon (a-Si:H) has been a focus for intensive investigation for many years [1–11]. Defects play an important role in shaping this response. The distinctive broadening exhibited in the low energy region of the imaginary part of the dielectric function associated with a-Si:H,  $\epsilon_2(\hbar\omega)$ , for example, is attributable to the presence of distributions of defect states [12, 13]. While there has been some basic work performed on developing an understanding as to how the underlying distributions of defect states shape the optical response of this material [14–16], the role that the individual types of optical transitions play in determining the character of this response remains unknown. Considering that fundamentally the optical response that occurs within a-Si:H is determined by the number of allowed optical transitions and by the magnitude of the optical transition matrix elements which couple the electronic states between which these optical transitions occur [17], this present state of affairs is lamentable.

In an earlier letter, Malik and O’Leary [18] determined the contributions to the optical response associated with a-Si:H corresponding to the various types of optical transitions that occur. The empirical model for the density of states (DOS) functions employed by Malik and O’Leary [18] considered valence band band (VBB) states, valence band tail (VBT) states, conduction band band (CBB) states, and conduction band tail (CBT) states. As optical transitions occur between the occupied valence band states and the unoccupied conduction band states, only optical transitions from the VBB states to the CBB states (VBB-CBB optical transitions), from the VBB states to the CBT states (VBB-CBT optical transitions), from the VBT states to the CBB states (VBT-CBB optical transitions), and from the VBT states to the CBT states (VBT-CBT optical transitions) are considered in the analysis of Malik and

O’Leary [18]; the presence of defect states was neglected.

In this Chapter, we aim to enrich the analysis of Malik and O’Leary [18], examining the role that defect states play in shaping the optical response of a-Si:H. We do so by generalizing the empirical DOS model of Malik and O’Leary [18] to include defect states. In particular, both valence band defect (VBD) states and conduction band defect (CBD) states are added to the distributions of VBB, VBT, CBB, and CBT states considered by Malik and O’Leary [18]. Accordingly, optical transitions from the VBB states to the CBD states (VBB-CBD optical transitions), from the VBT states to the CBD states (VBT-CBD optical transitions), from the the VBD states to the CBB states (VBD-CBB optical transitions), from the VBD states to the CBT states (VBD-CBT optical transitions), and from the VBD states to the CBD states (VBD-CBD optical transitions), in addition to the aforementioned VBB-CBB, VBB-CBT, VBT-CBB, and VBT-CBT optical transitions, are accounted for within the framework of this more generalized empirical model for the DOS functions. Using this enriched model, initially the contrast between results obtained with and without defect states is used in order to examine how distributions of defect states influence the corresponding optical response. Then, with defect states included, the contributions to the optical response attributable to the various types of optical transitions will be determined. Finally, we demonstrate how we are able to capture the spectral dependence of the optical absorption coefficient associated with a defect absorption influenced sample of a-Si:H using our empirical DOS model with defect states included.

## 5.2 Analytical framework

For the specific case of a-Si:H, Jackson *et al.* [19] demonstrate that

$$\epsilon_2(\hbar\omega) = 4.3 \times 10^{-45} \mathcal{R}^2(\hbar\omega) J(\hbar\omega), \quad (5.1)$$

where  $\mathcal{R}^2(\hbar\omega)$ , the normalized dipole matrix element squared average, is in units of  $\text{\AA}^2$  and  $J(\hbar\omega)$ , the joint density of states (JDOS) function, is in units of  $\text{cm}^{-6}\text{eV}^{-1}$ . The experimental results of Jackson *et al.* [19] suggest, for  $\hbar\omega$  between 0.6 and 3.0 eV, that  $\mathcal{R}^2(\hbar\omega) \simeq 10 \text{\AA}^2$ . As a result, for this range of photon energies, our analysis reduces to the determination of the JDOS function itself. Assuming zero-temperature statistics, this JDOS function may be expressed as an integral over the valence band and conduction band DOS functions. That is,

$$J(\hbar\omega) \equiv \int_{-\infty}^{\infty} N_v(E) N_c(E + \hbar\omega) dE, \quad (5.2)$$

where  $N_v(E)$  and  $N_c(E)$  denote the valence band and conduction band DOS functions, respectively,  $N_v(E) \Delta E$  and  $N_c(E) \Delta E$  representing the number of one-electron valence band and conduction band states, between energies  $[E, E + \Delta E]$ , per unit volume.

For the purposes of this analysis, we adopt an elementary empirical model for these DOS functions that captures the basic expected features. In particular, in the absence of defect states, we follow the approach of Jiao *et al.* [20] and O'Leary *et al.* [18, 21–26], and assume exponential distributions of tail states and square-root

distributions of band states. That is, we set

$$N_v(E) = N_{vo} \begin{cases} \sqrt{E_v - E_{vT}} \exp\left(\frac{E_{vT} - E_v}{\gamma_v}\right) \exp\left(\frac{E_v - E}{\gamma_v}\right), & E > E_{vT} \\ \sqrt{E_v - E}, & E \leq E_{vT} \end{cases}, \quad (5.3)$$

and

$$N_c(E) = N_{co} \begin{cases} \sqrt{E - E_c}, & E \geq E_{cT} \\ \sqrt{E_{cT} - E_c} \exp\left(\frac{E_c - E_{cT}}{\gamma_c}\right) \exp\left(\frac{E - E_c}{\gamma_c}\right), & E < E_{cT} \end{cases}, \quad (5.4)$$

where  $N_{vo}$  and  $N_{co}$  denote the valence band and conduction band DOS prefactors, respectively,  $E_v$  and  $E_c$  represent the valence band and conduction band band edges,  $\gamma_v$  and  $\gamma_c$  are the breadths of the valence band and conduction band tails, and  $E_{vT}$  and  $E_{cT}$  are the critical energies at which the exponential and square-root distributions interface; this model is identical to that employed by Malik and O'Leary [18]. It should be noted that this model implicitly requires that  $E_v - E_{vT} \geq 0$  and  $E_{cT} - E_c \geq 0$ . It should also be noted that  $N_v(E)$  and  $N_c(E)$  are continuous functions of energy.

With defect states included, we follow the spirit of the analysis Shur and Hack [27], Shaw and Hack [28], Shur, Hack, and Shaw [29], and Slade [30] and spline additional exponential distributions, of greater breadths than the valence band and conduction band tails, onto the valence band and conduction band tails.<sup>1</sup> As a result, our

---

<sup>1</sup>An exact use of the model of Shur and Hack [27], in which the conduction band DOS below the band edge is modeled by the sum of two exponential distributions, a narrow exponential distribution corresponding to the tail states and a broad exponential distribution corresponding to the defect states, makes it difficult to clearly dilenate between the tail and defect state distributions. The same problem is found for the models of Shaw and Hack [28], Shur, Hack, and Shaw [29], and Slade [30]. Given that a clear separation between these states is vital to our analysis, we proposed an alternate model for the DOS functions which does provide for a clear dileneation between the states. With an appropriate selection of parameters, the differences between these models are relatively minor.

empirical model for the DOS functions becomes

$$N_v(E) = N_{vo} \left\{ \begin{array}{l} \sqrt{E_v - E_{v_T}} \exp\left(\frac{E_{v_T} - E_v}{\gamma_v}\right) \exp\left(\frac{E_v - E_{v_D}}{\gamma_v}\right) \exp\left(\frac{E_{v_D} - E}{\gamma_{v_D}}\right), \\ \hspace{15em} E > E_{v_D} \\ \\ \sqrt{E_v - E_{v_T}} \exp\left(\frac{E_{v_T} - E_v}{\gamma_v}\right) \exp\left(\frac{E_v - E}{\gamma_v}\right), \\ \hspace{15em} E_{v_T} > E \geq E_{v_D} \\ \\ \sqrt{E_v - E}, \\ \hspace{15em} E \leq E_{v_T} \end{array} \right. , \quad (5.5)$$

and

$$N_c(E) = N_{co} \left\{ \begin{array}{l} \sqrt{E - E_c}, \\ \hspace{15em} E \geq E_{c_T} \\ \\ \sqrt{E_{c_T} - E_c} \exp\left(\frac{E_c - E_{c_T}}{\gamma_c}\right) \exp\left(\frac{E - E_c}{\gamma_c}\right), \\ \hspace{15em} E_{c_D} \leq E < E_{c_T} \\ \\ \sqrt{E_{c_T} - E_c} \exp\left(\frac{E_c - E_{c_T}}{\gamma_c}\right) \exp\left(\frac{E_{c_D} - E_c}{\gamma_c}\right) \exp\left(\frac{E - E_{c_D}}{\gamma_{c_D}}\right), \\ \hspace{15em} E < E_{c_D} \end{array} \right. , \quad (5.6)$$

where  $\gamma_{v_D}$  and  $\gamma_{c_D}$  represent the breadths of the valence band and conduction band defect distributions, and  $E_{v_D}$  and  $E_{c_D}$  denote the critical energies at which the valence band and conduction band tails interface with the corresponding defect distributions,

$N_{vo}$ ,  $N_{co}$ ,  $E_v$ ,  $E_c$ ,  $\gamma_v$ ,  $\gamma_c$ ,  $E_{v_T}$ , and  $E_{c_T}$  being as defined previously; as with the defect-free model, i.e., Eqs. (5.3) and (5.4), we note that  $N_v(E)$  and  $N_c(E)$  are continuous functions of energy. We assume that  $\gamma_{v_D} \geq \gamma_v$ ,  $\gamma_{c_D} \geq \gamma_c$ ,  $E_{v_D} > E_{v_T}$ , and  $E_{c_T} > E_{c_D}$  for the purposes of this analysis. Note that in the limit that  $\gamma_{v_D}$  reduces to  $\gamma_v$ , that Eq. (5.5) reduces to Eq. (5.3), and that in the limit that  $\gamma_{c_D}$  reduces to  $\gamma_c$ , that Eq. (5.6) reduces to Eq. (5.4), i.e., our generalized empirical DOS model with defect states included reduces to our defect-free empirical DOS model. For the purposes of this analysis, we adopt the same nominal a-Si:H modeling parameter selections as that employed by Malik and O’Leary [18], i.e., we set  $N_{vo} = N_{co} = 2 \times 10^{22} \text{ cm}^{-3} \text{ eV}^{-3/2}$ ,  $E_v = 0.0 \text{ eV}$ ,  $E_c = 1.7 \text{ eV}$ ,  $\gamma_v = 50 \text{ meV}$ ,  $\gamma_c = 27 \text{ meV}$ , and  $E_v - E_{v_T} = E_{c_T} - E_c = 35 \text{ meV}$ , noting that these parameter selections are representative of a-Si:H [31, 32]. We complete our specification of parameters by borrowing from the analysis of Slade [30], setting  $\gamma_{v_D} = 130 \text{ meV}$ ,  $\gamma_{c_D} = 80 \text{ meV}$ ,  $E_{v_D} - E_v = 400 \text{ meV}$ , and  $E_c - E_{c_D} = 200 \text{ meV}$ .<sup>2</sup> These nominal a-Si:H modeling parameter selections, employed for the purposes of this analysis, are tabulated in Table 5.1. The resultant DOS functions are depicted in Figure 5.1, the distributions of VBB, VBT, VBD, CBB, CBT, and CBD electronic states being clearly depicted. Representative VBB-CBB, VBB-CBT, VBT-CBB, VBT-CBT, VBD-CBB, and VBD-CBT optical transitions are depicted. Representative VBB-CBD, VBT-CBD, and VBD-CBD optical transitions are not depicted as they are found to make relatively minor contributions to the JDOS function.

### 5.3 Results

In Figure 5.2, we plot the JDOS function associated with a-Si:H,  $J(\hbar\omega)$ , determined through an evaluation of Eq. (5.2). In order to determine the role that

---

<sup>2</sup>These values are actually rounded values from the selections of Slade [30].

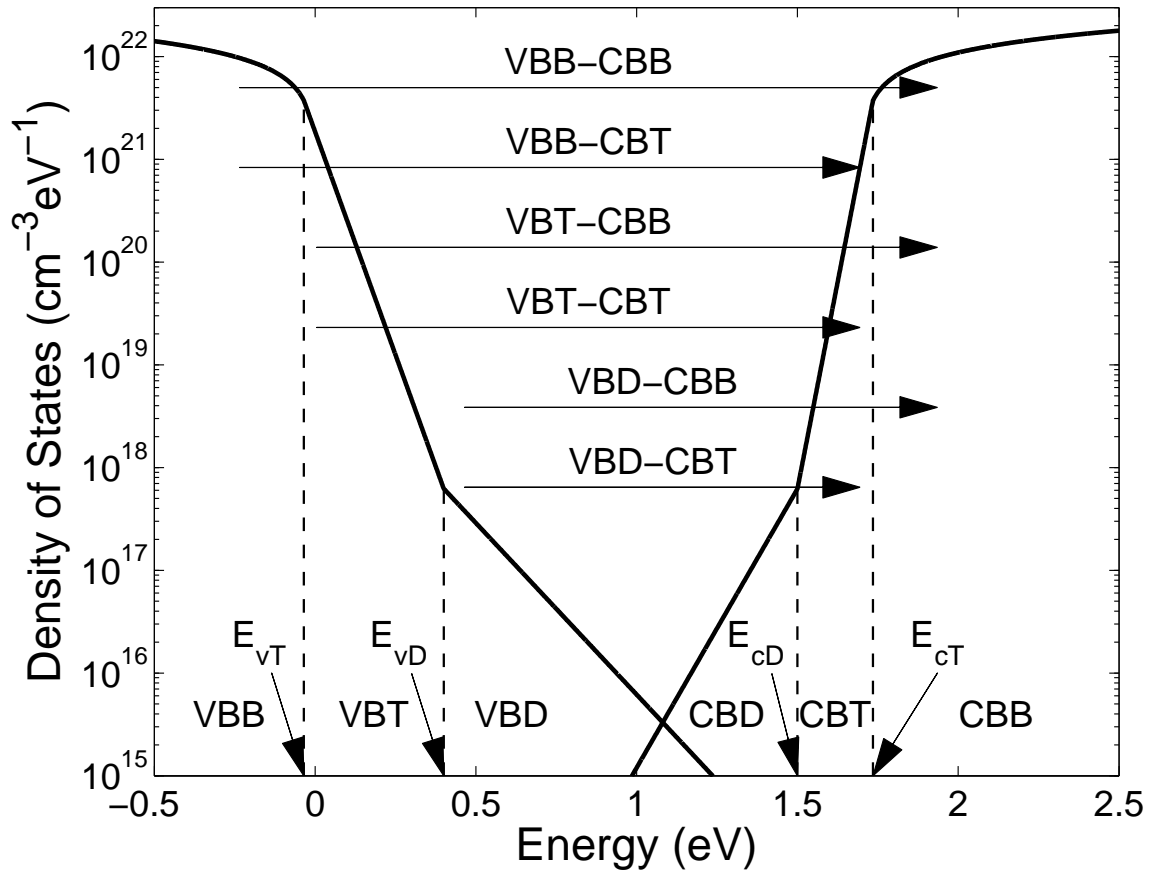


**Figure 5.1:** The valence band and conduction band DOS functions associated with a-Si:H. The valence band DOS function,  $N_v(E)$ , specified in Eq. (5.5), is determined assuming the nominal a-Si:H parameter selections  $N_{vo} = 2 \times 10^{22} \text{ cm}^{-3} \text{ eV}^{-3/2}$ ,  $E_v = 0.0 \text{ eV}$ ,  $\gamma_v = 50 \text{ meV}$ ,  $E_v - E_{vT} = 35 \text{ meV}$ ,  $\gamma_{vD} = 130 \text{ meV}$ , and  $E_{vD} - E_v = 400 \text{ meV}$ . The conduction band DOS function,  $N_c(E)$ , specified in Eq. (5.6), is determined assuming the nominal parameter selections  $N_{co} = 2 \times 10^{22} \text{ cm}^{-3} \text{ eV}^{-3/2}$ ,  $E_c = 1.7 \text{ eV}$ ,  $\gamma_c = 27 \text{ meV}$ ,  $E_{cT} - E_c = 35 \text{ meV}$ ,  $\gamma_{cD} = 80 \text{ meV}$ , and  $E_c - E_{cD} = 200 \text{ meV}$ . The critical points at which the band states and tail states interface,  $E_{vT}$  and  $E_{cT}$ , are clearly marked with the dashed lines and the arrows. The critical points at which the tail states and defect states interface,  $E_{vD}$  and  $E_{cD}$ , are also marked with the dashed lines and the arrows. Representative VBB-CBB, VBB-CBT, VBT-CBB, VBT-CBT, VBD-CBB, and VBD-CBT optical transitions are depicted. Representative VBB-CBD, VBT-CBD, and VBD-CBD optical transitions are not depicted as they are found to make relatively minor contributions to the JDOS function.

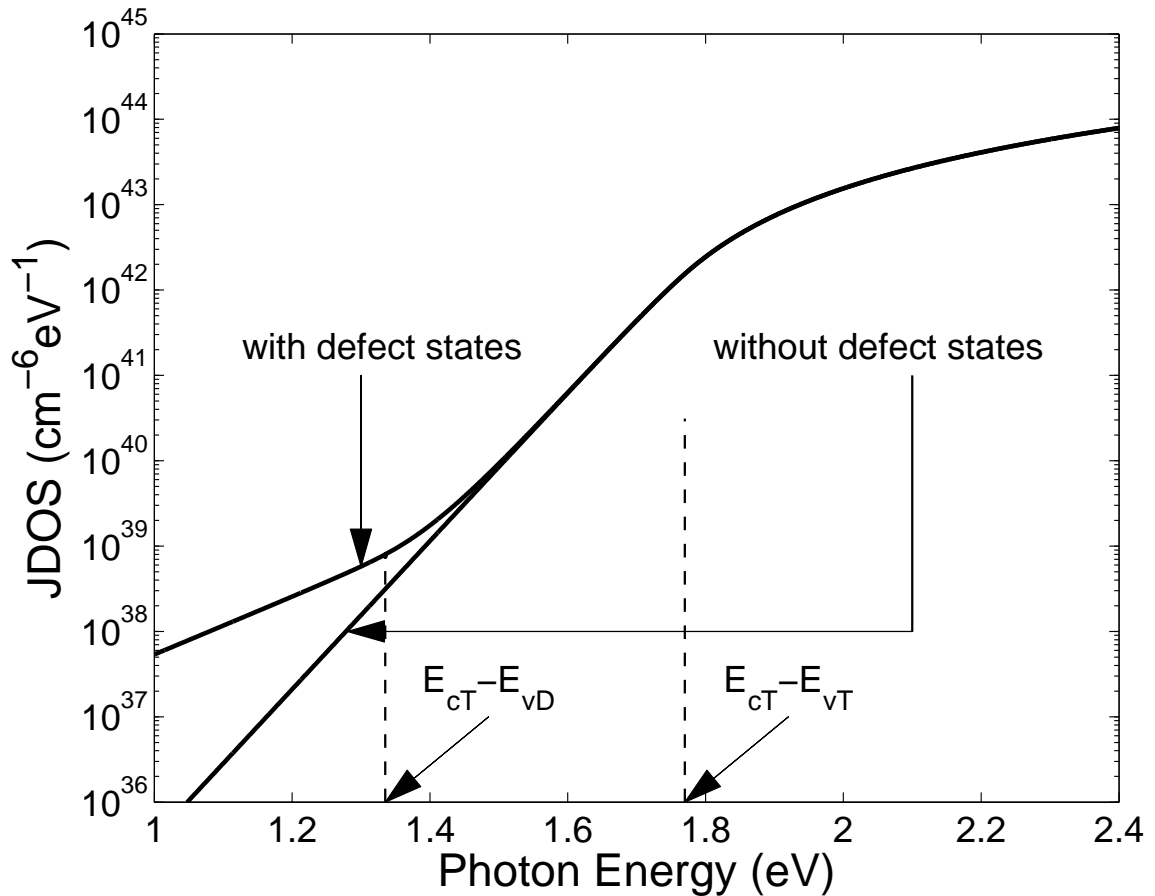


**Figure 5.2:** The JDOS function,  $J(\hbar\omega)$ , associated with a-Si:H, determined through an evaluation of Eq. (5.2). For the purposes of this analysis, we performed this evaluation with and without the defect states taken into account. In the absence of defects,  $N_v(E)$  and  $N_c(E)$  are as specified in Eqs. (5.3) and (5.4), respectively. With defects taken into account,  $N_v(E)$  and  $N_c(E)$  are as specified in Eqs. (5.5) and (5.6), respectively. The modeling parameters are set to their nominal a-Si:H values for the purposes of this analysis; recall Table 5.1.  $E_{cT} - E_{vT}$  and  $E_{cT} - E_{vD}$ , critical energies in our JDOS analysis, are clearly marked with the dashed lines and the arrows.

**Table 5.1:** The nominal a-Si:H modeling parameter selections employed for the purposes of this analysis.

parameter (units)	value
$N_{vo}$ ( $\text{cm}^{-3}\text{eV}^{-3/2}$ )	$2 \times 10^{22}$
$N_{co}$ ( $\text{cm}^{-3}\text{eV}^{-3/2}$ )	$2 \times 10^{22}$
$E_v$ (eV)	0.0
$E_c$ (eV)	1.7
$\gamma_v$ (meV)	50
$\gamma_c$ (meV)	27
$E_v - E_{v_T}$ (meV)	35
$E_{c_T} - E_c$ (meV)	35
$\gamma_{v_D}$ (meV)	130
$\gamma_{c_D}$ (meV)	80
$E_{v_D} - E_v$ (meV)	400
$E_c - E_{c_D}$ (meV)	200

defect states play in influencing this JDOS function, we perform this evaluation with and without defect states taken into account. The modeling parameters are set to their nominal a-Si:H values for the purposes of this analysis; recall Table 5.1. We note that in the absence of defect states, the JDOS function exhibits the spectral response characteristic of an ‘ideal’ amorphous semiconductor, i.e., an algebraic functional dependence beyond the optical gap and a sub-gap exponential tail [19]. This exponential tail, whose onset corresponds to the onset of optical transitions involving the exponentially distributed tail states, i.e.,  $\hbar\omega < E_{c_T} - E_{v_T}$ , has a breadth that is determined by the dominant tail breadth, i.e.,  $\gamma_v$  for the case of a-Si:H. With defect states included, however, the JDOS function broadens considerably at low photon energies, corresponding to the onset of significant optical transitions involving the VBD states, i.e.,  $\hbar\omega < E_{c_T} - E_{v_D}$ . The breadth of the JDOS function for this range of photon energies is determined by the dominant defect distribution breadth, i.e., for our nominal a-Si:H parameter selections,  $\gamma_{v_D}$ .

In order to quantitatively assess the impact of each type of optical transition on the overall JDOS function associated with a-Si:H, in Figure 5.3 we plot the fractional

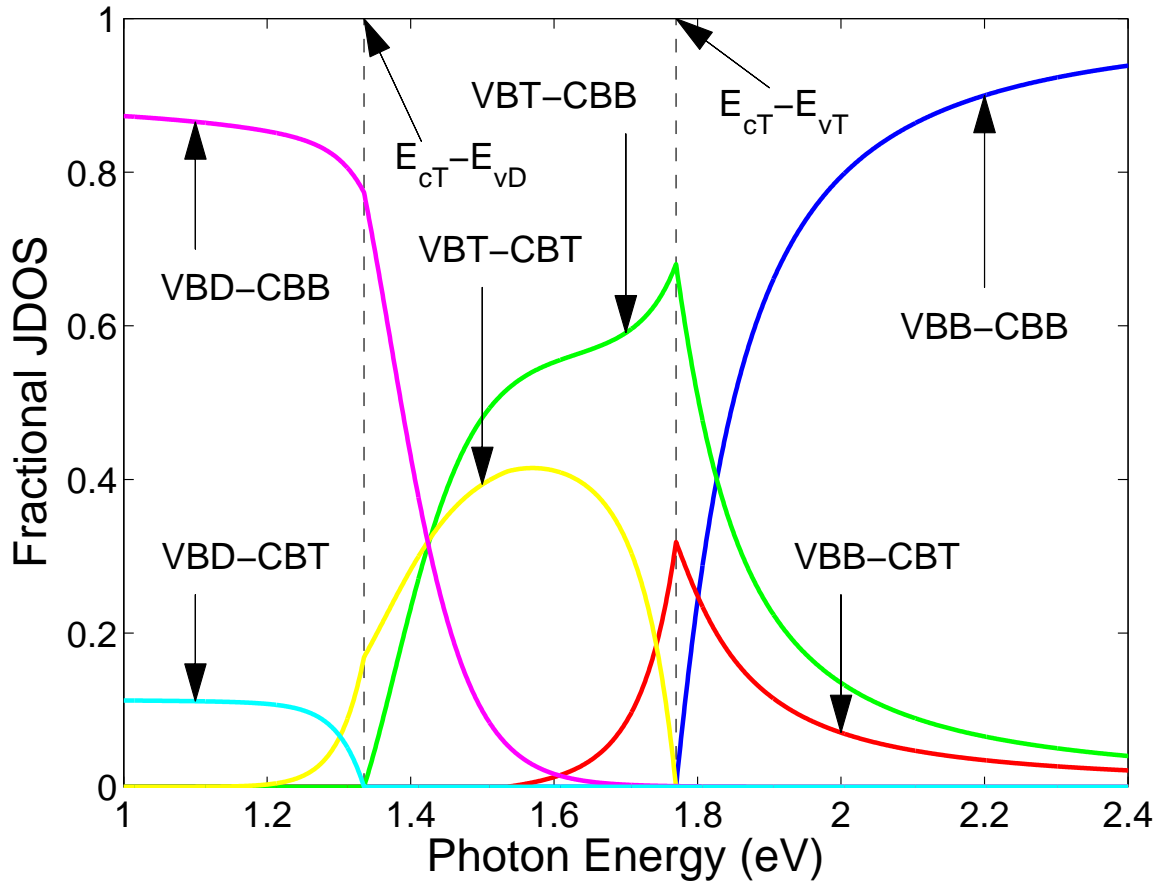


**Figure 5.3:** The fractional contributions to the overall JDOS function associated with the various types of a-Si:H optical transitions. The contribution attributable to the VBB-CBB optical transitions is shown with the solid blue line. The contribution attributable to the VBB-CBT optical transitions is shown with the solid red line. The contribution attributable to the VBT-CBB optical transitions is shown with the solid green line. The contribution attributable to the VBT-CBT optical transitions is shown with the solid yellow line. The contribution attributable to the VBD-CBB optical transitions is shown with the solid purple line. The contribution attributable to the VBD-CBT optical transitions is shown with the solid light blue line. The contributions to the JDOS function attributable to the VBB-CBD, VBT-CBD, and VBD-CBD optical transitions are not depicted as they are found to make relatively minor contributions to the JDOS function. The modeling parameters are set to their nominal a-Si:H values for the purposes of this analysis; recall Table 5.1.  $E_{cT} - E_{vT}$  and  $E_{cT} - E_{vD}$ , critical energies in our JDOS analysis, are clearly marked with the dashed lines and the arrows. The online version is in color.

contributions of the VBB-CBB, VBB-CBT, VBT-CBB, VBT-CBT, VBD-CBB, and VBD-CBT optical transitions on the overall JDOS function as a function of the photon energy,  $\hbar\omega$ ;<sup>3</sup> the fractional contributions of the VBB-CBD, VBT-CBD, and VBD-CBD optical transitions are not depicted as they are found to make relatively minor contributions to the JDOS function. Once again, our modeling parameters are set to their nominal a-Si:H values for the purposes of this analysis; recall Table 5.1. We note that the contribution to the overall JDOS function attributable to VBB-CBB optical transitions is nil until  $\hbar\omega$  exceeds  $E_{c_T} - E_{v_T}$ , beyond which it monotonically increases with increasing  $\hbar\omega$ . While VBB-CBB optical transitions dominate the form of the overall JDOS for  $\hbar\omega$  well in excess of the optical gap, other types of optical transitions also play a role, albeit a diminishing one, as  $\hbar\omega$  is increased for values of  $\hbar\omega$  in excess of the optical gap. For  $\hbar\omega$  set to 2 eV, 79.42, 7.04, and 13.53 % of the overall JDOS function is attributable to the VBB-CBB, VBB-CBT, and VBT-CBB optical transitions, respectively, VBT-CBT and VBD-CBT optical transitions making no contribution to the JDOS function for this value of  $\hbar\omega$ ; small contributions to the JDOS function attributable to VBB-CBD and VBD-CBB optical transitions are also found, the VBT-CBD and VBD-CBD optical transitions making no contribution to the JDOS function for this value of  $\hbar\omega$ . For selections of  $\hbar\omega$  well below the optical gap, VBD-CBB and VBD-CBT optical transitions dominate, the contributions attributable to the VBB-CBD and VBT-CBD optical transitions also playing a role, albeit a diminishing one, as  $\hbar\omega$  decreases. For  $\hbar\omega$  set to 1.0 eV, 0.74, 0.69, 87.30, and 11.23 % of the overall JDOS function is attributable to VBB-CBD, VBT-CBD, VBD-CBB, and VBD-CBT optical transitions, respectively, VBB-CBB, VBB-CBT, VBT-CBB, and VBT-CBT optical transitions making no contribution to the JDOS

---

<sup>3</sup>In order to determine the contribution to the JDOS function attributable solely to VBB-CBB, VBB-CBT, VBB-CBD, VBT-CBB, VBT-CBT, VBT-CBD, VBD-CBB, VBD-CBT, and VBD-CBD optical transitions, we integrate Eq. (5.2) over the appropriate energy intervals.

function for this value of  $\hbar\omega$ ; small contributions to the JDOS function attributable to VBD-CBD optical transitions are also found.

## 5.4 Comparison with experiment

We now demonstrate that our approach is able to capture the spectral dependence of the optical absorption coefficient associated with a defect absorption influenced sample of a-Si:H using our generalized empirical DOS model with defect states included. The experimental optical absorption a-Si:H data set considered corresponds to a sample prepared by Reměs [33] (this experimental data set corresponds to the “standard GD-a” data set depicted in Figure 5.2 of Reměs [33]). Details, on the means of sample preparation and on the approach taken whereby this optical absorption spectrum has been experimentally determined, are provided in the literature [33]. In order to determine the spectral dependence of the optical absorption coefficient,  $\alpha(\hbar\omega)$ , we note that

$$\alpha(\hbar\omega) = \frac{\omega}{n(\hbar\omega)c} \epsilon_2(\hbar\omega), \quad (5.7)$$

where  $n(\hbar\omega)$  denotes the spectral dependence of the index of refraction and  $c$  represents the speed of light in a vacuum. The spectral dependence of the refractive index,  $n(\hbar\omega)$ , is determined by fitting a tenth-order polynomial to the experimental results of Klazes *et al.* [34] (the experimental data considered corresponds to that presented in Figure 4 of Klazes *et al.* [34]); this approach was used previously by Mok and O’Leary [25] and Thevaril and O’Leary [35], the deviations from this model for  $n(\hbar\omega)$  not being expected to be significant.  $\mathcal{R}^2(\hbar\omega)$  is set to  $10 \text{ \AA}^2$ . From Eqs. (5.1), (5.2), (5.5), (5.6), and (5.7), the spectral dependence of  $\alpha(\hbar\omega)$  may be determined. We find that by setting  $N_{vo} = N_{co} = 2.38 \times 10^{22} \text{ cm}^{-3} \text{ eV}^{-3/2}$ ,  $E_v = 0.0 \text{ eV}$ ,  $E_c = 1.571 \text{ eV}$ ,  $\gamma_v = 75 \text{ meV}$ ,  $\gamma_c = 43 \text{ meV}$ ,  $E_v - E_{vT} = E_{cT} - E_c = 35 \text{ meV}$ ,

$\gamma_{v_D} = 675$  meV,  $\gamma_{c_D} = 600$  meV,  $E_{v_D} - E_v = 425$  meV, and  $E_c - E_{c_D} = 425$  meV, we are able to achieve a reasonably satisfactory fit with the a-Si:H experimental data of Reměš [33], this fit being shown in Figure 5.4. These a-Si:H modeling parameter selections, employed for the purposes of this fit, are tabulated in Table 5.2. The large values assigned to  $\gamma_{v_D}$  and  $\gamma_{c_D}$ , 675 and 600 meV, respectively, are consistent with that determined directly through the fit of an exponential function,  $\alpha_{o_D} \exp\left(\frac{\hbar\omega}{E_{o_D}}\right)$ , to the lower energy portion of the experimental a-Si:H optical absorption spectrum of Reměš [33]; we find that such a fit yields an  $E_{o_D}$  value equal to  $700 \pm 40$  meV. The resultant fit is depicted in Figure 5.4.

**Table 5.2:** The a-Si:H modeling parameter selections employed for the purposes of the fit to the experimental data of Reměš [33] shown in Figure 5.4.

parameter (units)	value
$N_{vo}$ ( $\text{cm}^{-3}\text{eV}^{-3/2}$ )	$2.38 \times 10^{22}$
$N_{co}$ ( $\text{cm}^{-3}\text{eV}^{-3/2}$ )	$2.38 \times 10^{22}$
$E_v$ (eV)	0.0
$E_c$ (eV)	1.571
$\gamma_v$ (meV)	75
$\gamma_c$ (meV)	43
$E_v - E_{v_T}$ (meV)	35
$E_{c_T} - E_c$ (meV)	35
$\gamma_{v_D}$ (meV)	675
$\gamma_{c_D}$ (meV)	600
$E_{v_D} - E_v$ (meV)	425
$E_c - E_{c_D}$ (meV)	425

## 5.5 Conclusions

In conclusion, using an empirical model for the DOS functions associated with a-Si:H, with defect states taken into account, we examined how the distributions of such states shape the optical response of this material. The contributions to this response attributable to the various types of optical transitions were also determined.

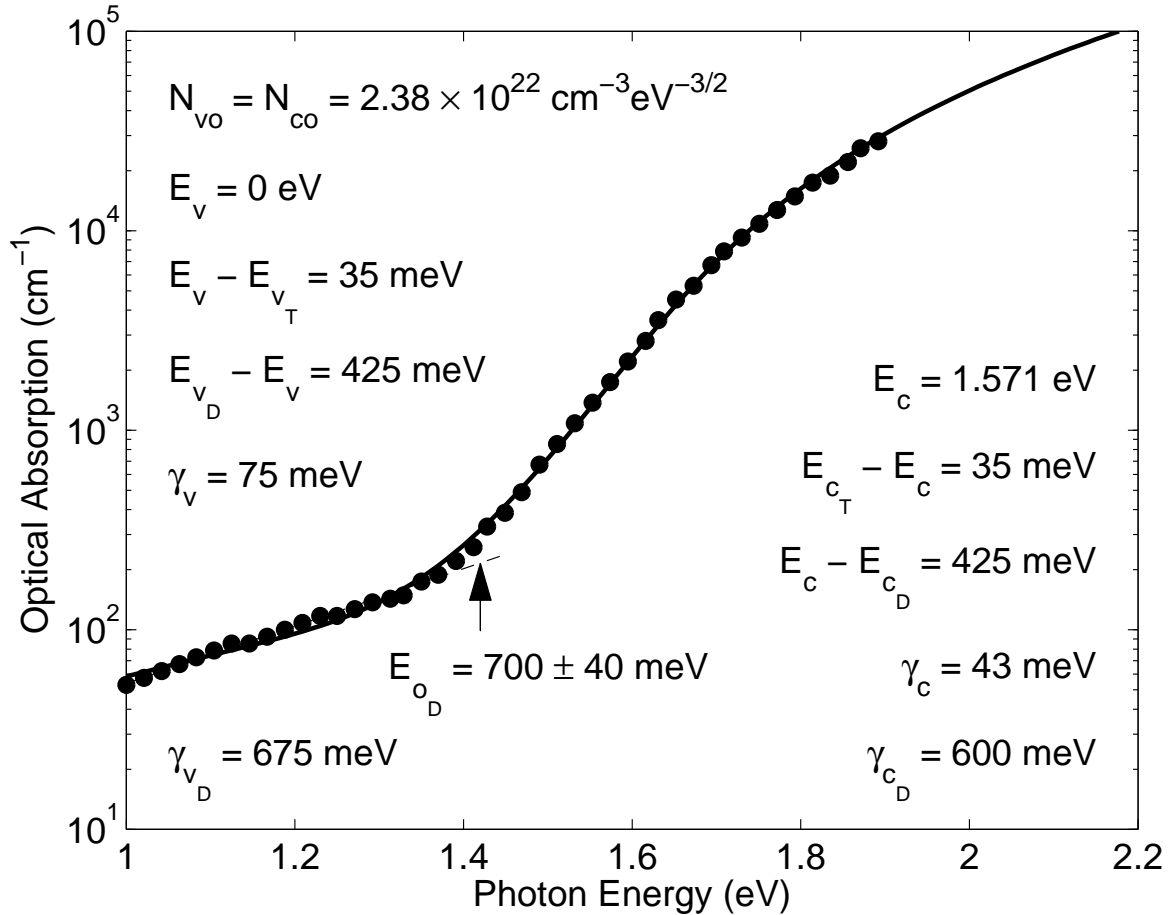


**Figure 5.4:** The optical absorption spectrum,  $\alpha(\hbar\omega)$ , associated with a-Si:H. The experimental data of Remeš [33] is depicted with the solid points; this experimental data set corresponds to the “standard GD-a” data set depicted in Figure 5.2 of Remeš [33]. The fit to this data set, determined using the modeling parameter selections specified in Table 5.2, is shown with the solid line. The fit of the lower portion of this spectrum to an exponential function,  $\alpha_{\text{oD}} \exp\left(\frac{\hbar\omega}{E_{\text{oD}}}\right)$ , is shown with the dashed line; the fit was obtained for experimental data with  $\hbar\omega < 1.4 \text{ eV}$ . The dashed line corresponding to this fit has been extrapolated out to 1.45 eV so that it is observable. The determined value of  $E_{\text{oD}}$  corresponding to this fit is  $700 \pm 40 \text{ meV}$ .

Finally, we demonstrated that we are able to capture the spectral dependence of the optical absorption coefficient associated with a defect absorption influenced sample of a-Si:H using our empirical formalism for the DOS functions associated with this material.

**Acknowledgements:** The authors gratefully acknowledge financial support from the Natural Sciences and Engineering Research Council of Canada.

## References

- [1] M. H. Brodsky, R. S. Title, K. Weiser, and G. D. Pettit, "Structural, optical, and electrical properties of amorphous silicon films," *Physical Review B*, vol. 1, no. 6, pp. 2632-2641, 1970.
- [2] E. C. Freeman and W. Paul, "Optical constants of rf sputtered hydrogenated amorphous Si," *Physical Review B*, vol. 20, no. 2, pp. 716-728, 1979.
- [3] T. Datta and J. A. Woollam, "Generalized model for the optical absorption edge in a-Si:H," *Physical Review B*, vol. 39, no. 3, pp. 1953-1954, 1989.
- [4] S. K. O'Leary, S. Zukotynski, and J. M. Perz, "Semiclassical density-of-states and optical-absorption analysis of amorphous semiconductors," *Physical Review B*, vol. 51, no. 7, pp. 4143-4149, 1995.
- [5] S. K. O'Leary, S. Zukotynski, and J. M. Perz, "Optical absorption in amorphous semiconductors," *Physical Review B*, vol. 52, no. 11, pp. 7795-7797, 1995.
- [6] S. K. O'Leary, "Optical absorption, disorder, and the disorderless limit in amorphous semiconductors," *Applied Physics Letters*, vol. 72, no. 11, pp. 1332-1334, 1998.
- [7] B. J. Fogal, S. K. O'Leary, D. J. Lockwood, J.-M. Baribeau, M. Noël, and J. C. Zwinkels, "Disorder and the optical properties of amorphous silicon grown by molecular beam epitaxy," *Solid State Communications*, vol. 120, no. 11, pp. 429-434, 2001.
- [8] S. K. O'Leary, B. J. Fogal, D. J. Lockwood, J.-M. Baribeau, M. Noël, and J. C. Zwinkels, "Optical dispersion relationships in amorphous silicon grown by molecular beam epitaxy," *Journal of Non-Crystalline Solids*, vol. 290, no. 1, pp. 57-63, 2001.
- [9] D. J. Lockwood, J.-M. Baribeau, M. Noël, J. C. Zwinkels, B. J. Fogal, and S. K. O'Leary, "Optical absorption in an amorphous silicon superlattice grown by molecular beam epitaxy," *Solid State Communications*, vol. 122, no. 5, pp. 271-275, 2002.
- [10] L.-L. Tay, D. J. Lockwood, J.-M. Baribeau, M. Noël, J. C. Zwinkels, F. Orapunt, and S. K. O'Leary, "Influence of growth temperature on order within silicon films grown by ultrahigh-vacuum evaporation on silica," *Applied Physics Letters*, vol. 88, no. 12, pp. 121920-1-3, 2006.
- [11] E. Malainho, M. I. Vasilevskiy, P. Alpuim, and S. A. Filonovich, "Dielectric function of hydrogenated amorphous silicon near the optical absorption edge," *Journal of Applied Physics*, vol. 106, no. 7, pp. 073110-1-9, 2009.

- [12] R. A. Street, *Hydrogenated Amorphous Silicon*, Cambridge, New York, 1991.
- [13] F. Orapunt and S. K. O’Leary, “A quantitative characterization of the optical absorption spectrum associated with hydrogenated amorphous silicon,” *Journal of Materials Science: Materials in Electronics*, vol. 20, no. 10, pp. 1033-1038, 2009.
- [14] C. R. Wronski, B. Abeles, T. Tiedje, and G. D. Cody, “Recombination centers in phosphorus doped hydrogenated amorphous silicon,” *Solid State Communications*, vol. 44, no. 10, pp. 1423-1426, 1982.
- [15] M. Vaněček, J. Kočka, J. Stuchlík, Z. Kožíšek, O. Štika, and A. Tríska, *Solar Energy Materials*, vol. 8, pp. 411, 1983.
- [16] G. Nobile and T. J. McMahon, “Limitations of the integrated sub-band-gap absorption for determining the density of defects in amorphous silicon,” *Journal of Applied Physics*, vol. 67, no. 1, pp. 578-580, 1990.
- [17] S. K. O’Leary, “Spectral dependence of the squared average optical transition matrix element associated with hydrogenated amorphous silicon,” *Applied Physics Letters*, vol. 82, no. 17, pp. 2784-2786, 2003.
- [18] S. M. Malik and S. K. O’Leary, “Optical transitions in hydrogenated amorphous silicon,” *Applied Physics Letters*, vol. 80, no. 5, pp. 790-792, 2002.
- [19] W. B. Jackson, S. M. Kelso, C. C. Tsai, J. W. Allen, and S.-J. Oh, “Energy dependence of the optical matrix element in hydrogenated amorphous and crystalline silicon,” *Physical Review B*, vol. 31, no. 8, pp. 5187-5198, 1985.
- [20] L. Jiao, I. Chen, R. W. Collins, C. R. Wronski, and N. Hata, “An improved analysis for band edge optical absorption spectra in hydrogenated amorphous silicon from optical and photoconductivity measurements,” *Applied Physics Letters*, vol. 72, no. 9, pp. 1057-1059, 1998.
- [21] S. K. O’Leary, S. R. Johnson, and P. K. Lim, “The relationship between the distribution of electronic states and the optical absorption spectrum of an amorphous semiconductor: an empirical analysis,” *Journal of Applied Physics*, vol. 82, no. 7, pp. 3334-3340, 1997.
- [22] S. K. O’Leary and S. M. Malik, “A simplified joint density of states analysis of hydrogenated amorphous silicon,” *Journal of Applied Physics*, vol. 92, no. 8, pp. 4276-4282, 2002.
- [23] S. K. O’Leary, “An analytical density of states and joint density of states analysis of amorphous semiconductors,” *Journal of Applied Physics*, vol. 96, no. 7, pp. 3680-3686, 2004.

- [24] S. K. O’Leary, “An empirical density of states and joint density of states analysis of hydrogenated amorphous silicon: a review,” *Journal of Materials Science: Materials in Electronics*, vol. 15, pp. 401-410, 2004.
- [25] T. M. Mok and S. K. O’Leary, “The dependence of the Tauc and Cody optical gaps associated with hydrogenated amorphous silicon on the film thickness:  $\alpha l$  experimental limitations and the impact of curvature in the Tauc and Cody plots,” *Journal of Applied Physics*, vol. 102, no. 11, pp. 113525-1-9, 2007.
- [26] F. Orapunt and S. K. O’Leary, “Optical transitions and the mobility edge in amorphous semiconductors: A joint density of states analysis,” *Journal of Applied Physics*, vol. 104, no. 7, pp. 073513-1-6, 2008.
- [27] M. Shur and M. Hack, “Physics of amorphous silicon based alloy field-effect transistors,” *Journal of Applied Physics*, vol. 55, no. 10, pp. 3831-3842, 1984.
- [28] J. G. Shaw and M. Hack, “An analytic model for calculating trapped charge in amorphous silicon,” *Journal of Applied Physics*, vol. 64, no. 9, pp. 4562-4566, 1988.
- [29] M. Shur, M. Hack, and J. G. Shaw, “A new analytic model for amorphous silicon thin-film transistors,” *Journal of Applied Physics*, vol. 66, no. 7, pp. 3371-3380, 1989.
- [30] H. C. Slade, “Device and material characterization and analytic modeling of amorphous silicon thin film transistors,” *Ph. D. Thesis*, University of Virginia, Charlottesville, Virginia, 1997.
- [31] S. M. Malik and S. K. O’Leary, “Deviations from square-root distributions of electronic states in hydrogenated amorphous silicon and their impact upon the resultant optical properties,” *Journal of Non-Crystalline Solids*, vol. 336, no. 1, pp. 64-70, 2004.
- [32] S. M. Malik and S. K. O’Leary, “An analysis of the distributions of electronic states associated with hydrogenated amorphous silicon,” *Journal of Materials Science: Materials in Electronics*, vol. 16, no. 3, pp. 177-181, 2005.
- [33] Z. Remeš, “Study of defects and microstructure of amorphous and microcrystalline silicon thin films and polycrystalline diamond using optical methods,” *Ph. D. Thesis*, Charles University, Prague, 1999.
- [34] R. H. Klazes, M. H. L. M. van den Broek, J. Bezemer, and S. Radelaar, “Determination of the optical bandgap of amorphous silicon,” *Philosophical Magazine B*, vol. 45, no. 4, pp. 377-383, 1982.

- [35] J. J. Thevaril and S. K. O’Leary, “A dimensionless joint density of states formalism for the quantitative characterization of the optical response of hydrogenated amorphous silicon,” *Journal of Applied Physics*, vol. 107, no. 8, pp. 083105-1-6, 2010.

---

## CHAPTER 6

---

# Conclusions

A quantitative model for the spectral dependence of the optical properties associated with amorphous semiconductors, which allows for the ready determination of the underlying modeling parameters from the results of experiment, has been devised. This model stems directly from a simplified empirical model for the DOS functions,  $N_v(E)$  and  $N_c(E)$ , that only considers VBB, VBT, and CBB electronic states, i.e., the CBT electronic states are neglected. This model assumes square-root distributions of VBB and CBB electronic states, and an exponential distribution of VBT states. The optical properties of a-Si:H were then determined through the evaluation of the corresponding JDOS function,  $J(\hbar\omega)$ . A comparison with the results of experiment was used in order to validate the model and in order to gain insight into the character of the optical response of a-Si:H.

In order to justify the neglect of the CBT states, initially, for the specific case of a-Si:H, it was shown that the neglect of the CBT states has no real impact on the obtained JDOS function, and that, therefore, the optical properties of a-Si:H may be accurately determined using this simplified empirical model for the DOS functions. This was done through the use of a general empirical model for the DOS functions of O'Leary *et al.* [1], this model including VBB, VBT, CBB, and CBT electronic states. Square-root distributions of VBB and CBB states were assumed

and exponential distributions of VBT and CBT were assumed. By examining the role that the conduction band tail breadth,  $\gamma_c$ , plays in determining the form of the resultant JDOS function,  $J(\hbar\omega)$ , it was shown that when the conduction band tail breadth,  $\gamma_c$ , is significantly less than the valence band tail breadth,  $\gamma_v$ , the CBT states can be ignored in the determination of the JDOS function,  $J(\hbar\omega)$ . Experimental evidence was presented that confirmed this to be the case for the specific case of a-Si:H. Thus, the use of a simplified empirical DOS model, that neglects CBT states, was justified for the specific case of this material.

In order to further simplify this empirical model for the DOS functions, it was further assumed that the derivative of the valence band DOS function is continuous at the energy at which the square-root and exponential functional dependencies interface; it was already assumed that the valence band DOS function is continuous at this interface. This simplification allowed for the casting of the JDOS evaluation into a dimensionless format. This dimensionless formalism for the JDOS function was shown to provide a platform for the comparison of disparate optical absorption spectra, with differing energy gaps and Urbach tail breadths. The applicability of this formalism was then tested through an analysis of a large number of a-Si:H experimental data sets. From this analysis, insights into the optical response of this material were gleaned. In particular, the similarity in the results suggest a ‘universal’ character common to the spectral dependence of all the optical absorption spectra associated with this material.

Finally, the role that defect states play in shaping the optical response of a-Si:H was probed. In order to perform this analysis, the empirical model for the DOS functions was modified in order to include VBD and CBD states. This was done by splining exponential tails, of greater breadth than the VBT and CBT tail breadths, onto the VBT and CBT states, these new exponential distributions modeling the dis-

tributions of defect states. With this model for the VBD and CBD states established, the contributions to the JDOS function, attributable to the various types of optical transitions involving these defect states, was then assessed. A comparison with the results of experiment was used in order to validate this modeling approach.

There are a number of further developments that can be pursued in order to further develop this body of work. Whether or not this ‘universal’ relationship, found for the case of a-Si:H, also applies to other materials, is certainly worthy of further investigation. There is also the question as to whether or not, through the use of this dimensionless JDOS formalism, there are efficient and effective means of extracting the underlying parameters from the results of experiment more directly rather than just a visual examination of the tightness of the resultant fit? Can this process be systematized within the framework of a formal error analysis? There is also the question as to whether or not it is possible to “map out” the optical response of a-Si:H. Through an exhaustive examination of as many a-Si:H experimental optical absorption data sets as possible, as yet unknown correlations between these modeling parameters may be discovered. This may allow one to effectively reduce the number of independent modeling parameters in the analysis of this material, allowing for the entire parameter space to be probed much more efficiently and effectively. Finally, there is the matter of using the obtained model in order to quantitatively predict and improve on the device performance of a-Si:H based electron devices.

## References

- [1] S. K. O’Leary, “An analytical density of states and joint density of states analysis of amorphous semiconductors,” *Journal of Applied Physics*, vol. 96, no. 7, pp. 3680-3686, 2004.

---

## APPENDIX A

---

# Copyright Release - Journal of Applied Physics

*Permission is granted - subject to the conditions outlined below - for the following:*

*A dimensionless joint density of states formalism for the quantitative characterization of the optical response of hydrogenated amorphous silicon, J. J. Thevaril and Dr. S. K. O'Leary, J. of Applied Physics, vol. 107, no. 8, 083105-1-6, 15 April 2010.*

*To be used in the following manner:*

*Reproduced in your Ph. D. thesis to be submitted to the Electrical and Computer Engineering Department at the University of Windsor.*

- 1. The American Institute of Physics grants you the right to reproduce the material indicated above on a one-time, non-exclusive basis, solely for the purpose described. Permission must be requested separately for any future or additional use.*
- 2. This permission pertains only to print use and its electronic equivalent, including CD-ROM or DVD.*
- 3. The following copyright notice must appear with the material: "Reprinted with permission from Thevaril, J.J. and O'Leary, S.K., A dimensionless joint density of states formalism for the quantitative characterization of the optical response of hydrogenated amorphous silicon, Vol. 107, n 8, p 083105-1-6, Copyright [2010], American Institute of Physics."*
- 4. This permission does not apply to any materials credited to sources other than the copyright holder.*
- 5. If you have not already done so, please attempt to obtain permission from at least one of the authors. The author's address can be obtained from the article.*

*Please let us know if you have any questions.*

*Sincerely,  
Susann Brailey*

*Office of the Publisher, Journals and Technical Publications  
Rights & Permissions  
American Institute of Physics  
Suite 1NO1  
2 Huntington Quadrangle  
Melville, NY 11747-4502*

---

## APPENDIX B

---

# Copyright Release - Solid State Communications

*Please note that, as one of the Authors of this article, you retain the right to include the journal article, in full or in part, in a thesis or dissertation.*

### *Authors' Rights*

*What rights do you retain as a journal author?*

*As a journal author, you retain rights for a large number of author uses, including use by your employing institute or company. These rights are retained and permitted without the need to obtain specific permission from Elsevier. These include the right to include the journal article, in full or in part, in a thesis or dissertation.*

# VITA AUCTORIS

Jasmin Joseph Thevaril was born in 1979 in Kerala, India. She graduated from Michael Power/St. Joseph's High School in 1998. From there she went on to Ryerson University where she obtained Bachelor's and Master's degrees in Electrical Engineering in 2002 and 2004, respectively. She is currently a candidate for the Doctoral degree in Electrical Engineering at the University of Windsor and hopes to graduate in the Spring of 2011.